UNIVERSIDAD DE INVESTIGACIÓN DE TECNOLOGÍA EXPERIMENTAL YACHAY

Escuela de Ciencias Químicas e Ingeniería

TÍTULO: A dual theoretical-experimental study of Iron complexing with N-ligand: understand and design a catalyst

Trabajo de integración curricular presentado como requisito para la obtención del título de Químico

Autor

Carlos Michael Jimenez Muñoz

Tutor

Thibault Terencio, Ph.D

Co - Tutor

Juan Pablo Saucedo, Ph.D

Urcuquí, Abril 2021

Urcuquí, 18 de junio de 2021

SECRETARÍA GENERAL
(Vicerrectorado Académico/Cancillería)
ESCUELA DE CIENCIAS QUÍMICAS E INGENIERÍA
CARRERA DE QUÍMICA
ACTA DE DEFENSA No. UITEY-CHE-2021-00008-AD

A los 18 días del mes de junio de 2021, a las 17:00 horas, de manera virtual mediante videoconferencia, y ante el Tribunal Calificador, integrado por los docentes:

Presidente Tribunal de Defensa	Dr. CAETANO SOUSA MANUEL , Ph.D.
Miembro No Tutor	Dra. LOPEZ GONZALEZ, FLORALBA AGGENY , Ph.D.
Tutor	Dr. TERENCIO THIBAULT , Ph.D.

El(la) señor(ita) estudiante **JIMENEZ MUÑOZ, CARLOS MICHAEL**, con cédula de identidad No. **0604968289**, de la **ESCUELA DE CIENCIAS QUÍMICAS E INGENIERÍA**, de la Carrera de **QUÍMICA**, aprobada por el Consejo de Educación Superior (CES), mediante Resolución **RPC-SO-39-No.456-2014**, realiza a través de videoconferencia, la sustentación de su trabajo de titulación denominado: **A dual theoretical-experimental study of Iron complexing with N-ligand: understand and design a catalyst**, previa a la obtención del título de **QUÍMICO/A.**

El citado trabajo de titulación, fue debidamente aprobado por el(los) docente(s):

Tutor	Dr. TERENCIO THIBAULT , Ph.D.

Y recibió las observaciones de los otros miembros del Tribunal Calificador, las mismas que han sido incorporadas por el(la) estudiante.

Previamente cumplidos los requisitos legales y reglamentarios, el trabajo de titulación fue sustentado por el(la) estudiante y examinado por los miembros del Tribunal Calificador. Escuchada la sustentación del trabajo de titulación a través de videoconferencia, que integró la exposición de el(la) estudiante sobre el contenido de la misma y las preguntas formuladas por los miembros del Tribunal, se califica la sustentación del trabajo de titulación con las siguientes calificaciones:

Tipo	Docente	Calificación
Tutor	Dr. TERENCIO THIBAULT , Ph.D.	10,0
Presidente Tribunal De Defensa	Dr. CAETANO SOUSA MANUEL , Ph.D.	10,0
Miembro Tribunal De Defensa	Dra. LOPEZ GONZALEZ, FLORALBA AGGENY , Ph.D.	10,0

Lo que da un promedio de: **10 (Diez punto Cero)**, sobre 10 (diez), equivalente a: **APROBADO**

Para constancia de lo actuado, firman los miembros del Tribunal Calificador, el/la estudiante y el/la secretario ad-hoc.

Certifico que *en cumplimiento del Decreto Ejecutivo 1017 de 16 de marzo de 2020, la defensa de trabajo de titulación (o examen de grado modalidad teórico práctica) se realizó vía virtual, por lo que las firmas de los miembros del Tribunal de Defensa de Grado, constan en forma digital.*

JIMENEZ MUÑOZ, CARLOS MICHAEL
Estudiante

MANUEL CAETANO SOUSA
Digitally signed by MANUEL CAETANO SOUSA
Date: 2021.06.21 15:39:13 -05'00'
Dr. CAETANO SOUSA MANUEL , Ph.D.
Presidente Tribunal de Defensa

THIBAULT TERENCIO

Dr. TERENCIO THIBAULT , Ph.D.
Tutor

FLORALBA AGGENY LOPEZ GONZALEZ

Digitally signed by FLORALBA AGGENY LOPEZ GONZALEZ
Date: 2021.06.21 16:51:07 -05'00'

Dra. LOPEZ GONZALEZ, FLORALBA AGGENY , Ph.D.
Miembro No Tutor

CARLA SOFIA YASELGA NARANJO

Digitally signed by CARLA SOFIA YASELGA NARANJO
Date: 2021.06.21 14:34:14 -05'00'

YASELGA NARANJO, CARLA
Secretario Ad-hoc

AUTORÍA

Yo, **CARLOS MICHAEL JIMENEZ MUÑOZ**, con cédula de identidad 0604968289, declaro que las ideas, juicios, valoraciones, interpretaciones, consultas bibliográficas, definiciones y conceptualizaciones expuestas en el presente trabajo; así cómo, los procedimientos y herramientas utilizadas en la investigación, son de absoluta responsabilidad de el/la autor(a) del trabajo de integración curricular. Así mismo, me acojo a los reglamentos internos de la Universidad de Investigación de Tecnología Experimental Yachay.

Urcuquí, Abril 2021

Carlos Michael Jimenez Muñoz

CI: 0604968289

AUTORIZACIÓN DE PUBLICACIÓN

Yo, **CARLOS MICHAEL JIMENEZ MUÑOZ**, con cédula de identidad 0604968289, cedo a la Universidad de Tecnología Experimental Yachay, los derechos de publicación de la presente obra, sin que deba haber un reconocimiento económico por este concepto. Declaro además que el texto del presente trabajo de titulación no podrá ser cedido a ninguna empresa editorial para su publicación u otros fines, sin contar previamente con la autorización escrita de la Universidad.

Asimismo, autorizo a la Universidad que realice la digitalización y publicación de este trabajo de integración curricular en el repositorio virtual, de conformidad a lo dispuesto en el Art. 144 de la Ley Orgánica de Educación Superior.

Urcuquí, Abril 2021

Carlos Michael Jimenez Muñoz

CI: 0604968289

ACKNOWLEDGMENTS

First, I want to express my gratitude to Yachay Tech University for the opportunity to receive a high-quality education that made my professional formation an unforgivable experience. Furthermore, I want to thank and congratulate the administrative and organizational work of the School of Chemical Science and Engineering that allowed me to obtain not only the best educational experience but also the opportunity to be immersed in the cusp of international education and global science.

I express my complete gratitude to my family. Especially emphasize my respect and honor for my parents Mirian and Ivan, I do not doubt that I would never have achieved anything without their trust, knowledge, love, and patience. I will never forget the sacrifices, the good days, the bad times, the happiness, and the love, both of you are the essential piece of my life. Thank you so much for let me dream.

Also, I want to recognize the effort of professor Thibault Terencio for being my guide into the theoretical chemistry field and for the unconditional help in this work. I want to thank the time invested in my formation, the patience, and the friendship that showed me since we met. Thank you for the opportunity to develop my potential and for believing in me; I will always be grateful to you.

I want to express my gratitude to professor Juan Pablo Saucedo for motivating me during my career and show me how to love chemistry. Thank you for the unconditional help you always give to me.

Also, I am entirely grateful to all my professors during the career at Yachay Tech University; especially with Kamil Makowski, Fernando Albericio, Marta Lopez, Juan Rosales, Vivian Morera, Manuel Caetano, and Stalyn Avila, also with my high school teacher Carlos Calán, that were not only my teachers but also my friends, I will never forget the support, the trust and the help in my professional and personal life.

Finally, I would like to thank all my friends, all of you changed my life and made me the person I am. I want to thank my closest friends Carlos Andrés L., Carlos V., Emily Daniela G., María Belen C., Josseline A., Kimberly C., Erick P., Jonathan C., Erick O., Fernanda R., Gabriela P., Carolina I., Ma. Emilia M., Juan Andrés C., the family Jimenez-Muñoz, the family Abad Peña and, the family López-Mejia. Especially, I want to thank Dayanara C. for being the closest person to me for a long time at university; thanks for

staying with me and helping me in all life aspects. Thank all of you for supporting me in the bad times of my life and staying with me in the happiest ones. I am convinced that all of you saw in me the person that I want to be.

To life, thank you so much for the depressive times, the euphoric times, the poetry, the chess, and the books. I think that I owe a lot of thanks and some apologies.

DEDICATION

To my parents, Mirian and Ivan.

To my brothers, Carlos Ivan and Juan Pablo.

To my whole family, especially to family Jimenez-Muñoz.

To Yachay Tech University and Ecuador.

To my professors.

To all my friends.

To the science.

To the literature art.

To the depressive, happy, challenging, and exciting times in my life.

To all the moments when I thought I was not capable.

RESUMEN

El hierro es un elemento que está presente tanto en compuestos inorgánicos como en la naturaleza y en el interior de nuestro cuerpo, por ejemplo, en la hemoglobina y los sideróforos. Desde el punto de vista de la química inorgánica, el hierro es un elemento fascinante que se encuentra en estados variables de oxidación y espín dependiendo de la naturaleza de los ligantes, mostrando propiedades interesantes.[1] Los ligantes que contienen nitrógeno son particularmente interesantes ya que son capaces de estabilizar incluso hierro (IV) o hierro (V) a través de diferentes geometrías. La afinidad de los ligantes no hémicos con el hierro ha mostrado ser específica por los átomos de nitrógeno, lo que implica una relación directa entre el número de enlaces en un complejo y el contenido de nitrógeno. La naturaleza del enlace, iónica o covalente, es un aspecto crítico que influye en las propiedades y la reactividad del hierro. En la búsqueda de entendimiento, la química teórica y computacional han sido particularmente eficientes. [2] En este trabajo se desarrolló el estudio teórico de los factores energéticos que influyen sobre el efecto catalítico en la reacción de deshidrogenación oxidativa de un compuesto de hierro coordinado con un ligante nitrogenado. Este tipo de reacciones son interesantes por sus características exotérmicas y su presencia en reacciones fundamentales como la producción de alquenos a partir de alcanos o incluso la síntesis de aminoácidos. [3,4] En este trabajo, se demostró que el complejo promueve la oxidación del ligante coordinado, lo cual contribuye a formar una imina a partir de una amina a través de la influencia del metal de transición. El centro metálico de Fe^{3+} coordinado con los ligantes 1,9-bis(2'-piridil)-2,5,8-triazanonano o 1,9-bis(3'-piridil)-2,5,8-triazanonano muestra un comportamiento muy diferente, no solo en la conformación sino también en la respuesta catalítica. Además, los resultados experimentales ilustrados en la literatura están respaldados por los resultados teóricos obtenidos. [5,6] A través de estudios DFT, se estudió el mecanismo de reacción para explicar las diferencias observadas entre ambos complejos. Además, los mecanismos se probaron bajo la acción de diferentes solventes para estimar qué condición favorecería la deshidrogenación oxidativa, mostrando mayor afinidad por el agua. Y finalmente, los estudios teóricos nos permitieron no solo explicar sino también diseñar modificaciones adicionales de este ligante, que serán probadas para predecir su actividad catalítica. [7]

Palabras Clave: complejos de hierro, ligandos nitrogenados, DFT, deshidrogenación oxidativa, mecanismos de reacción, catálisis.

ABSTRACT

Iron is a ubiquitous element, present in organic and inorganic compounds, in nature and inside our bodies, for example, in hemoglobin and siderophores. From an inorganic chemistry standpoint, iron is a fascinating element found in variable oxidation and spin states depending on the nature of the binding ligands showing exciting properties.jajaja[1] N-containing ligands are particularly interesting as they can stabilize even iron (IV) or iron (V) through different geometries. The affinity of nonheme ligands with iron already showed a specific affinity for nitrogen atoms, which implies a direct relationship between the number of bonds in a complex and the nitrogen content. The binding nature, ionic or covalent, is one critical aspect influencing iron properties and reactivity. In this quest of understanding, theoretical and computational chemistry have been particularly efficient.[2] In this work, the theoretical study of the energetic factors that influence the catalytic effect in the oxidative dehydrogenation reaction of an iron compound coordinated with a nitrogenated ligand was developed. These reactions are very interesting because of their exothermic characteristics and their presence in fundamental reactions like alkene production from alkanes or amino acid synthesis.[3,4] In this work, we demonstrate that the complex promotes the oxidation of the coordinated ligand, which contributes to form an imine from an amine through the influence of the transition metal. The metallic Fe^{3+} center coordinated with 1,9-bis(2'-pyridyl)-2,5,8-triazanonane or 1,9-bis(3'-pyridyl)-2,5,8-triazanonane ligands show a highly different behavior, not only in conformation but also in catalytic response. Moreover, the experimental results illustrated in the literature are supported by the theoretical results obtained.[5,6] Through DFT studies, the reaction mechanism was studied to explain the observed differences between both complexes. Furthermore, the mechanisms were probed under different solvents' actions to estimate which condition would favor oxidative dehydrogenation, showing a higher affinity for water. And finally, the theoretical studies allowed us not only to explain but also to design additional modifications of the ligands, which will be tested to predict its catalytic activity. [7]

Keywords: iron complexes, N-ligands, DFT, oxidative dehydrogenation, reaction mechanisms, catalysis.

TABLE OF CONTENT

LIST OF TABLES

LIST OF FIGURES

ABBREVIATIONS

N-ligand	Nitrogenated ligand
IUPAC	International Union of Pure and Applied Chemistry
HSAB	Interpretation of Hard and Soft Acids and Bases
TON	Turnover number
TOF	Turnover frequency
OD	Oxidative Dehydrogenation
picdien	1,9-bis(2’-pyridyl)-2,5,8-triazanonane
L2	1,9-bis(2’-pyridyl)-2,5,8-triazanonane
L3	1,9-bis(3’-pyridyl)-2,5,8-triazanonane
L4 in water	1,9-bis(2’-pyridyl)-5-[hydroxy-2’’-pyridyl)methyl]-2,5,8-triazanonane
L4 in methanol	1,9-bis(2’-pyridyl)-5-[methoxy-2’’-pyridyl)methyl]-2,5,8-triazanonane
L4 in ethanol	1,9-bis(2’-pyridyl)-5-[ethoxy-2’’-pyridyl)methyl]-2,5,8-triazanonane
HAT	Hydrogen Atom Transfer
HF	Hartree-Fock
DFT	Density-Functional Theory
RHF	Restricted Hartree-Fock
UHF	Unrestricted Hartree-Fock
ROHF	Restricted Open-shell Hartree-Fock
SCF	Self-Consistent Field
LDA	Local Density Approximation
GGA	Generalized Gradient Approximation
D3BJ	D3 with Becke-Johnson damping
SVP	Split Valence Polarization
TZVP	Triple-Zeta Valence Polarization
MP2	Second-Order Møller–Plesset Perturbation
CPCM	Conductor-like Polarizable Continuum Model
DMSO	Dimethyl sulfoxide
MOs	Molecular Orbitals
HOMO	Highest Occupied Molecular Orbital
SOMO	Single Occupied Molecular Orbital
LUMO	Lowest Unoccupied Molecular Orbital

CHAPTER I

1. Introduction

Nowadays and also before, catalysis can be initially defined as a kinetic process that changes the reaction rate by using a substance called "catalyst" that reduces the activation energy of the reaction and is not consumed during the process. The reaction where the catalyst is used should be repeatable, and the rate change should occur only in the presence of the catalyst. The catalytic effect is observed in different environments and under other characteristics depending on the nature of the catalyst.

The catalysts could be an atom, a molecule, an enzyme, a biomolecule, or a macrostructure. However, catalysis, as science, takes into account the chemical nature and physicochemical characteristics of the catalyst as well as the reaction attributes to define the types of catalytic processes.[8]

Homogeneous catalysis is based on the principle that both substrates and catalysts are present in the same phase, in most cases, the liquid phase.[9] More recently, the concept of homogeneous catalysis has been updated to the organometallic approach [10–12]; this new vision is based on the metallic complexes catalytic character produced by the ligands and the metallic center. The organometallic catalyst structure is based on a central metal atom surrounded by ligands that could be organic or inorganic. The properties of the catalyst are determined by the interaction between the ligand and the metallic center; the activity of the catalyst lies in the capability to modify the ligand environment.[9] From this approach, the biochemical importance of organometallic catalysts and homogeneous catalysis is fundamental to understanding life mechanisms.

For metal-containing compounds involved in catalysis, the aim is to integrate spectroscopic, thermodynamic, and kinetic studies. The Density Functional Theory (DFT) contributes to studying the effects of metal centers on the catalysis process from a theoretical approach. Also, molecular modeling allows a spatial study to obtain predictable states. The catalytic intermediates and rate-determining steps are fundamental data to the analysis of the catalyst activity. Furthermore, chemical characteristics as the activity, chemoselectivity, regioselectivity, and stereoselectivity give a guideline about the strength of the organometallic catalysts.[13]

This study aims to develop a theoretical study of an iron coordination compound with a nitrogenated ligand (N-ligand) in order to understand the catalytic effect achieved for the oxidative dehydrogenation reaction. This reaction yields oxidation that contributes to forming an imine from an amine through the transition metal intervention as a coordination center. The metallic iron center coordinated with the ligand 1,9-bis(**2'**-pyridyl)-2,5,8-triazanonane and 1,9-bis(**3'**-pyridyl)-2,5,8-triazanonane, shows a highly different behavior not only in spatial conformation but also in catalytic response for both cases. The ligand substituted in position two of the pyridine rings is reported in the literature as *picdien* [5,6]. Through theoretical studies, the nature of the bond between the ligand and the metallic iron center, the reaction mechanisms, and the catalytic behavior of both ligands can be analyzed.

1.1. Problem Approach

The interest in oxidative dehydrogenation arises from the capacity of the system to generate oxidized species from amines coordinated to metal centers, for example, nitriles, nitro species, and carbonyl groups through cleavage reactions. Furthermore, this reaction is widespread in biochemical systems (known as oxidative amine dehydrogenation), in reactions like lysyl oxidation in crosslinking collagen, and in the regulation of neurotransmitters such as dopamine and serotonin. [14] The most recent application for this group of reactions is based on the developing of electrocatalytic reactions, production of non-fossil-dependent batteries, alkanes treatment, nanotubes synthesis, and other homogeneous/heterogeneous catalytic reactions. [15–18] Many efforts have been made to propose a mechanism for this reaction; however, due to the energetic factors involved in the kinetics of the reaction, a most profound study or new mechanism possibilities are necessary. The theoretical background of this reaction in homogeneous catalysis is being studied with different complexes and macrocyclic compounds. In an effort to contribute to the understanding of the reaction mechanism for oxidative dehydrogenation in amine ligands, this study presents the theoretical analysis of an inorganic system experimentally studied previously.[19] This study explains a possible reaction mechanism for reducing amine ligands and proposes possible modifications to obtain more selective and efficient catalytic reactions based on the solvent used.

1.2. Objectives

1.2.1. General Objective

- To understand the differences in the oxidative dehydrogenation reaction mechanisms of two iron complexes with two poly-nitrogenated ligands with a structural difference in the position of substitution in the pyridine rings of the ligands.

1.2.2. Specific Objectives

- To carry out a computational analysis of the ligand substituted in two different positions to compare the stability of both possibilities.
- To perform modifications in the ligand based on the solvent used for the OD reaction and analyze its stability.
- To compare the coordination of both ligands with the iron center, contrasting the energy of the possible multiplicities of the ligands and the stability of the formed complexes.
- To study the possible reaction mechanism for the oxidative dehydrogenation reaction with modifications in the ligand and compare the catalytic impact in the energy of each stage.
- To found the transition state for each hydrogen transfer involved in the mechanism evaluated.
- To evaluate the reaction mechanism under the influence of different solvents and establish the thermodynamics of the reaction for each case.

CHAPTER II

1. Background and Literature Review

1.1. Chemical Fundamentals

1.1.1. Chemoselectivity, Regioselectivity, and Stereoselectivity

The term "selectivity" refers to the affinity that a reagent (A) shows for a different reagent (B) in presence of other reagents (C, D…). Also, selectivity can be interpreted as the discrimination of different reaction pathways between two reactants (A and B). Chemoselectivity refers to the preference to break or form a chemical bond. According to the International Union of Pure and Applied Chemistry (IUPAC), chemoselectivity is defined as "the preferential reaction of a chemical reagent with one of two or more different functional groups." In this way, the functional groups could be extraordinarily reactive or completely inert; these characteristics are the chemoselectivity pillar.[20,21]

According to the IUPAC, regioselectivity directs the reaction to forming or breaking a specific bond preferentially over all other possibilities. Depending on the capability of discriminating the bond formation or breaking, the reactions can be 100% regioselective or partially if a product predominates over another. [20]

Stereoselectivity refers to the control of the stereochemical interaction in the reaction. [22] In this case, IUPAC defines stereoselectivity as "forming a stereoisomer over another in a chemical reaction". Furthermore, the effect can be more specific if the stereoisomer is an enantiomer or a diastereoisomer; the stereoselectivity changes to enantioselectivity and diastereoselectivity, respectively. [20]

1.1.2. Homolytic and Heterolytic Bond Cleavage

The simple bond formation implies two electrons that are part of two different atoms reaching a most stable state. The chemical properties of the elements allow the construction of double or triple bonds, just increasing the number of electrons interacting to four and six, respectively. Depending on the nature of the atoms involved in the bond formation, it can be identified as covalent, ionic, metallic, or coordinated. [23] Regarding this, the break-down of a bond is a process of fundamental importance for chemistry in all its branches.

The bond break-down can be divided into two different pathways; the first is the homolytic bond cleavage, which is defined as the bond-breaking where each one of the

electrons forming the bond goes with each of the different atoms involved in the bond.[24] In Equation 1, the homolytic bond cleavage is represented, the elements that intervene are represented as X and Y, and the electrons are represented as dots.

$$X : Y \rightarrow X \cdot + \cdot Y \quad (1)$$

The second pathway is the heterolytic bond cleavage; in this case, both of the electrons that are part of the bond go with one of the atoms, then the other atom does not have any of the electrons of the bond. [24] This process depends on the electronegativity of the elements and produces an anion (negatively charged atom) and a cation (positively charged atom). Using the same nomenclature as in Equation 1:

$$X : Y \rightarrow X + : Y \quad or \quad X : + Y \quad (2)$$

1.1.3. Multiplicity

According to the IUPAC, the number of possible orientations of the spin angular moment that corresponds to a given total spin quantum number (spin multiplicity) is calculated as follows, where S is the total spin angular momentum, as shown in Equation 3 [20]:

$$2S + 1 \quad (3)$$

The value of S is a non-negative integer or half-integer, considering that each electron has a value of S = 1/2.

1.2. Catalysis

The term "catalysis" was initially used by Jöns Jakob Berzelius in 1836 to appoint previous experiments based on ammonia decomposition by metals and modification of the decay rate of potassium chlorate, among others. Initially, the gross definition of catalysis was based on the inhibition break-down activity observed for some species. [25] However, the term has been evolving, taking account of the new approaches established in chemistry and the novel observations that are developed currently.

Catalysis was interpreted as an "affinity" force that guides the course of the chemical reaction. This understanding was adopted due to the ignorance of reaction mechanisms at the molecular level and the reaction rates. [26] The constant development of Chemistry has remodeled the catalysis description as the action of a substance that modifies the rate of a chemical reaction keeping itself unchanged during the process. [27]

Although catalysis intervenes directly in the increment of the rate of the reaction, its effect does not modify the thermodynamics of the reaction; the reaction will proceed without

the presence of the catalyst, some cases very fast (a catalyst is not necessary) and in other cases too slowly to be noted or valuable (a catalyst is necessary). [27] Also, the catalyst action does not alter the equilibrium composition of the reaction because the increment in the reaction rates is equal to the forward as the backward reactions. [27] The basic idea of catalysis is to provide an alternative and more accessible pathway than the original, reducing the activation energy and increasing the efficiency of the reaction in contrast with an uncatalyzed reaction.

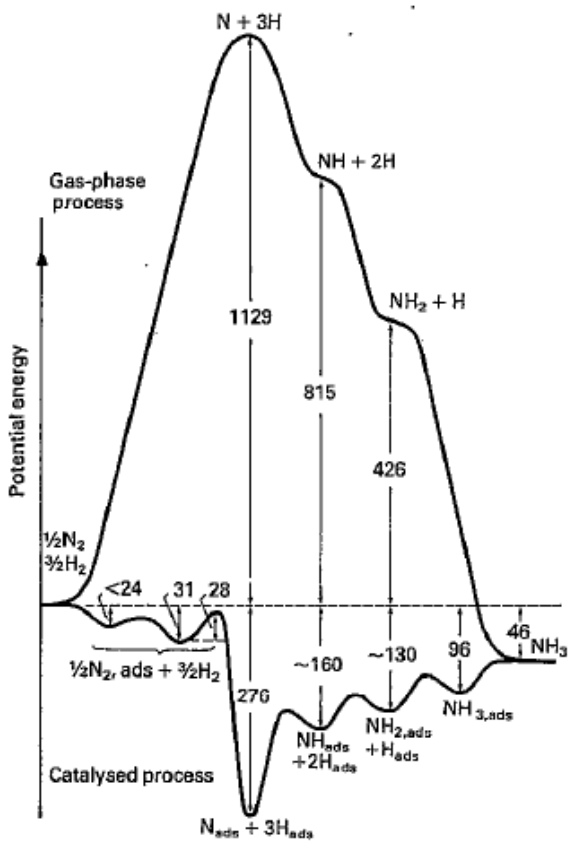

Figure 1. Catalytic process for the synthetic pathway of ammonia from hydrogen and nitrogen in gas-phase iron-catalyzed. Taken from [28].

As shown in Figure 1, the interaction of the reagents with a catalyst derives from the access to thermodynamically more favorable mechanisms than the mechanism without the inclusion of the catalyst species. Usually, these reactions are activated by heat. [29] Furthermore, the new mechanism could be divided into sub-reactions that modify the initial energy required for the activation of the reaction in contrast with the one-step mechanism that needs high amounts of energy. It can be interpreted as a split of the necessary energy, taking small quantities of the thermal energy always present in the reaction environments, to achieve the same product.

1.2.1. Catalyst

Catalyst is a substance that performs a catalytic effect in a chemical reaction, which means, it increases the reaction rate. [30] The reaction of the catalyst with the reactants is established by forming chemical bonds that allow the interaction among the reactants to create the products under the catalytic effect. The elementary idea of catalysis sets that catalyst is recovered after the reaction is catalyzed; however, it does not have an infinite useful life. [30] The physical-chemical state of the catalyst defines its characteristics on the reaction dynamics; this creates different branches to study catalysts' effects and features.

The most relevant characteristics of catalysts are activity and selectivity. Focusing on chemical activity, it is expressed in terms of turnover number (TON) which is the number of molecules of the product obtained per molecule of catalyst. [31] As can be inferred, the turn over frequency (TOF) has units of turnover number per unit time. The chemical selectivity can be analyzed through different perspectives, dividing it into chemoselectivity, regioselectivity, and stereoselectivity. Besides, it is essential to consider the catalyst life, the susceptibility to poisoning, the diffusion of the reactant, and the mechanistic understanding for performance control. [31]

1.2.2. Autocatalysis

The autocatalytic effect is referred to the reaction where one of the products is the catalyst of the same reaction that produces it. In terms of kinetics, the autocatalytic reaction curve of the concentration of A reactant ([A]) vs time always shows an "inverted s" behavior, as is illustrated in Figure 2, where the [A] vary in time according Equation 4.[32]

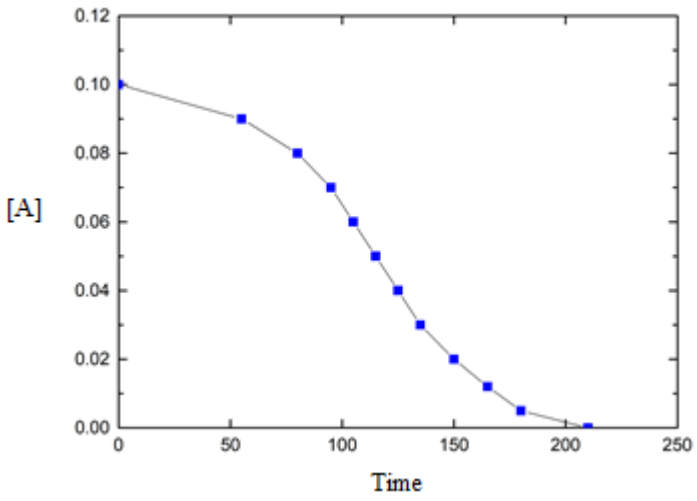

Figure 2. Autocatalytic reaction behavior, [A] vs. t. Adapted from [32].

$$[A] = \frac{[A]_0 + [B]_0}{1 + \frac{[A]_0}{[B]_0} e^{-([A]_0+[B]_0)kt}} \quad (4)$$

This behavior occurs due to the small quantity of catalyst at the beginning of the reaction, producing a prolonged degradation of an initial reagent A. In contrast, as the reaction goes forward, the amount of catalyst generated increases, and the rate of degradation of the reagent A also increases, decreasing its concentration. [32] At the final of the reaction, the rate goes slower than before because of the almost complete reagent A consumption.

This catalytic process can be demonstrated through the exponential rate of the appearance of the product and the correlation of the initial product concentration and reaction rate. This type of catalysis describes complex behaviors of biological systems; however, extending the definition to the biologic field, the appropriate term is "autocatakinesis." [33] Furthermore, autocatalysis is a fundamental theory to understand the chemical evolution and the origin of life, the dissipative chemical systems, and information processing systems. [34]

1.2.3. Heterogeneous Catalysis

Heterogeneous catalysis is based on the physical state of the catalyst. In difference to homogeneous catalysis and autocatalysis, in this case, the catalytic reaction takes place on the surface of a solid catalyst. Processes such as the adsorption and the reaction of the adsorbed reactant (called adsorbate) with the species in the gas or liquid phase, and the desorption process of the reaction products are crucial for the overall analysis of this type of catalysis [35]. Heterogeneous catalysis has essential differences from homogeneous catalysis despite working under the same chemical principle.

This type of catalysis is widely used in industry (almost 85% of all catalytic processes, according to Bhaduri et al. [31]) due to the extent of its application and its higher thermal stability. Furthermore, in contrast with homogeneous catalysis, heterogeneous catalysis is involved in developing useful catalysts for cracking, reformation, ammonia synthesis, among other reactions with industrial interest that can be performed at high temperatures. Another critical advantage of heterogeneous catalysis is the easy recovery of the catalyst (filtration or decantation). [31]

1.2.4. Homogeneous Catalysis

Homogeneous catalysis refers to the chemical system where both the catalyst and the substrates are in the same phase (liquid or gaseous). Organometallic compounds and

coordination complexes are the principal groups of catalysts used in homogeneous catalysis; they also encompass other important processes as acid and base catalysis, organic catalysis, enzymatic processes, among others. [36]

The oxidative addition, the reductive elimination, the insertion reactions, the β-hydride elimination, and the nucleophilic attack on a coordinated ligand are common reactions in a large number of homogeneous catalytic reactions. Oxidative addition and reductive elimination are widespread and essential in coordination compounds; the metal ion suffers formal oxidation or reduction, changing its oxidation state and coordination sphere. [31] In Figure 3**,** a few examples of this type of reaction in coordinated complexes can be observed.

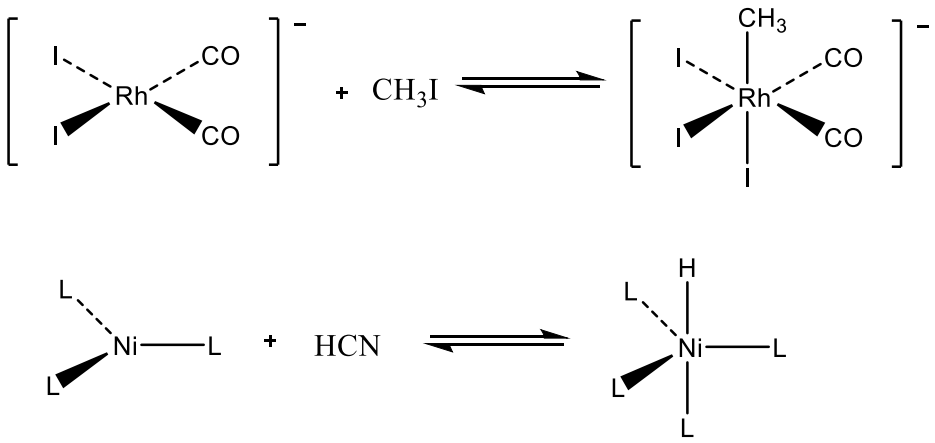

Figure 3. Examples of oxidative addition and reductive elimination reactions. Adapted from [31].

Focusing on coordination compounds, the chemistry of homogeneous catalysis of transition metal centers is governed by the fundamental rules of coordination chemistry, emphasizing the formation, stability, and reactivity. [37] Homogeneous catalysis with coordination compounds is characterized by high activity, high specificity reacting with specific substrates, and high selectivity reacting in a particular position. [38] Nowadays, classical industrial processes are developed under homogeneous catalysis with coordination compounds viewpoint, for example, polymerization on the Ziegler catalysts, olefin oxidation by molecular oxygen to aldehydes, hydroformylation, among others. [38]

1.3. Coordination Compounds

Coordination chemistry is based on the existence of coordination bonds. These bonds are a particular case of the covalent bond, regarding the principle of sharing electrons to

supply the lack of them in another atom. [39] In terms of shape, coordination compounds are formed by a central metallic atom (or ion) surrounded by electron-rich groups that can be atoms, ions, or molecules. The structure surrounding the metallic atom center is named the coordination sphere and it is occupied by a ligand. Usually, coordination compounds are called complexes because of their "complex" composition, charge, and structural properties.

1.3.1. Ligands

Ligands are atoms, ion or molecules that surround a metallic atom to form a coordination compound, the interaction (coordination) of the central metallic atom with its ligands establishes the inner coordination sphere of the compound.[39] The ligands accomplish specific functions as modulation of the electron density at the central metal (affecting its reactivity), managing the multiplicity and symmetry through the coordination sites at the metal, and enhancing the environment to benefits a reaction.[37]

1.3.2. Interpretation of Hard and Soft Acids and Bases Theory (HSAB)

The coordination chemistry of the metals is subdivided into two categories depending on the kind of binding: covalently or ionic binding metal ion. According to the theory of hard and soft acids and bases (HSAB) and Lewis's acid/base theory, the basic idea is that ions with small ionic radio and/or high oxidation states (Ca, Mg, Na, and K) are known as hard (class A) or ionic, while, ions with large ionic radii and more polarizable (Pt, Hg, Cd, and Pb) are known as soft (class B) or covalent. In this point, HSAB theory describes transition metals (Zn, Cu, Fe, and Co) that are placed in the frontier of class A and class B.[40]

Considering the before-mentioned HSAB theory and applying it to ligands, hard species or ionic ligands possess an oxygen donor group (carboxylate, alcohol), while soft species covalent ligands have sulfur or phosphorus donor atoms (thioethers, thiolates, phosphanes). As in the metal centers, a group of ligands also possess an intermediate characteristic between hard and soft species; the ligands with this character are nitrogen-donor ligands (imidazole). Furthermore, the ligand defines the coordination number, spin state, redox potential of the metal ion, and the coupling geometry among the ligand and metal center, a fundamental feature for catalysis. [40]

1.3.3. Nitrogenated ligands

The nitrogenated ligands (N-ligands) are particularly interesting in coordination compounds and homogeneous catalysis because of characteristics not observed in another type of ligands (as phosphorus-ligands). The capacity of N-donors to establish a π back-bonding is negligible, generally are unsuited for stabilizing low oxidation states of transition metal centers. Furthermore, the *trans* effect of N-donors is insignificant too, so the rates of substitution reactions are usually high. Also, the reactivity of complexes of transition metals with N-donors is high. [37] In Figure 4**,** it can be observed the interaction of pyridine (py) with different metallic centers.

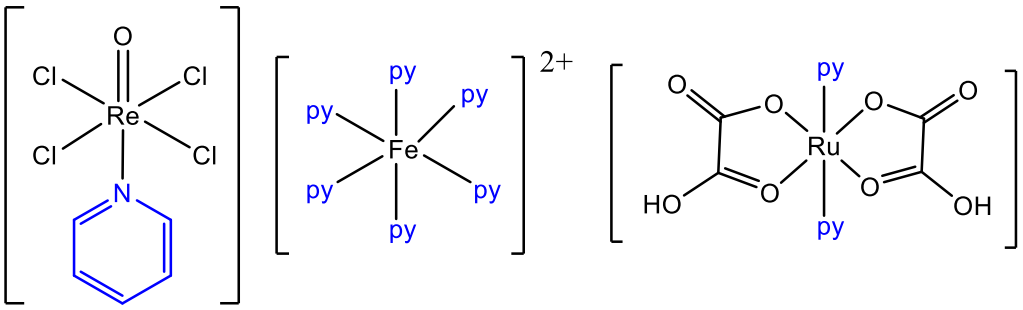

Figure 4. Pyridine interaction with a metal center. Adapted from [41].

1.3.4. Picdien ligand

The poly-nitrogenated ligand 1,9-bis(2'-pyridyl)-2,5,8-triazanonane, or also called *picdien*, is a pentadentate ligand used to study oxidative dehydrogenation reaction when is coordinated with iron or copper metal centers. This N-ligand has secondary amine groups signaled as responsible for forming stable imine iron (II) complexes through oxidative dehydrogenation. [6] In most cases, octahedral compounds that contain this type of ligands present a high geometrical and conformational isomerism due to the nature of the ligand.

This ligand has been studied in the interaction with a comprehensive list of metal centers, for example, Cr(III) [42], Co(III) [43], Ru(III) [44], Cu(II) [45], Ni(II) [45], Zn(II) [46], and Fe(III) [47] trying to elucidate its characteristics to promote the oxidative formation of imines as well as its reactivity, kinetical and thermodynamic characteristics. The ligand and its analog in position 3' are shown in Figure 5.

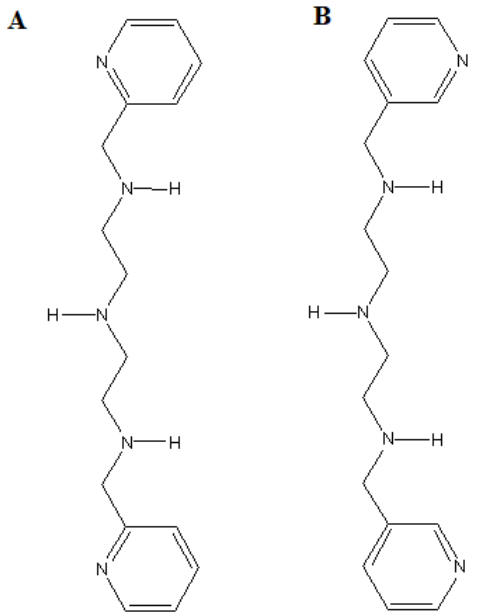

Figure 5. A) 1,9-bis(2'-pyridyl)-2,5,8-triazanonane (picdien) B) 1,9-bis(3'-pyridyl)-2,5,8-triazanonane

Then, the *picdien* ligand can be modified with a well-studied diol formation reaction; this transformation depends on the solvent where the synthesis is carried. The solvent induces a nucleophilic attack to oxidate the ligand in the imine group yielding the diol that will increase the denticity of the ligand. [19]

The reaction could be initiated in water, methanol, or ethanol as solvent. In the case of water, the reaction shown in Figure 6 is achieved; the result of this modification is the formation of the hexadentate ligand 1,9-bis(2'-pyridyl)-5-[hydroxy-2''-pyridyl)methyl]-2,5,8-triazanonane.

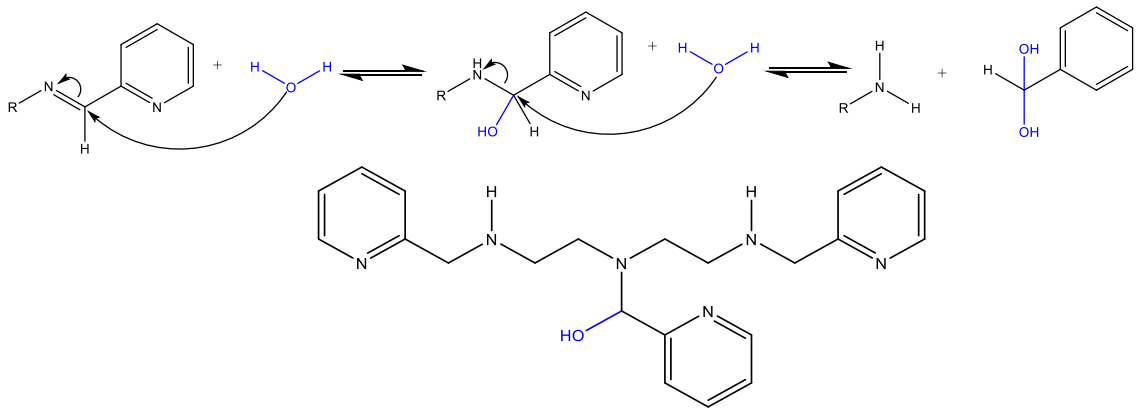

Figure 6. Synthesis of 1,9-bis(2'-pyridyl)-5-[hydroxy-2''-pyridyl)methyl]-2,5,8-triazanonane (nucleophilic attack of water)

In the case of methanol, the reaction shown in Figure 7 is achieved for the formation of the hexadentate ligand 1,9-bis(2'-pyridyl)-5-[methoxy-2''-pyridyl)methyl]-2,5,8-triazanonane.

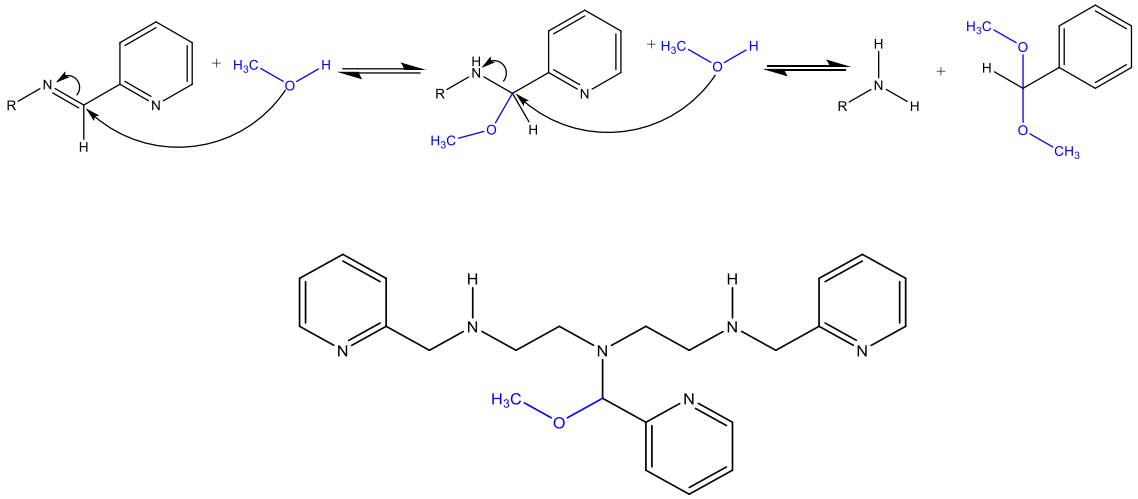

Figure 7. Synthesis of 1,9-bis(2'-pyridyl)-5-[methoxy-2''-pyridyl)methyl]-2,5,8-triazanonane (nucleophilic attack of methanol)

In this case, the use of ethanol as solvent led *picdien* to be transformed into a hexadentate ligand 1,9-bis(2'-pyridyl)-5-[ethoxy-2''-pyridyl)methyl]-2,5,8-triazanonane as can be observed in Figure 8. [6]

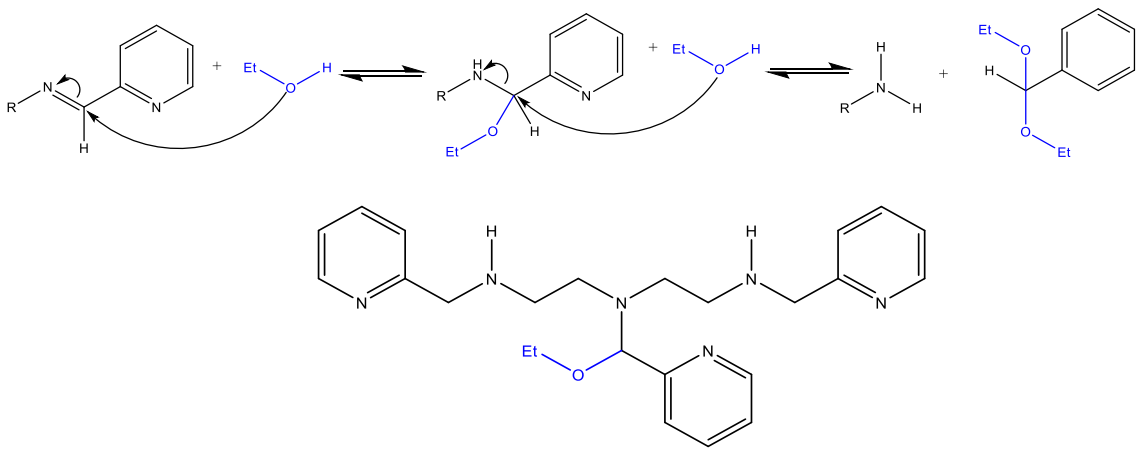

Figure 8. Synthesis of 1,9-bis(2'-pyridyl)-5-[ethoxy-2''-pyridyl)methyl]-2,5,8-triazanonane (nucleophilic attack of ethanol)

1.4. Oxidative Dehydrogenation

The interest in oxidative dehydrogenation (OD) was initiated with the study of such reactions in complexes with macrocyclic ligands. This reaction is interesting because the complexes oxidize their coordinated amines into nitriles, nitro species, and carbonyl

groups through cleavage reactions. [48] Furthermore, this reaction is widespread in biochemical systems (known as oxidative amine dehydrogenation) in reactions like lysyl oxidation in crosslinking collagen and the regulation of neurotransmitters such as dopamine or serotonin. [14]

In these reactions, the metal center is fundamental to define the oxidative characteristics of the ligand. The iron promotes the reaction because of its accessible potential redox value compared to other metal centers that show different electrochemical properties.

Establishing a contrast between iron and copper, which are critical metals for live beings, the difference lies in the electrochemical properties. The reduction potentials of Fe(III)/Fe(II) and Fe(II) at neutral pH are relative low and accessible in biochemical environments [Fe_2O_3 (hematite)/Fe(II):-0.2V, Fe(II)/Fe(0):-0.44V], while, cupper shows reduction potentials more thermodynamically impeded (Cu(II)/Cu(0):+0.34V, Cu(II)/Cu_2S:+0.2V). [49] The electrochemical characteristics of iron are the principal reason why iron is studied. It can be stabilized to uncommon multiplicities and improves the reaction in biochemical environments, for example, hydrogen transfers in OD.

From this overview, it can be suggested that the metallic complexes that induce specific reactions, as OD, are categorized as a catalyst.

The oxidative dehydrogenation is formed by a group of sub-reactions that involve proton and electron transfers. In the case of the amine to imine oxidation reaction with the presence of a transition metal, the mechanism begins with first oxidation followed by the deprotonation of the ligand, an electron transfer, and then final deprotonation reaction that allows the formation of the double bond of the imine group as can be observed in Figure 9.

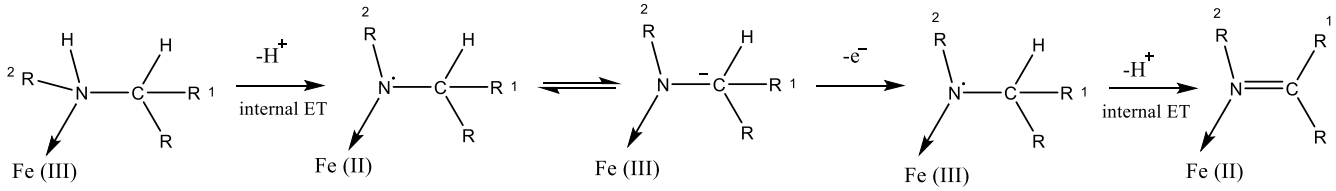

Figure 9. Oxidative dehydrogenation of an amine group to yield an imine group. Adapted from [50].

1.4.1. Electron-Proton Transfer

The presence of a catalyst that enhances a hydrogen transfer reaction tends to reduce multiple bonds to create a hydrogen donor. After that, the hydrogen is added to the hydrogen acceptor, which is characteristic of an unsaturated functional group that stabilizes the accepted atom. This process can be generalized when the hydrogen donor

(DH_2) and the hydrogen acceptor (A) interact through a catalyst to achieve hydrogen transference. [51] Equation 5 shows the description of an electron-proton transfer.

$$\gamma DH_2 + A \leftrightarrows D + AH_2 \quad (5)$$

Proton transfer is a fundamental step for a vast number of chemical reactions involved in all chemistry fields. This process is promoted by electron transfers that depend on the coupling strength and the transfer range. In this sense, three viewpoints will be discussed.[52]

1.4.1.1. Hydrogen Atom Transfer (HAT)

The first case is the hydrogen atom transfer (HAT), the simultaneous transference of the proton and the electron from the same donor to the same acceptor. [52]

1.4.1.2. Long Distance Transference

The second case is a long-distance transference of the electron directly from the proton transference that moves only a short distance. [53] These procedures are present in combustions, halogenations, and oxidations; the phenomena can be more complicated considering thermodynamics and kinetics of the reaction.

1.4.1.3. Hydrogen Transfer in Metal Complexes

This case can be divided into two paths; the first is the "hydridic route," and the second is the "direct hydrogen transfer." As its name specifies, the hydridic route forms a metal hydride as an intermediate due to the interaction of the catalyst with the hydrogen donor and the transference of the hydride from the metal to the acceptor. In direct hydrogen transfer, both the donor and the acceptor are held together by the catalyst allowing the hydrogen transference. [51]

1.5. Computational Background

Theoretical and computational chemistry is a powerful tool to understand the kinetics and thermodynamics of the reactions that are involved in a chemical reaction. For coordination compounds particularly, the computational study allows to propose and analyze reaction mechanisms, transition states, electron density localization, frequencies, solvent environments, among other important characteristics involved in the study of a reaction.

1.5.1. Hartree-Fock Approximation

The Hartree-Fock approximation (HF) is considered one of the fundamentals of modern chemistry because it was the first step to obtaining the Schrodinger equation's possible solution for multi-electronic systems. The principle of the HF method is based on the replacement of one electron problem that considers electron-electron repulsion instead of trying to solve many-electron problems. [54] The HF method assumes that the many-body wave function has an anti-symmetrized form due to the one-electron orbitals; the bases for this assumption are the independent particle approximation and the Pauli exclusion principle. [55] It is important to emphasize that is not an accurate method for organometallic systems.

HF present some difficulties in its application, first, a set of single particle wave functions is needed to calculate the single-electron nonlocal potential. Second, the inclusion of correlation corrections needed a complex process to be implemented. With this, complex many-electron systems become a too complicated calculation.[56]

1.5.2. Density-Functional Theory (DFT)

The Density-Functional Theory is based on understanding the physical-chemical phenomena of molecules and materials through the fundamental laws of quantum mechanics.[57] The objective is to obtain an approximation to the solution of the Schrodinger equation of N-electrons moving in an electrostatic potential (typically generated by the atomic nuclei). The DFT demonstrates the equivalence of the poly-electronic wave function and electron density; it identifies the ground state electronic structure and energy (E_0) of any chemical system. [58]

This estimation presents severe limitations to be considered as the definitive solution; the first is that the problem is highly nontrivial, even for a small number of electrons in the system; another limitation is that the computational demand of the calculations increases with the number of atoms in the system, the resolution for high number electrons becomes exorbitant.[59] For open-shell systems, DFT approximations allow a not perfectly accurate prediction of electron affinities and ionization energies from total energy difference calculation.[57] For the use of DFT approximations, different functionals are available considering accuracy, computational costs, and the exchange-correlation energy. [60]

1.5.3. ORCA – Quantum Chemistry Program

ORCA is a software characterized by its procedural and strongly typed nature.[61] The general purpose of the system is to include a wide range of theoretical and spectroscopic methods, be robust, effective and be mainly focused on transition metals. [62] ORCA is capable of working with closed-shell (RHF), spin-unrestricted (UHF), and restricted open-shell (ROHF) self-consistent field (SCF) calculations based on various methods of DFT or Hartree-Fock. [63]

ORCA uses Gaussian bases functions in conventional, semidirect, and direct integral handling models. ORCA is written in C^{++} language that is not based on any other previous electronic structure program package. ORCA can treat local density approximation (LDA), generalized gradient approximation (GGA), meta-GGA, hybrid, double-hybrid, and range separated functionals.[62] For this work, the input used for ORCA calculations is formed by a functional (B3LYP), a dispersion corrector (D3BJ), various optimization methods (OPT/OPTTS/FREQ) and basis set (def2-SVP/def2-TZVP) principally, but in some cases a solvation model is added (CPCM).

1.5.3.1. Functional: B3LYP

The B3LYP hybrid functional is formed by the combination of Becke's three-parameter exchange functional and the nonlocal correlation functional of Lee, Yang, and Parr. Becke's three-parameter exchange functional determines the relative weights of the exact, local, and gradient-corrected nonlocal contributions on the Hartree-Fock exchange-correlation.[64]

The B3LYP functional is one of the most popular density functional in the computational chemistry field due to its capacity of obtaining geometries, dipole moments, polarizabilities, and vibrational frequencies in fairly good agreement with experimental systems.[64] In comparison with DFT functionals as LSDA and BLYP, B3LYP showed impressive agreement with the experiment; furthermore, force fields as MP2 and SCF showed slightly less or much less accuracy than the DFT/B3LYP forcefield. B3LYP also demonstrated that while increasing the size of the basis set, the calculation converges faster.[65]

This functional was initially designed to study vibrational absorption and circular dichroism, achieving a moderate computational cost and accurate results; these characteristics led to B3LYP be considered as a standard method.[66] DFT calculation does

not evaluate the dispersion interactions produced by the instantaneous deformation of the electronic density (van der Waals interactions); however, in systems with biologic ligands or large ligands, this influence could not be negligible. Instead, B3LYP approximates DFT focused on exchange and correlation functional; it is based on Hartree-Fock, local density approximation, and general gradient approximation.

1.5.3.2. Dispersion Corrector: D3BJ

The problem of dispersion interactions in the DFT functional was tried to solve by considering intermolecular interactions. The consideration of the interactions is significant for the solution of liquid media, crystals, polymer, and biomolecules. The D2, D3, and D3BJ (D3 with Becke-Johnson damping) methods were proposed by Grimme, et al. [67,68] In the short-term, D3BJ is an atom-pairwise dispersion correction to the DFT energy with Becke-Johnson damping. [69]

1.5.3.3. Optimization Methods: OPT/OPTTS/ FREQ

The OPT command is used for geometry optimization of a structure; this means minimizing the total energy of the structure or atom for the input method. The optimization program automatically reassigns the coordinates of the atoms if become invalid, this assignation is evaluated through an algorithm that uses the variational principle.[69] The transition state optimization method (OPTTS) is based on locating transition states through the eigenvector-following algorithm. The objective is to find an approximate minimum energy path that connects 2 minima, then the transition state is located by the eigen-vector following method. [69]

The command FREQ is used in vibrational frequencies calculation in HF, DFT, and MP2. This command is applied to identify the harmonic vibrational frequencies of a system. Apart, form the possibility to simulate an IR spectrum, FREQ must be used to verify if the optimized structures are minimal. [70]

1.5.3.4. Basis Sets: def2-SVP/def2-TZVP

The second-generation default (def2) family of basis sets was developed by Ahlrichs and co-workers, the group is formed by def2-SVP, def2-TZVP, def2-TZVPP, def2-QZVP, and def2-QZVPP.[71] The basis set def2 represents the electronic wave function and considers the polarization function in all atoms. The particular case of def2-SVP is called split valence polarization. It is defined as the valence double-zeta basis set with “new”

polarization functions.[69] The def2-TZVP is called triple-zeta valence polarization. It is defined as the valence triple-zeta basis set with "new" polarization functions. [69]

The group of def2 basis sets showed a consistently increasing quality with the increasing of the basis set size in comparison with the predecessor def basis set group. For equilibrium geometries calculations (optimizations), def2 basis sets yield reasonable and qualitative correct results.[72] Furthermore, this group of basis sets presented a consistent accuracy for almost all elements in the periodic table.[73] Particularly, TZVP showed to be an excellent choice for general purposes applications of DFT in comparison with MG3S basis. Additionally, the SVP basis can be used when TZVP is unaffordable. [71]

1.5.3.5. CPCM

The dielectric continuum theories are widely used to describe the hydration in unification with quantum mechanics calculations with a relatively low computational cost.[74] The conductor-like polarizable continuum model is a method to implement the solvent effects in quantum chemical calculations in an implicit way. The solvent is represented as a dielectric polarizable continuum, and polarization charges that describe the solvent reaction field. [70] The solute molecule is embedded in a cavity surrounded by a dielectric continuum of permittivity ε that represents the solvent media. [74]

The accuracy of continuum solvation models depends on the proper boundary conditions on the surface of the cavity containing the solute, considering the cavity as spheres centered on atoms or atomic groups where inside the cavity the dielectric constant is the same as *in vacuo* and outside it takes the value of the desired solvent.[74] The charge distribution of the solute polarizes the dielectric continuum creating an electrostatic field the polarizes the solute.[75]

CHAPTER III

1. Methodology

In this work, the theoretical study of OD reaction mechanism was performed. However, before performing the calculations of the mechanism, previous calculations were performed to understand the stability of the coordination complex system at all its stages. The work follows the order presented in Figure 10.

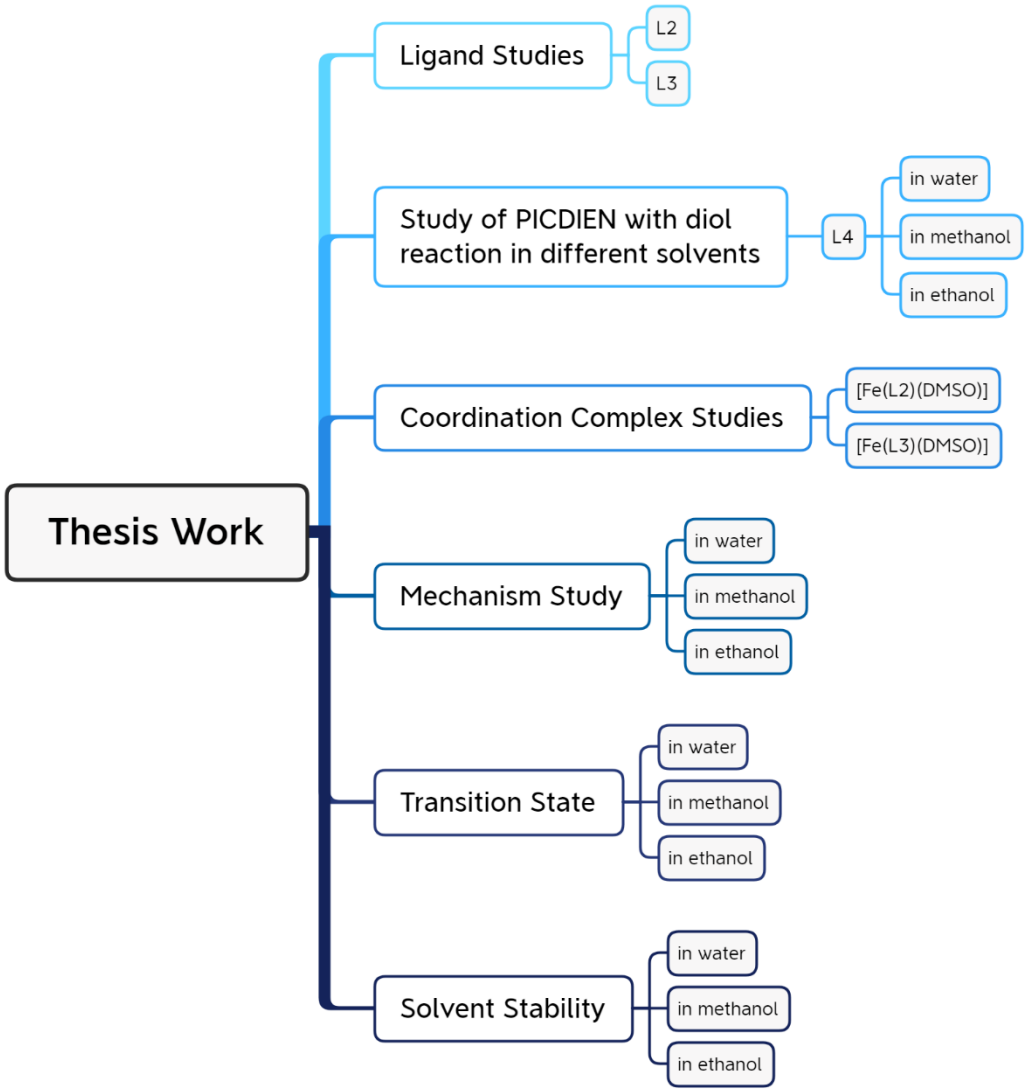

Figure 10. Graphical description of the methodology used for the development of the present work.

1.1. Ligand Studies

Following a sequence line, the first step was to analyze the stability of the ligand *picdien* and the 3' substituted derivative (Figure 5). A comparison of 1,9-bis(**2'**-pyridyl)-2,5,8-triazanonane (L2) ligand versus 1,9-bis(**3'**-pyridyl)-2,5,8-triazanonane (L3) that is the

same ligand substituted at position 3 pretends to explain the importance of the correct synthesis of the ligand and the repercussions of the hindrance effect in the formation of the complex, as well as the influence of the slightly structural difference in the OD reaction. The comparison of both ligands was established before the OD and after it.

In previous studies, the synthesis and stabilization of complexes with picdien and iron were experimentally demonstrated; also, it was demonstrated that the OD reaction is achieved.[47] However, the spatial conformation of the complex at the different stages of the mechanism as well as the reaction mechanism is not demonstrated theoretically so far.

In the first part of this work, the ligand L2 was studied through computational calculations. This process was performed to analyze its structure and stability before and after the oxidative step but without the presence of the metallic center. The input used was B3LYP D3BJ OPT def2-SVP. The same study was then performed for L3.

The objective of these calculations was to compare the optimization energy after achieved the optimization of the ligands. On the one hand, the comparison established was based on the energy of both ligands before the OD reaction, and, on the other hand, the same analysis was applied for the ligands once the OD was achieved. The initial and the final conformations of one ligand cannot be compared among them because the presence of the unsaturation caused by the OD reaction modifies the number of electrons in the ligand. However, this comparison could give an idea about the stability of the system.

Besides, the analysis of molecular orbitals (MOs) was performed. The MOs aims to understand the spatial characteristics and distribution of electrons on the structure. The MOs allow not only to analyze the electronic characteristics of the structures but also to justify the reactivity of the structure during the different modifications or mechanism steps. For obtaining MOs from ORCA calculations, the command that may be added to the ORCA input is the following:

```
%output
Print[ P_Basis ] 2
Print[ P_MOs ] 1
end
```

1.2. Study of L2 with diol reaction in different solvents

It is well known that L2 interacts with the solvent when the iron complex synthesis is realized. This is the reason why different solvents were tested for this part. At this point,

as was shown before, the ligand reacts with water, methanol, and ethanol forming a diol that increases the denticity of the ligand. A similar analysis as in the last section was performed again, which means studying the stability before the OD and after it. This calculation aims to define which of the solvents produce higher stability of the ligand, moreover, understand if the diol insertion in the ligand distorts the geometry or the stability of the ligand. The same input as before was used, B3LYP D3BJ OPT def2-SVP.

The L2 ligand reacts with the solvent to form the L4 ligand increasing the denticity from a pentadentate configuration to a hexadentate configuration. Three solvents were probed, each one was tested before and after the OD. Depending on the solvent used for the synthesis, the L4 ligand could be 1,9-bis(2'-pyridyl)-5-[hydroxy-2''-pyridyl)methyl]-2,5,8-triazanonane for water, 1,9-bis(2'-pyridyl)-5-[methoxy-2''-pyridyl)methyl]-2,5,8-triazanonane for methanol, and 1,9-bis(2'-pyridyl)-5-[ethoxy-2''-pyridyl)methyl]-2,5,8-triazanonane for ethanol. The increment in the number of carbons in the solvent-formed extra ring changes the total number of atoms in the ligand and impedes a rigorous comparative analysis. This intermediate reaction allows the formation of the octahedral complex and, in consequence, the presence of OD. In this part, the MOs were also studied.

1.3. Studies on iron coordination complexes

For the third part of this work, after studying the ligand and its possible variations, the optimization of the iron complex formed was performed. The contrast was established among the two conformations of the ligand with the metallic iron center, which means $[Fe(L2)(DMSO)]^{3+}$ and $[Fe(L3)(DMSO)]^{3+}$. These complexes are formed before the catalytic reactions happen. An energetic barrier was identified by comparing the two ligands; this barrier impossibilities OD.

The literature does not suggest a favored spin state produced by the coordination of L2 ligand to iron, but studies with other metal centers suggest a low spin ligand.[47] In this work, both low spin and high spin variants were proved to elucidate the nature of the complex formed by L2 and L3 with iron. The nitrogen atoms forming the ligand could be a hint of a low spin character.

To calculate the optimization energy of the complexes, different field splitting caused for the coordination of the ligand were considered. For both complexes, $[Fe(L2)(DMSO)]^{3+}$ and $[Fe(L3)(DMSO)]^{3+}$, the oxidation state was always Fe(III). Both possible complexes

were optimized in ORCA with the input B3LYP D3BJ OPT def2-SVP in all the possible multiplicities.

The possible multiplicities were calculated considering that the ligand could be high spin, low spin, or present the Jahn-Teller effect. Then, the multiplicities were 2 (Low Spin), 6 (High Spin), and 4 (Jahn-Teller Effect High Spin). For Jahn-Teller Effect with Low Spin, the number of unpaired electrons is the same as Low Spin ligands, as shown in the Figures 11-15. The representation of the fields is presented considering an octahedral geometry.

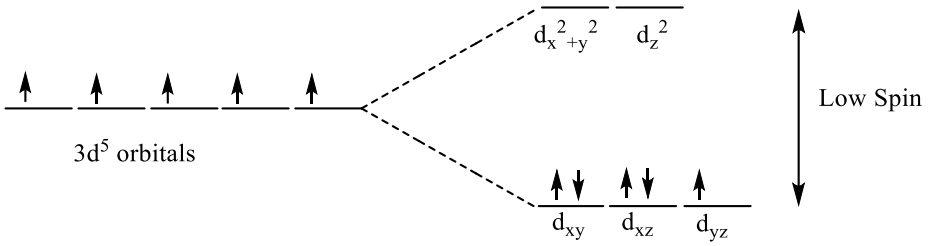

Figure 11. Low Spin Field for 3d5 metal.

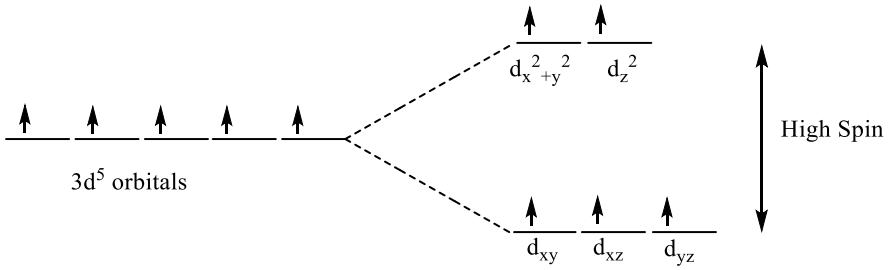

Figure 12. High Spin Field for 3d5 metal.

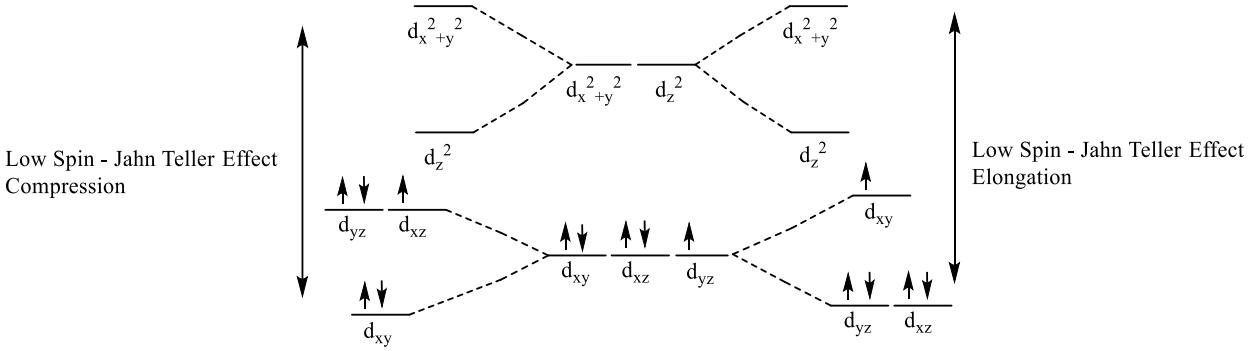

Figure 13. Jahn-Teller Effect for Low Spin 3d5 metal.

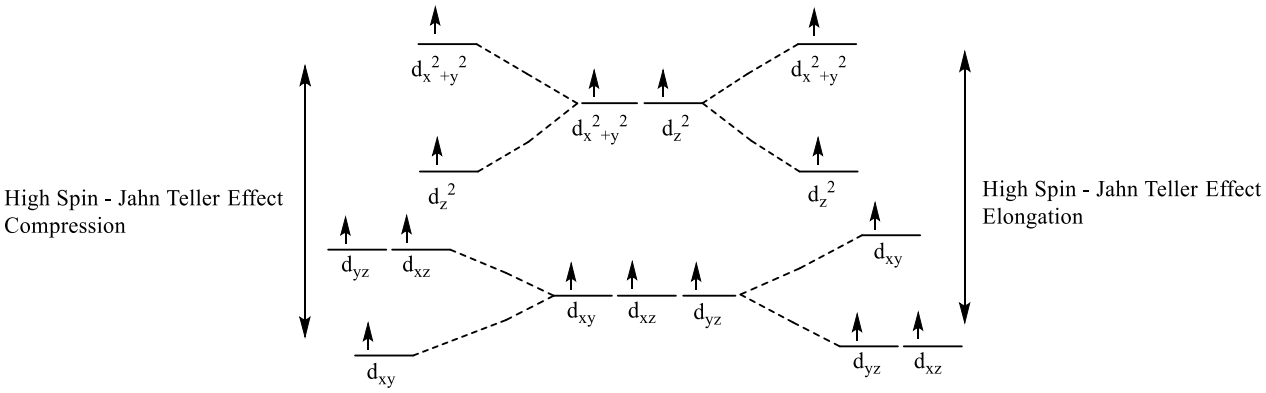

Figure 14. Jahn-Teller Effect for High Spin 3d5 metal.

1.4. Reaction Mechanism

Next, for the study of the reaction mechanism, a tentative mechanism was taken from a previous paper published by Saucedo et al [76]. The experimental results in the mentioned work suggest that L2 reacts in the presence of ethanol to produce L4; however, the same principle can be used for solvents such water and methanol, as was demonstrated before.

At this point, OD is the foremost step to be understood. To calculate the reaction mechanism of this complex, it was necessary to identify a set of stages that describes the flux of electrons and atoms through the mechanism. Four significative stages were identified; in each of them, optimization was performed to obtain the most stable tridimensional conformation. For this, the same optimization step in ORCA was accomplished through the input B3LYP D3BJ OPT def2-SVP. Furthermore, to obtain accurate results, another basis set was used to calculate the exact mechanism; the input was B3LYP D3BJ OPT def2-TZVP. This implementation allowed to establish a critical comparison of both computational methods and, at the same time, to corroborate the results of each stage.

The reaction mechanism calculation was not restrained to optimizing the complex structures; other molecules should also be included in the entire mechanism. To achieve the OD of this complex, a solvent molecule and an oxygen molecule needed to be presented to justify the electrons flux.

In this case, the analysis of molecular orbitals was performed only for the water mechanism with the basis set def2-SVP. The reason is that the different mechanisms with both basis sets probably could show a highly similar behavior. Furthermore, the analysis of all orbitals for each structure would result too extensive for this work.

1.5. Transition States

After obtaining the optimization for all the proposed mechanism stages, it was necessary to find the transition states. The transition states were found through a previous optimization of the complex with the molecule of solvent where the hydrogen is transferred. After that, the hydrogen bond distance was changed to an intermediate distance from the nitrogen of the complex to the oxygen of the solvent molecule. The input used for this calculation was B3LYP D3BJ OPTTS def2-SVP. The distances to found the transition state were varied to reach the optimal distance, from an upper limit to a lower limit and decreasing the interval of the measure until the optimal distance is to be as close as possible. Each attempt for a distance was performed in a separate calculation file.

After found both transition states, a calculation of the frequencies was performed. This calculation allowed to confirm that the result obtained is a transition state and not a local optimization minimum or a higher-order critical point (with more than one negative frequency). From the frequency list, one should be negative; this means that the transition state was achieved. The input to perform frequency calculation was B3LYP def2-SVP FREQ.

1.6. Mechanism and Solvent Stability

As the last step for analyzing the reaction energies, the optimized mechanism with different solvents depending on the L4 formation was studied. It means that the final complex structure that depends on the solvent was tested in the corresponding solvent to understand the stabilization energies. This new calculation was performed by adding the command CPCM in the ORCA input. The input in this case was B3LYP D3BJ CPCM(solvent) OPT def2-SVP, where the corresponding solvent in each case replaces the word “solvent”.

CHAPTER IV

Results and Discussion

1. Ligand Studies

As was explained in the methodology section, the first part of this work is to study the optimization of the ligand during the OD reaction.

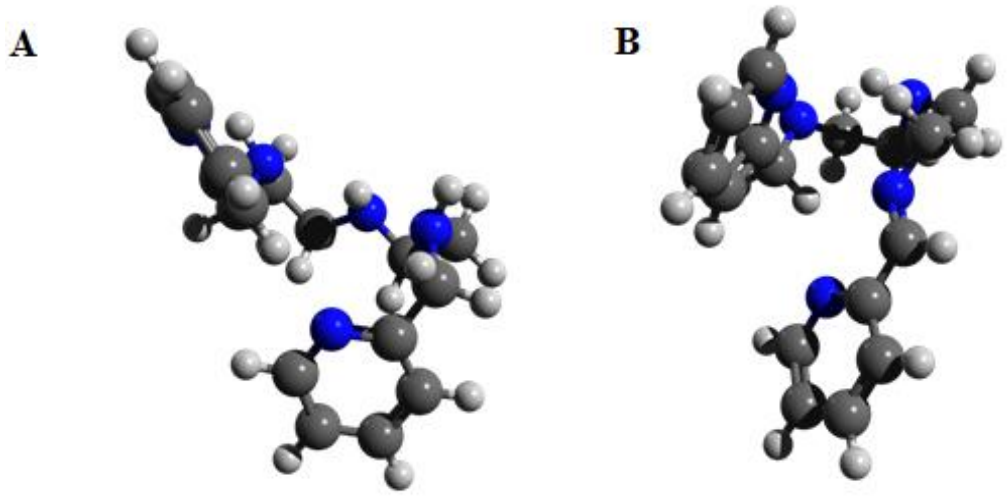

Figure 15. A) L2 before OD B) L2 after OD

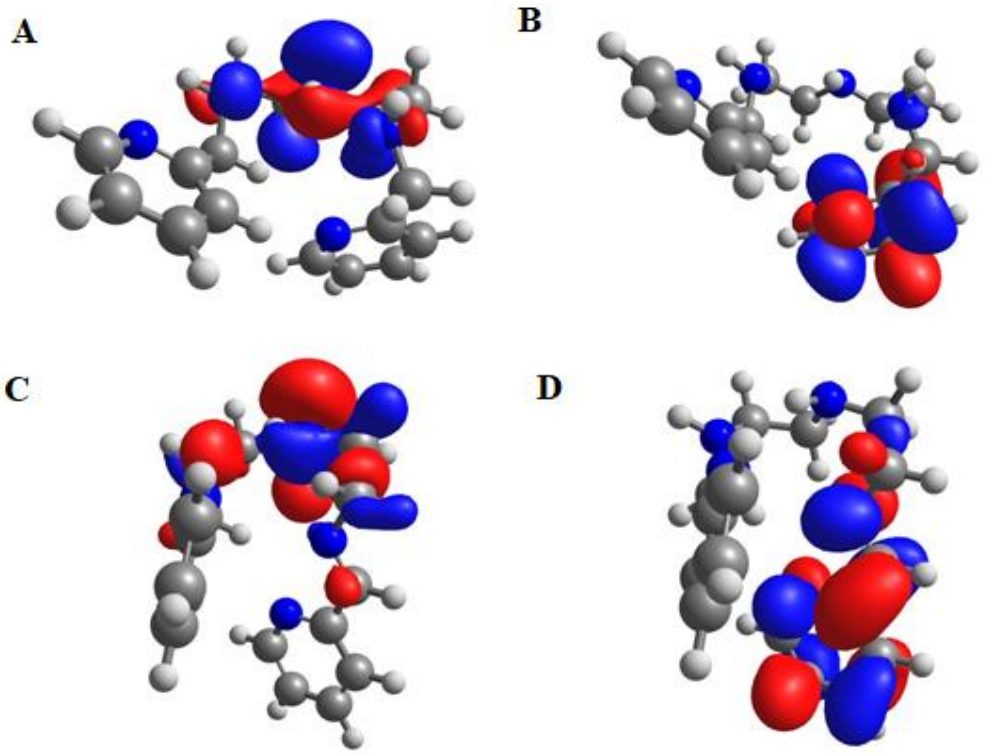

Figure 16. Molecular Orbitals for L2 Ligand A) HOMO before OD B) LUMO before OD C) HOMO after OD D) LUMO after OD

The ligand stabilization in both cases was achieved fast. In the case of L2 ligand is easy to observe that the spatial conformation describes a pentadentate ligand considering the position of the nitrogen atoms. In Figure 15, the L2 ligand is shown before and after achieved the OD reaction. The molecular orbital analysis is presented in Figure 16 where the highest occupied molecular orbital (HOMO) and the lowest unoccupied molecular orbital (LUMO) before and after the OD can be observed.

In the case of L3, shown in Figure 17, the optimization is also achieved with slight differences in optimization energy as is indicated in Table 1. However, the spatial response at the optimization of the ligand is different from L2, especially in the pyridine rings orientation. The orbital analysis for L3 is presented in Figure 18 where the orbitals HOMO and LUMO before and after the OD can be observed.

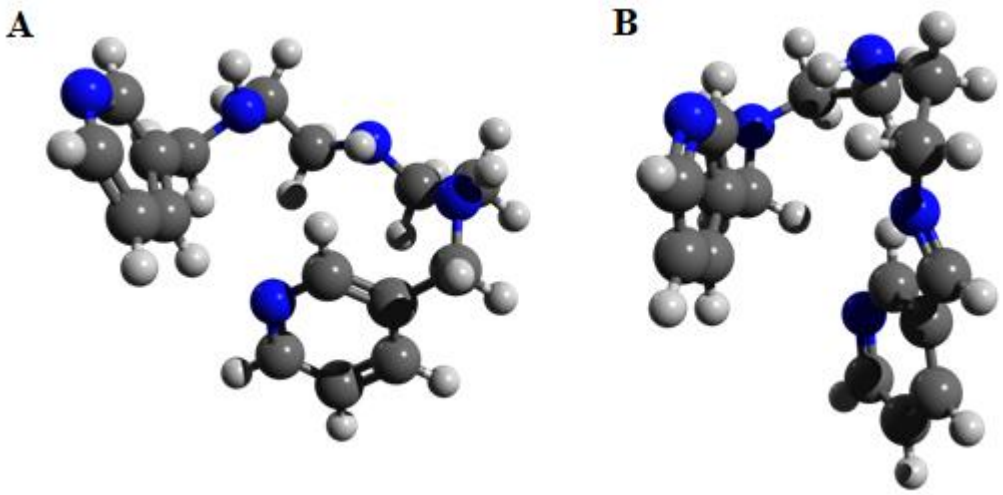

Figure 17. A) L3 before OD B) L3 after OD

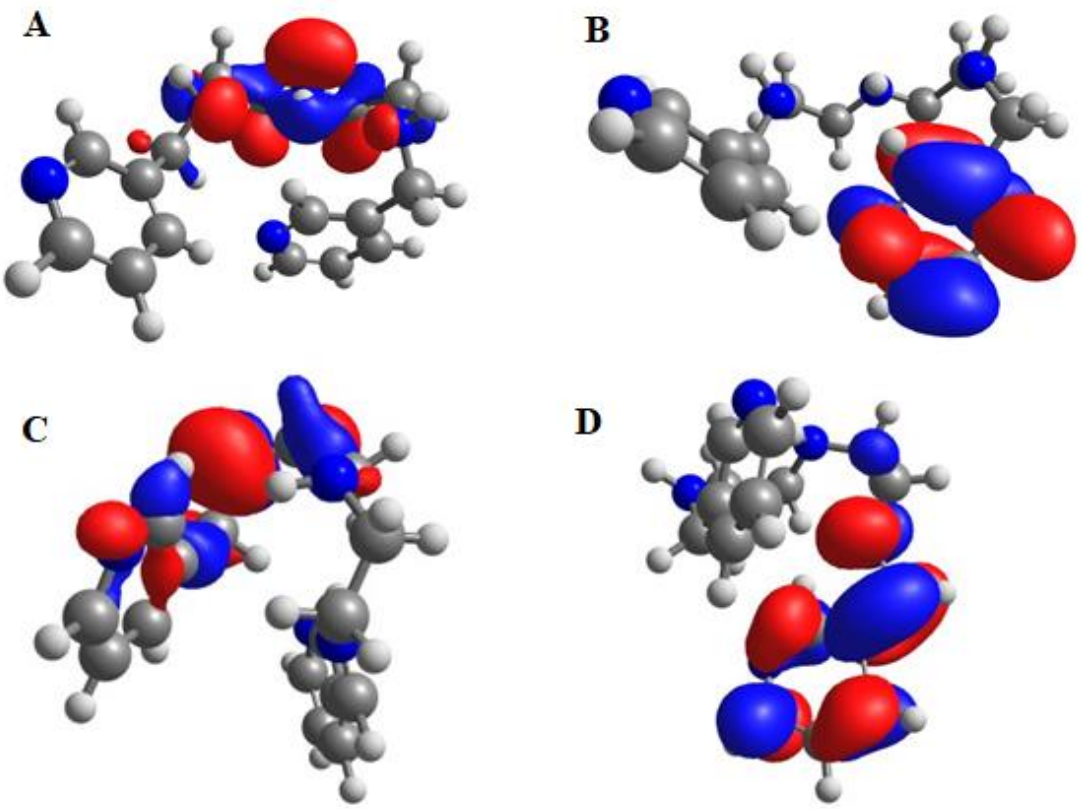

Figure 18. Molecular Orbitals for L3 Ligand A) HOMO before OD B) LUMO before OD C) HOMO after OD D) LUMO after OD

1.1. Discussion

Table 1 shows the results of the computational calculations to compare L2 vs. L3 before and after the OD reaction. In this table, it can be observed that the L2 ligand is more stable than L3 before OD, L3 is near to the energy of L2, with just a 7.4 kJ/mol difference. During the OD reaction, the results show that L3 ligand is more stable than L2 after OD, L3 is near to the energy of L2, with just a -8.6 kJ/mol difference.

Table 1. Optimization energy comparison between L2 vs. L3

Before OD	Electrons	Charge	Spin	Final Energy (Hartree)	Energy Difference (kJ/mol)
L2	154	0	1	-896.155760	0.0
L3	154	0	1	-896.152924	7.4

After OD	Electrons	Charge	Spin	Final Energy (Hartree)	Energy Difference (kJ/mol)
L2	152	0	1	-894.940179	0.0
L3	152	0	1	-894.943468	-8.6

For the MOs analysis of L2 and L3, the HOMO and LUMO were considered and shown in Figure 16 and Figure 18. Considering the ligands before OD, the localization of the

HOMOs is highly similar, it means, in the middle of the ligand between the pyridine rings. The remarkable difference among both conformations is the sign of the orbitals that are inverse and that for L3, the HOMO orbital slightly deviates to a pyridine ring. The LUMOs before OD for both conformations are very similar, located at one pyridine ring; however, for L2, a minor deviation of the orbital to the next carbon is observed.

After OD, the changes are more significant. The HOMO for L2 is strictly located in the linear zone of the ligand, while for L3, the HOMO is located nearest to one of the pyridine rings. In LUMOs, the similarity is again high; however, in L2, a minor deviation to the side carbon is observed again. With this in mind, it is important to emphasize that not only the spatial conformation could affect the coordination of the ligand, also the electronic distribution could be a remarkable factor.

2. Study of L2 with diol reaction in different solvents

At this point, the same study was performed for the hexadentate form of the ligand. The hexadentate ligand is reached when the L2 ligand reacts with the solvent, in which the synthesis is carried out. With this in mind, the study for the complex may be performed for the variation with water, methanol, and ethanol and considering the different possible multiplicities. The results for the ligands are shown as L4 in water (Figure 19, 20 and Table 2), methanol (Figure 21, 22 and Table 3), or ethanol (Figure 23, 24 and Table 4). The computational methods described in the Methodology section are exactly equal for all L4 possibilities.

2.1. L4 in water

Table 2. Optimization energies for L4 in water

L4 in Water	Electrons	Charge	Spin	Final Energy (Hartree)	Energy Difference (kJ/mol)
Initial	210	0	1	-1,257.326079	0
After OD	208	0	1	-1,256.123973	3,156.1

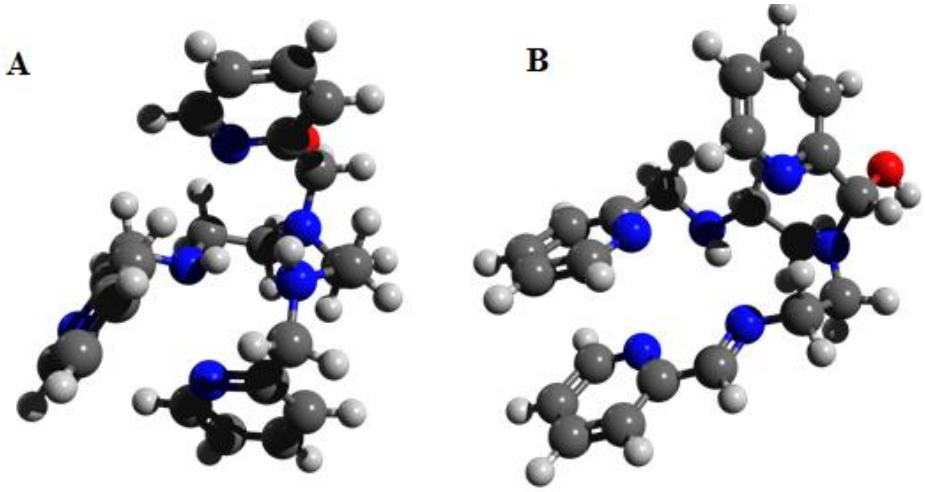

Figure 19. A) L4 in water before OD B) L4 in water after OD

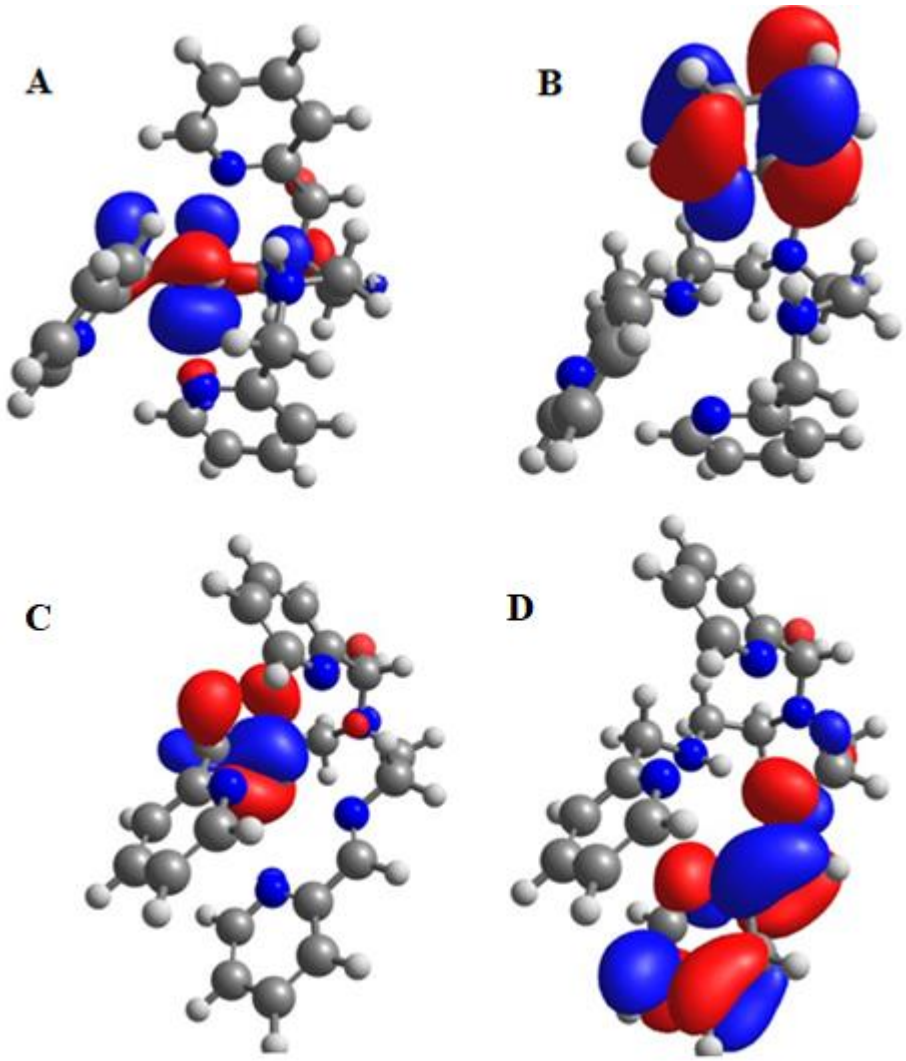

Figure 20. Molecular Orbitals for L4 ligand in water A) HOMO before OD B) LUMO before OD C) HOMO after OD D) LUMO after OD

2.2. L4 in methanol

Table 3. Optimization energies for L4 in methanol

L4 in Methanol	Electrons	Charge	Spin	Final Energy (Hartree)	Energy Difference (kJ/mol)
Initial	218	0	1	-1,296.587103	0
After OD	216	0	1	-1,295.374797	3,182.9

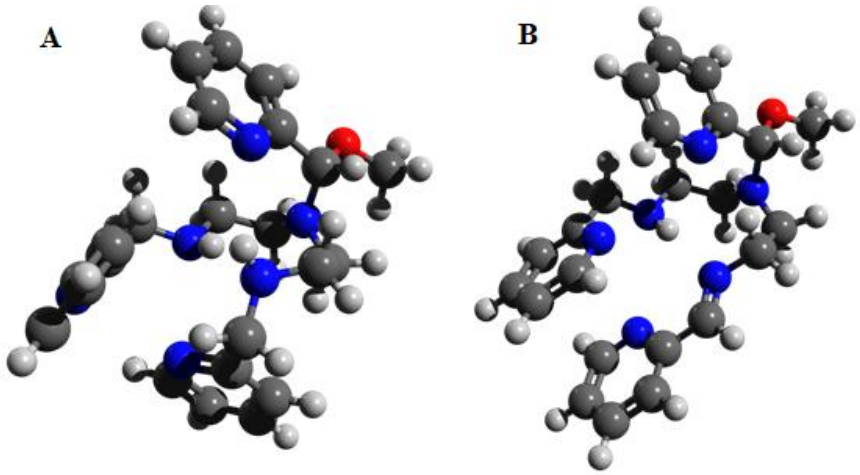

Figure 21. A) L4 in methanol before OD B) L4 in methanol after OD

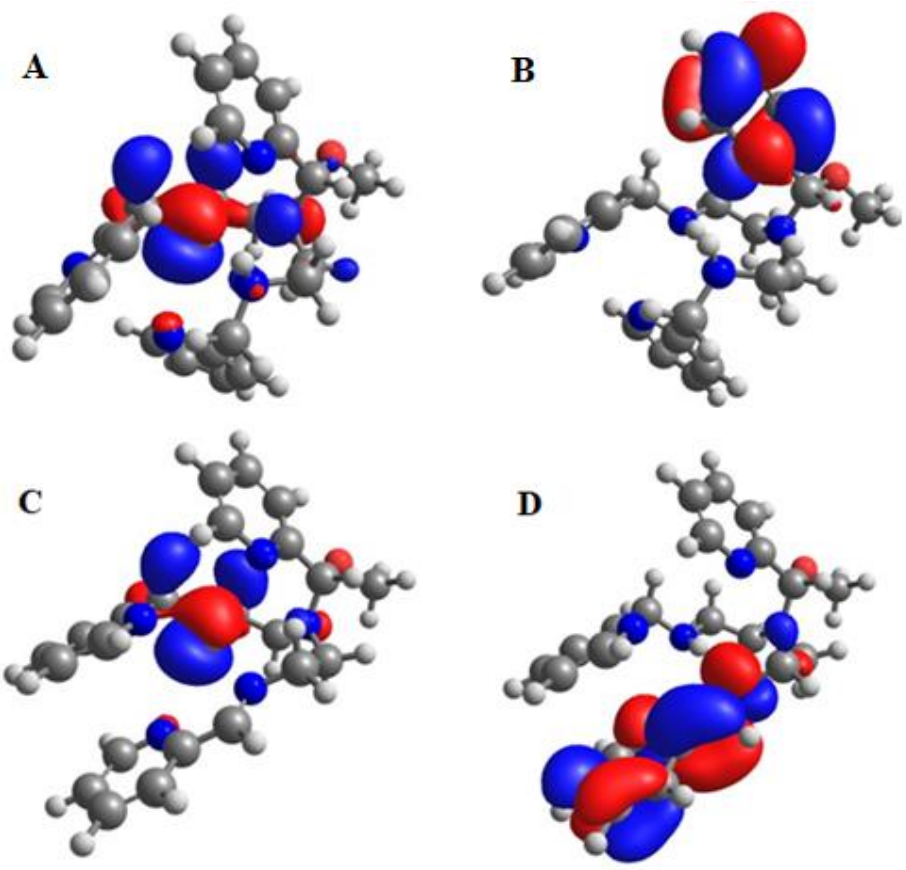

Figure 22. Molecular Orbitals for L4 ligand in methanol A) HOMO before OD B) LUMO before OD C) HOMO after OD D) LUMO after OD

2.3. L4 in ethanol

Table 4. Optimization energies for L4 in ethanol

L4 in Ethanol	Electrons	Charge	Spin	Final Energy (Hartree)	Energy Difference (kJ/mol)
Initial	226	0	1	-1,335.837609	0
After OD	224	0	1	-1,334.639860	3,144.7

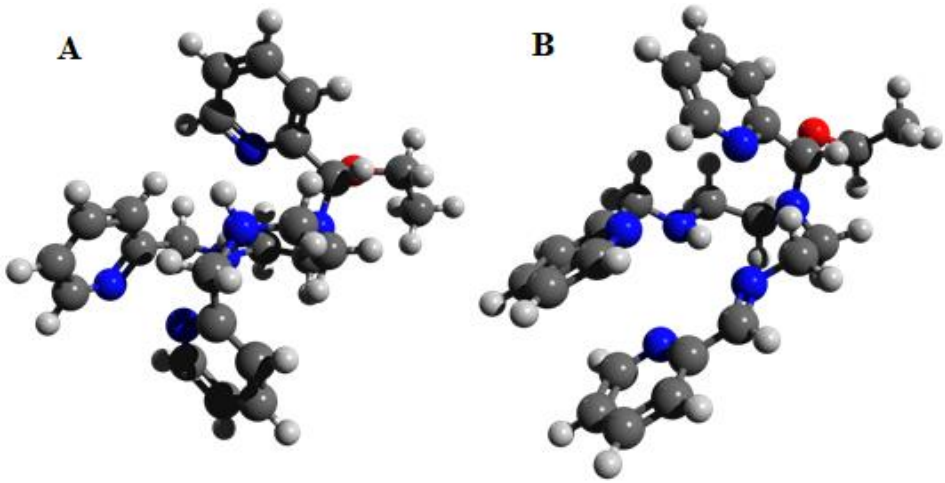

Figure 23. A) L4 in ethanol before OD B) L4 in ethanol after OD

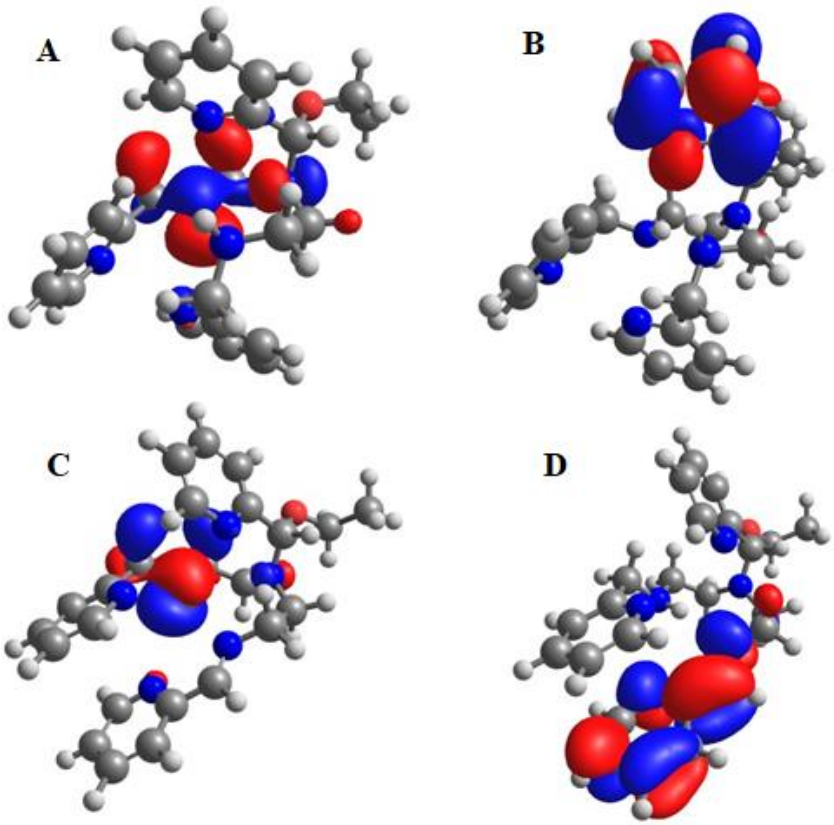

Figure 24. Molecular Orbitals for L4 ligand in ethanol A) HOMO before OD B) LUMO before OD C) HOMO after OD D) LUMO after OD

2.4. Discussion

The results for the optimization of the L4 ligand show that the behavior of the ligand, in terms of spatial conformation and geometry, is highly similar. This conclusion means that the ligand maintains a tendency to form an octahedral geometry and preserve the orientation of the rings despite the solvent used. The evident change is based on the final energies. As is shown in Figure 25, the first point to be analyzed is that the optimization energy before OD is always more negative. This difference between the optimization energy before and after OD is minimal; however, it represents enough to conclude that the ligands are more stable before than after OD. If the evaluation approach is focused on the structures before and after OD, it can be observed that a small difference of stabilization energy is identified between the structures. In all cases before OD the structures are more stable, however, the presence of the solvent and the other molecules in the system will contribute to stabilizing OD structures.

The second conclusion is that a significant difference in the optimization energies can be identified depending on the solvent used for the reaction. In Figure 25, it can be observed that in both cases, before and after OD, the ligand in ethanol is more stable than in water or methanol. The difference of energy between the ligands is almost 40 Hartree or more, which is a too high difference of stability. From this, the mechanism in ethanol is favored over the reaction in water or methanol.

Figure 25. Summary of L4 studies in different solvents A) Before OD and B) After OD

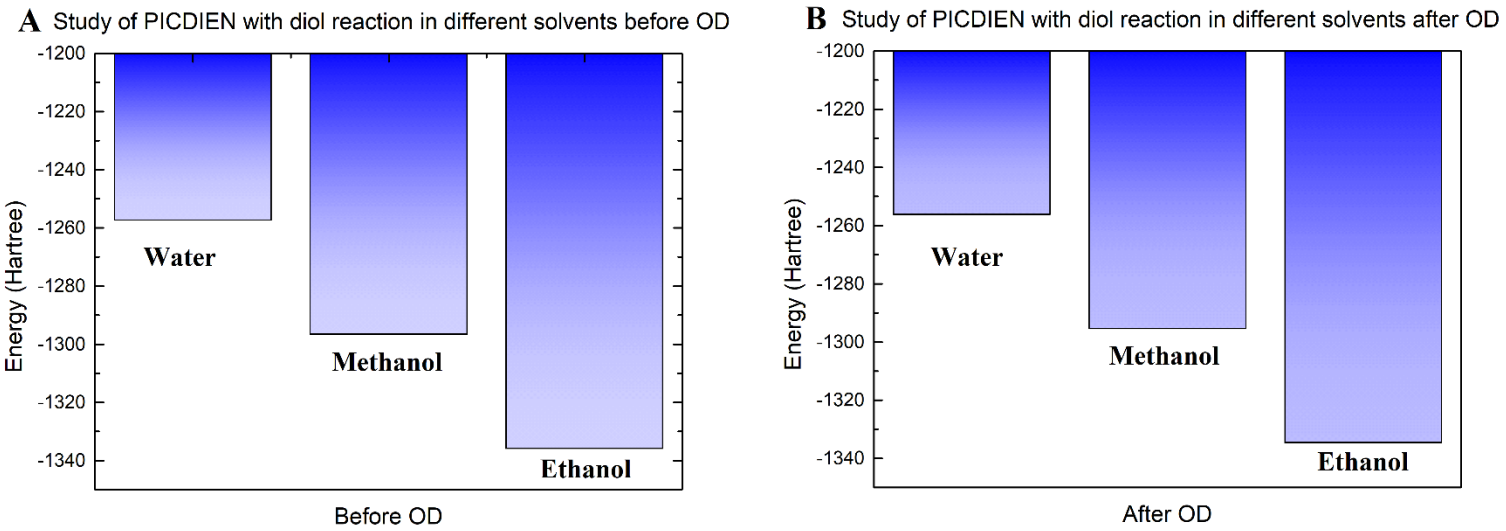

The MOs were obtained for L4 in water, methanol, and ethanol; the HOMO and LUMO were considered and shown in Figure 20, Figure 22, and Figure 24, respectively. For the HOMOs before and after OD, no major differences can be observed. Also, LUMOs are

highly similar, and no shows relevant differences. This characteristic supports that the reactivity of the ligands is similar; furthermore, the successful OD in all cases can be supported for this similarity. Additionally, the Mulliken charges of the oxygen that is part of the solvent-implemented diol, before and after OD, show values of -0.27 for water to -0.38 for methanol and ethanol. Mulliken charges values support the similar reactivity of the mechanism in different solvents and the energy changes according to the modification in the solvent (carbon number and polarity).

3. Studies on iron coordination complexes

After the first analysis of the free ligands, the complexes derived from such ligands coordinated with the iron center were carefully studied. For the case of $[Fe(L2)(DMSO)]^{3+}$, the optimization calculations in all the possible multiplicities shown very similar results among them despite being calculated taking the same structure as a base; the input for the calculations was B3LYP D3BJ OPT def2-SVP. From a spatial conformational view, all the possibilities show similar behavior (see Figure 26); it means a hexacoordinated iron center forming an octahedral geometry and a pentadentate ligand. However, from an energetical point of view, it can be observed sharp differences in the final optimization energy as shown in Table 5.

Table 5. Optimization energy of the possible multiplicities for [Fe(L2)(DMSO)]3+

[Fe(L2)(DMSO)]3+	Electrons	Charge	Spin	Final Energy (Hartree)	Energy Difference (kJ/mol)
Weak Field (High Spin)	219	3	6	-2,711.732990	0.0
Strong Field (Low Spin)	219	3	2	-2,711.730136	7.5
Jahn-Teller Effect (Intermediate Spin)	219	3	4	-2,711.716077	44.4

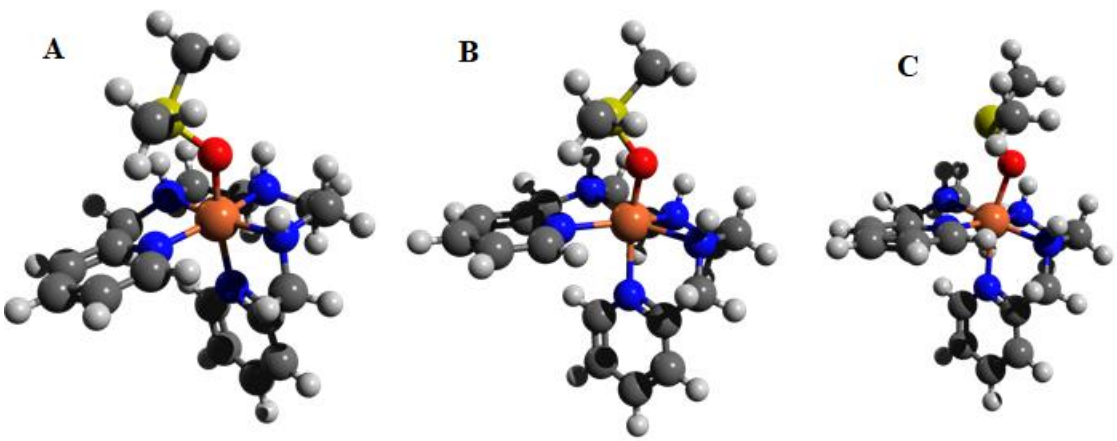

Figure 26. A) $[Fe(L2)(DMSO)]^{3+}$ Low Spin B) $[Fe(L2)(DMSO)]^{3+}$ High Spin C) $Fe(L2)(DMSO)]^{3+}$ Jahn-Teller

For the $[Fe(L3)(DMSO)]^{3+}$ complex, the observed geometries are entirely different depending on the multiplicity; in all cases, the input used was B3LYP D3BJ OPT def2-SVP. The first attempt was the complex with multiplicity 2, which means a low spin character. In this case, it can be observed that the optimization of the complex implies a coordination sphere change (see Figure 27). The pyridine rings substituted at position 3 cannot maintain the coordination of the nitrogen atom with the metallic center because of the effect produced by the intermediate carbon at position 2. The geometry of the coordination center obtained by the calculation to reach stability is tetrahedral.

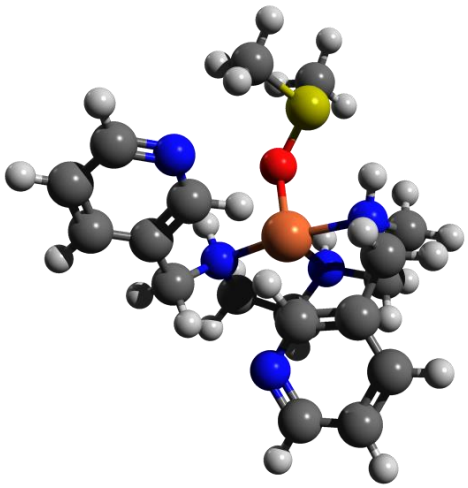

Figure 27. $[Fe(L3)(DMSO)]^{3+}$ Low Spin

After, the multiplicity of the complex was changed to 6. However, in this case, despite the octahedral geometry of the Fe^{3+} center is obtained, the coordination with the pyridine rings is changed (see Figure 28). As is shown, the pyridine ring coordinates to the metal center with the position 2 carbon instead with the nitrogen, and this is not shown in experimental trials.

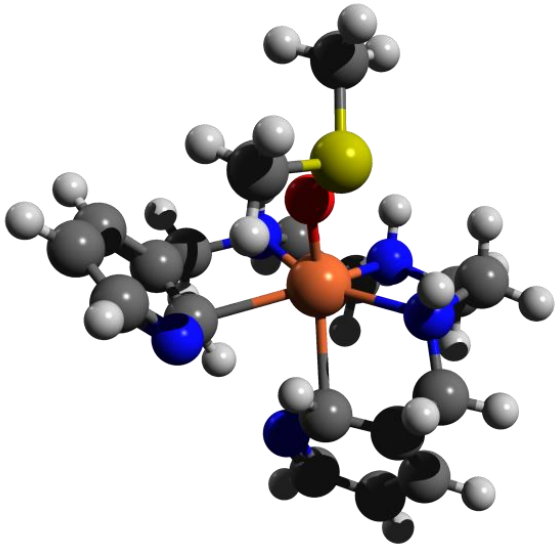

Figure 28. $[Fe(L3)(DMSO)]^{3+}$ High Spin

Finally, the calculation was performed with multiplicity 4 that corresponds to a Jahn-Teller effect with an intermediate spin character. In this case, neither a tetrahedral geometry of the coordination sphere nor the coordination of the nitrogen atoms of pyridine rings are achieved (see Figure 29). The geometry of this complex reaches a distorted tetrahedral shape.

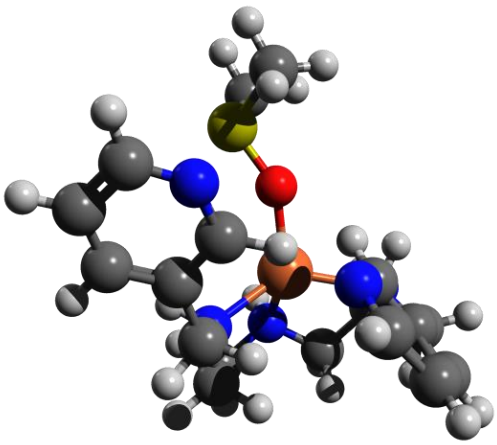

Figure 29. $[Fe(L3)(DMSO)]^{3+}$ Jahn-Teller High Spin

Table 6 shows a comparison among the structures of the ligand and the tested field characters. According to the results, the most stable geometry structure is reached with the Jahn-Teller Effect with an intermediate spin character.

Table 6. Optimization energy of the possible multiplicities for [Fe(L3)(DMSO)]3+

[Fe(L3)(DMSO)]3+	Electrons	Charge	Spin	Final Energy (Hartree)	Energy Difference (kJ/mol)
Weak Field (High Spin)	219	3	6	-2,711.608052	0.0
Strong Field (Low Spin)	219	3	2	-2,711.595003	34.3
Jahn-Teller Effect (Intermediate Spin)	219	3	4	-2,711.626181	-47.6

3.1. Discussion

As was discussed previously in this section, the case of $[Fe(L2)(DMSO)]^{3+}$ shows similar spatial conformations in all the variations of spin possible for the compound-complex. The difference between the three possible spins is focused on the optimization energy. As can be observed in Table 5, the $[Fe(L2)(DMSO)]^{3+}$ compound with low spin character is the most stable due to higher negative optimization energy, in contrast with the same compound with high spin character or Jahn-Teller Effect. Furthermore, after performed the spatial analysis for $[Fe(L3)(DMSO)]^{3+}$, it can be observed that the octahedral conformation of the metallic center is never achieved. The hindrance effect occurred by the substitution in position three instead of position two results in an extreme barrier for the compound formation. Figure 30 summarizes the results obtained in this section.

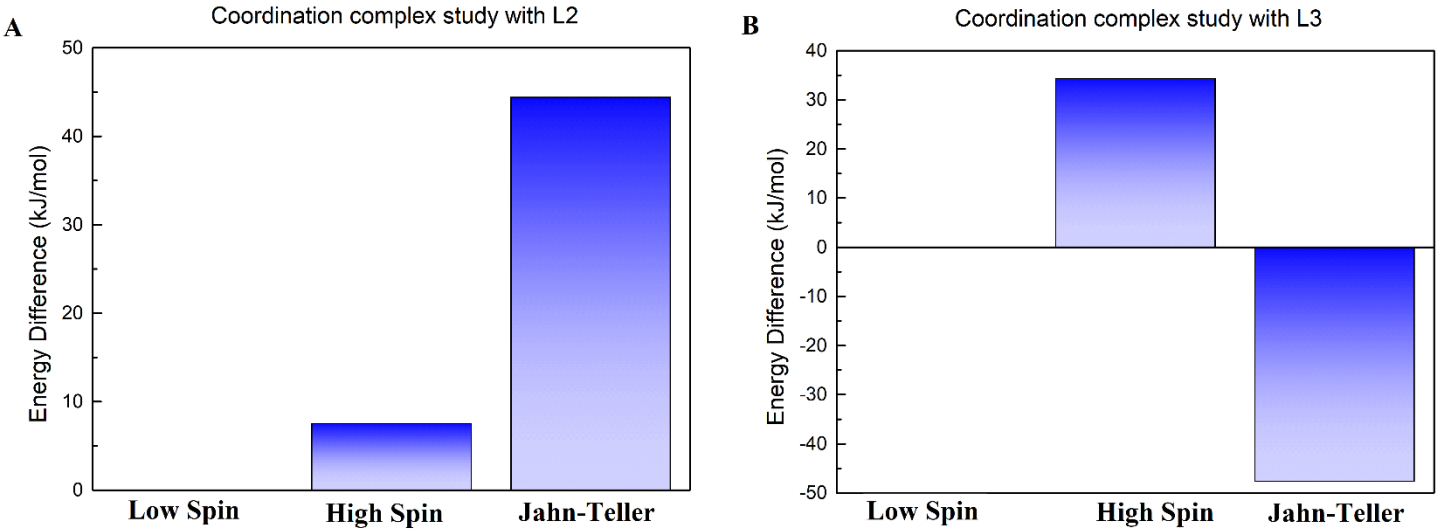

Figure 30. Summary of coordination complex studies A) For L2 complex and B) For L3 complex.

As Figure 30 shows, in the case of $[Fe(L2)(DMSO)]^{3+}$, the low spin character of the ligand shows higher stability than the other possibilities, the energy difference barrier between the three conformations is very marked. Furthermore, the octahedral metallic center is achieved. With this in mind, the low spin character of the ligand can be considered the best way to continue with the next steps of the study.

In fact, for $[Fe(L3)(DMSO)]^{3+}$, the Jahn-Teller distortion spin achieves a negative energy difference, which means a more stable conformation, even more stable than low spin $[Fe(L2)(DMSO)]^{3+}$. However, Jahn-Teller $[Fe(L3)(DMSO)]^{3+}$ does not achieve the octahedral metallic center that is demonstrated in the literature [19]; this geometry allows the OD reaction in further steps. Considering this argument, the mechanism cannot be used as a solution due to the divergent characteristics in comparison with the interest system.

4. Reaction Mechanism

The reaction mechanism is a four-stage mechanism with 3 kinetics steps proposed by Saucedo-Vázquez *et al*. [76] that explains the iron-promoted OD reaction. As shown before, in the mechanism (see Figure 31), the final structure of ligand L4 depends on the solvent used for the synthesis; consequently, R should be replaced with the molecule that corresponds to the three possible solvents used in this work.

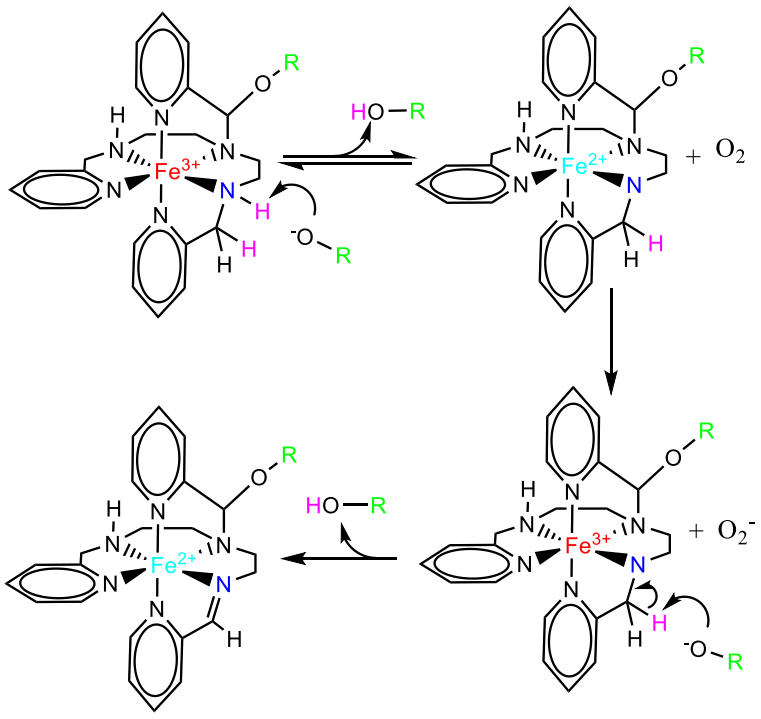

R= H, CH_3, CH_3CH_2

Figure 31. Proposed 4-stage reaction mechanism for OD reaction.

4.1. Mechanism with water-synthesized ligand

The first stage proposed for the water-synthesized ligand mechanism was optimized considering that the initial oxidation state of the metallic center of iron is 3^+, which corresponds to $[Ar]3d^5$ electronic configuration. From the performed studies of the

ligand, a tendency to be a low spin ligand was identified, and, with this in mind, the assumption of a strong field complex is established.[76] Besides, considering the electronic distribution of the metallic center and the strong field complex, the multiplicity of the compound is 2 (see Figure 32). In this case, the molecular orbitals were also obtained (see Figure 33).

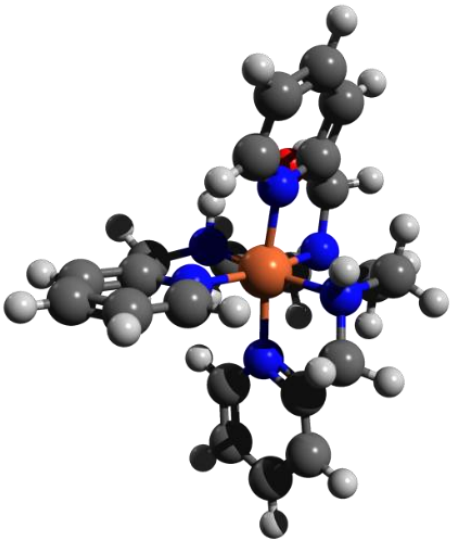

Figure 32. Stage 1 with water-synthesized ligand (def2-SVP)

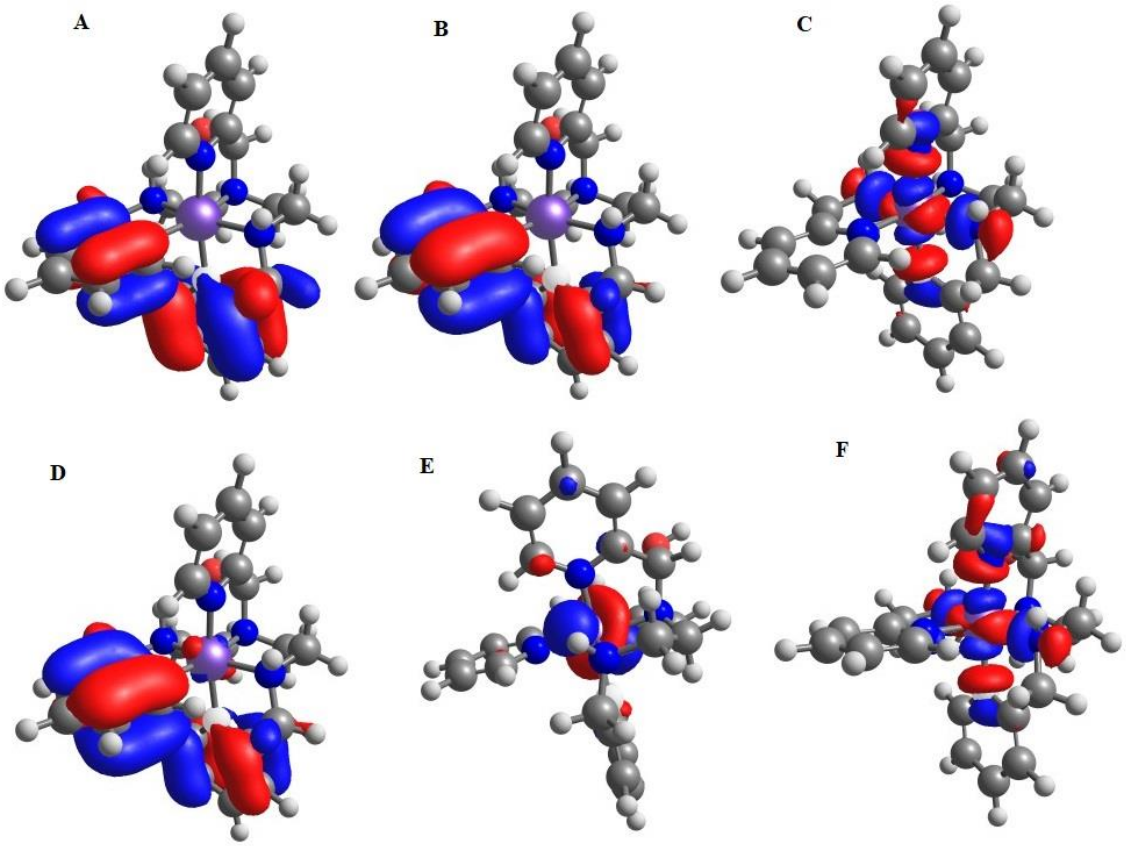

Figure 33. Molecular Orbitals for Stage 1 in water A) HOMO alpha B) SOMO alpha C) LUMO alpha D) HOMO beta E) SOMO beta F) LUMO beta

For the first stage, it can be observed in Figure 33 that the HOMO alpha and beta (depending on the spin of the electron, alpha for spin up and beta for spin down) has an almost equal distribution over the two initial pyridine rings of the ligand. Then, considering the single occupied molecular orbital (SOMO) which is associated to a radical for example, it can be observed that the SOMO alpha has a distribution over the initial pyridine rings of the ligand, while the SOMO beta is located surrounding the metal center. This distribution could be due to the oxidation state of the iron center and its electronic distribution, the shape of the orbital matches with a d molecular orbital. Finally, the LUMO alpha and beta are distributed over the iron center and the bonds established with the multiple nitrogen atoms of the ligand.

For the second stage of the proposed mechanism, the optimization was performed considering the proton removal from the nitrogen where OD occurs. It is also important to emphasize that the electrons that form part of the bond between the nitrogen and hydrogen stay in the nitrogen atom. With this, the oxidation state of the metallic center changed to 2^+ because of the intermolecular electron transfer process; one of the electrons of the nitrogen-hydrogen bond changes the metallic center oxidation state, and the other

electron stays in the nitrogen. The electronic distribution of the metallic center changes to [Ar]$3d^6$; however, the free radical generated in the mentioned nitrogen produces the multiplicity of the complex to be still 2 (Figure 34). The molecular orbitals were also obtained (see Figure 35).

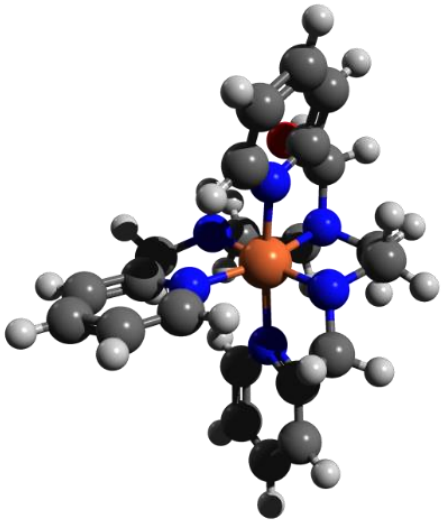

Figure 34. Stage 2 with water-synthesized ligand (def2-SVP)

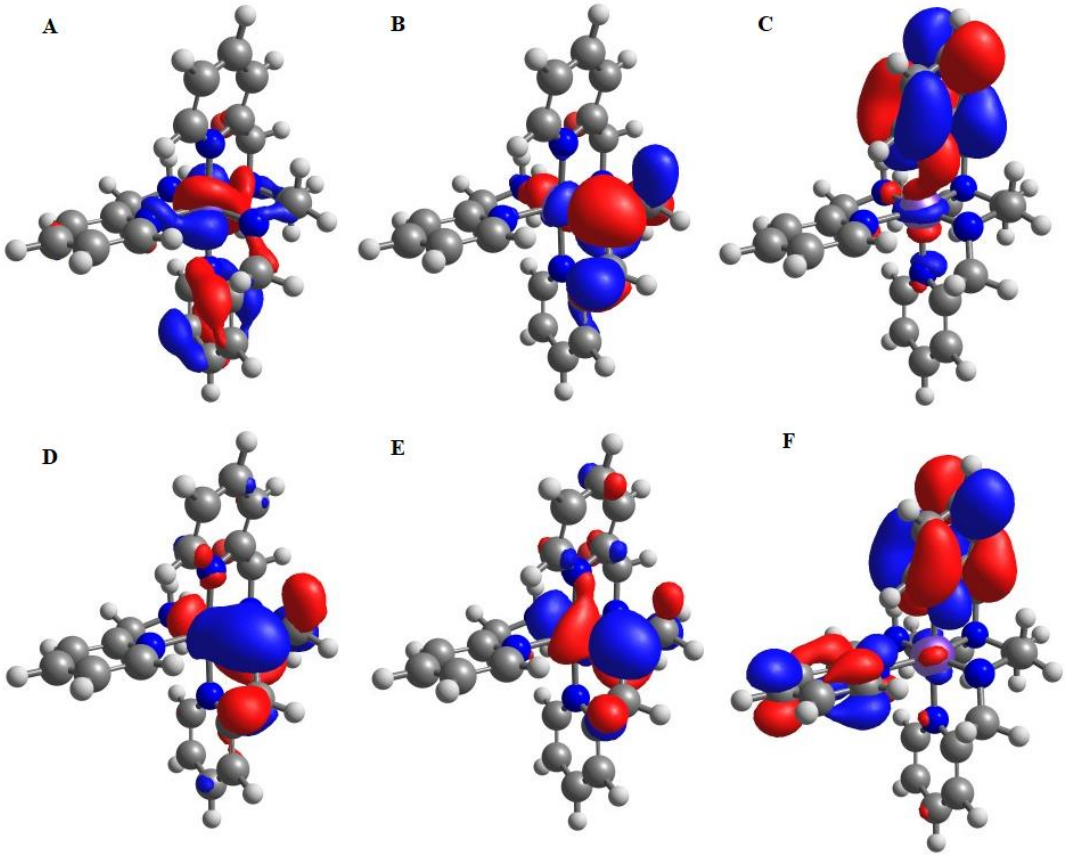

Figure 35. Molecular Orbitals for Stage 2 in water A) HOMO alpha B) SOMO alpha C) LUMO alpha D) HOMO beta E) SOMO beta F) LUMO beta

For the second stage, it can be observed in Figure 35 that the HOMO (alpha and beta) presents a change in shape and localization in comparison with the first stage. In this case, they are distributed over the iron center and in the nitrogen, where the OD is achieved. Then considering the SOMO, it can be observed that the SOMO alpha and beta have similar behavior as the HOMO, changing its location to the nitrogen where the first proton is removed and over the region where the electron rearrangement is happening. It may be considered that in this stage, the iron center changes its oxidation state to 2^+; this is the reason why SOMOs are located in the metal center region. Finally, the LUMO alpha and beta are distributed over the pyridine ring produced by the diol formation; this could support that its inclusion in the molecule is fundamental to achieve the OD reaction.

For the third stage, a dioxygen molecule induces an intermolecular electron transfer from the metallic center produces a change in the oxidation state of iron center 2^+ to 3^+. This transference can be interpreted as a long-distance electron transference. Nevertheless, the free radical located in the nitrogen is not altered in this electron interchange. This change in the electronic profile inside the complex could be responsible for the second proton

extraction derived from the double bond formation that finalizes the OD reaction (see Figure 36). The molecular orbitals were also obtained (see Figure 37).

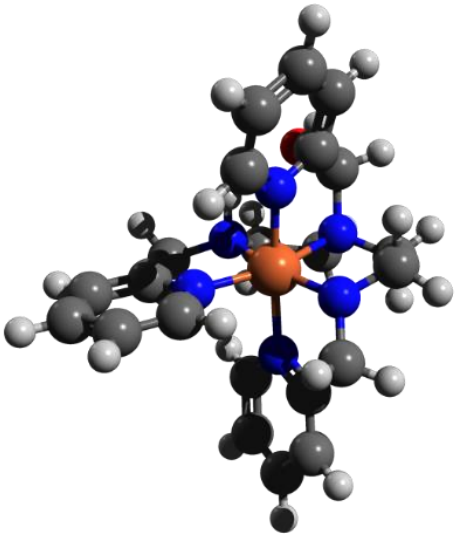

Figure 36. Stage 3 with water-synthesized ligand (def2-SVP)

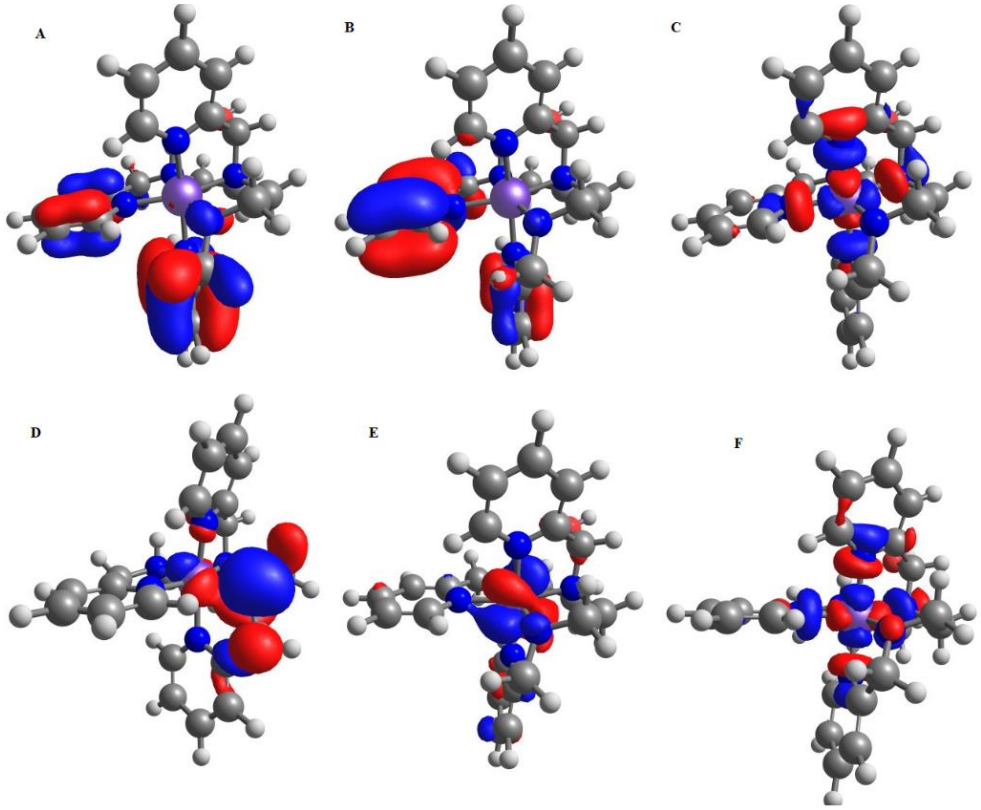

Figure 37. Molecular Orbitals for Stage 3 in water A) HOMO alpha B) SOMO alpha C) LUMO alpha D) HOMO beta E) SOMO beta F) LUMO beta

It can be observed in Figure 37 that the HOMO alpha is again distributed on the initial pyridine rings of the ligand as in the first stage; however, the HOMO beta is located over

the nitrogen where the OD is happening, as in the second stage. This distribution is happening due to the free-electron located in the nitrogen that is not part of the metal center. Then considering the SOMO, it can be observed that the SOMO alpha is also located over the initial pyridine rings of the ligand, while SOMO beta is located around the metal center. This can be explained by the change of oxidation state of the iron center to 3^+ and the loss of one electron in contrast with the last stage. Finally, the LUMO alpha and beta are distributed over the iron center again, as in the first stage, and the bond established with the multiple nitrogen atoms of the ligand is recovered to stabilize the octahedral center.

The last stage of the mechanism shows the complex with the presence of the unsaturation provoked by OD. To reach this structure, the proton adjacent to the nitrogen with the free electron was removed. The electrons of the released hydrogen establish the double bond with the nitrogen atom, and, in a quick step, the bond formation pushes the free electron to the metallic center changing one more time its oxidation state from 3^+ to 2^+. This multiplicity of the complex in the final state (the product) is 1 since the charge of the metallic center is 2^+ with an electronic distribution $[Ar]3d^6$; also, considering the strong field character induced by the low spin ligand are no free charges in the metal nor the atoms involved in the double bond (see Figure 38). The molecular orbitals were also obtained (see Figure 39).

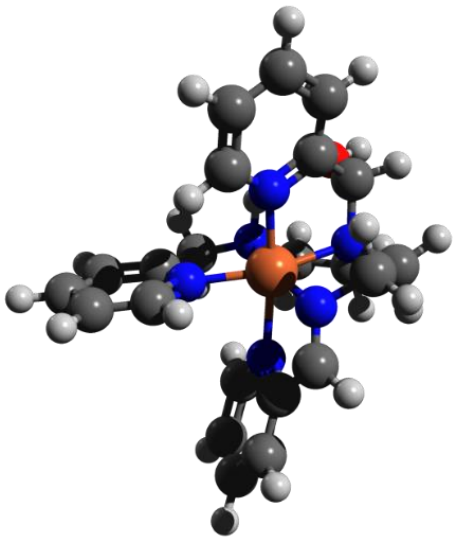

Figure 38. Stage 4 with water-synthesized ligand (def2-SVP)

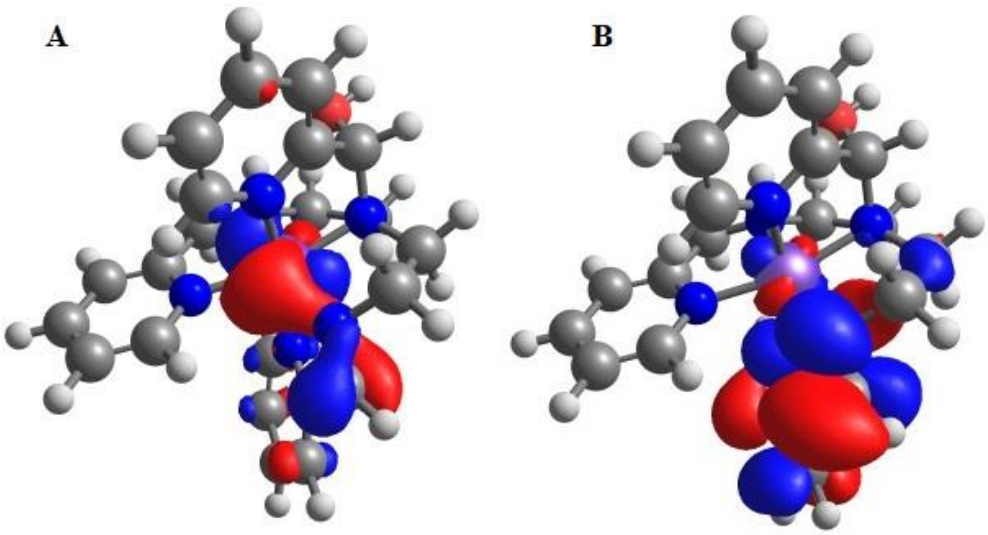

Figure 39. Molecular Orbitals Stage 4 in water A) HOMO B) LUMO

In this last stage, the presence of HOMO is observed instead of SOMO. The reason is that the oxidation state of the iron center is [Ar]3d^6, and not free-electrons are located at any point of the structure, so a single occupied orbital is not possible. Considering this, the HOMO is located at the iron center, and the nitrogen where the OD is achieved, while LUMO is located over the nitrogen where OD is achieved and the side pyridine ring; the unsaturation provoked by OD could support this.

In following tables 7 and 8, the computational results of each stage with def2-SVP basis set are shown. Considering the presence of other molecules in the mechanism, such as dioxygen, oxide, water, and hydroxide, the corresponding results for the calculations for the def2-SVP basis set are shown in Annexes section A. The results obtained from the optimizations of each stage of the mechanism are shown in Table 7. Also, in Table 8 are shown the final energies of the system for each stage expressed in Hartree and transformed to kJ/mol to be compared. Finally, in Figure 40, an energy diagram to compare and resume the final energies for the mechanism is shown.

Table 7. Calculations of the mechanism with water-synthesized ligand (def2-SVP)

def2-SVP	Electrons	Charge	Spin	Energy (Hartree)
Stage A	233	3+	2	-2,520.066994
Stage B	233	2+	2	-2,519.874555
Stage C	232	3+	3	-2,519.405382
Stage D	232	2+	1	-2,519.282844

Table 8. Final energies of mechanism with water-synthesized ligand (def2-SVP)

	Total Electrons	Final Energy (Hartree)	Energy Difference (Hartree)	Energy Difference (kJ/mol)
Stage A	269	-2,821.399338	0	0
Stage B	269	-2,821.903477	-0.504138	-1,323.6
Stage C	269	-2,821.470889	-0.071551	-187.9
Stage D	269	-2,822.044929	-0.645590	-1,695.0

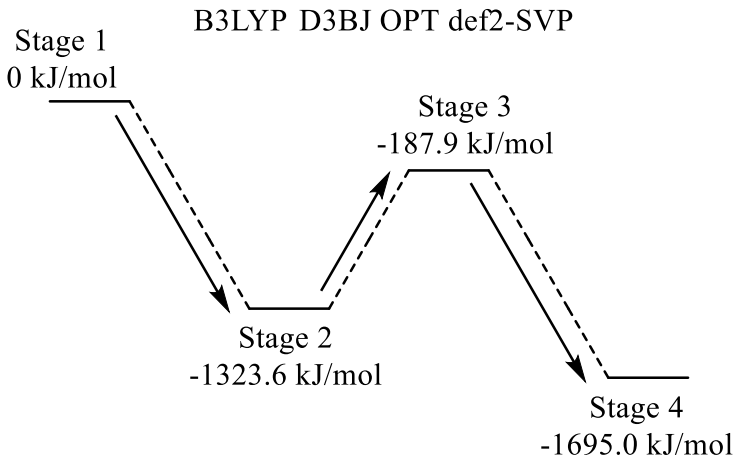

Figure 40. Energy diagram for the mechanism with water-synthesized ligand (def2-SVP)

For obtaining accurate and supported results, the exact mechanism calculations were performed using a different basis set (see Figure 41). In this case, a more significant basis set was used, then the input of ORCA optimization was B3LYP D3BJ OPT def2-TZVP.

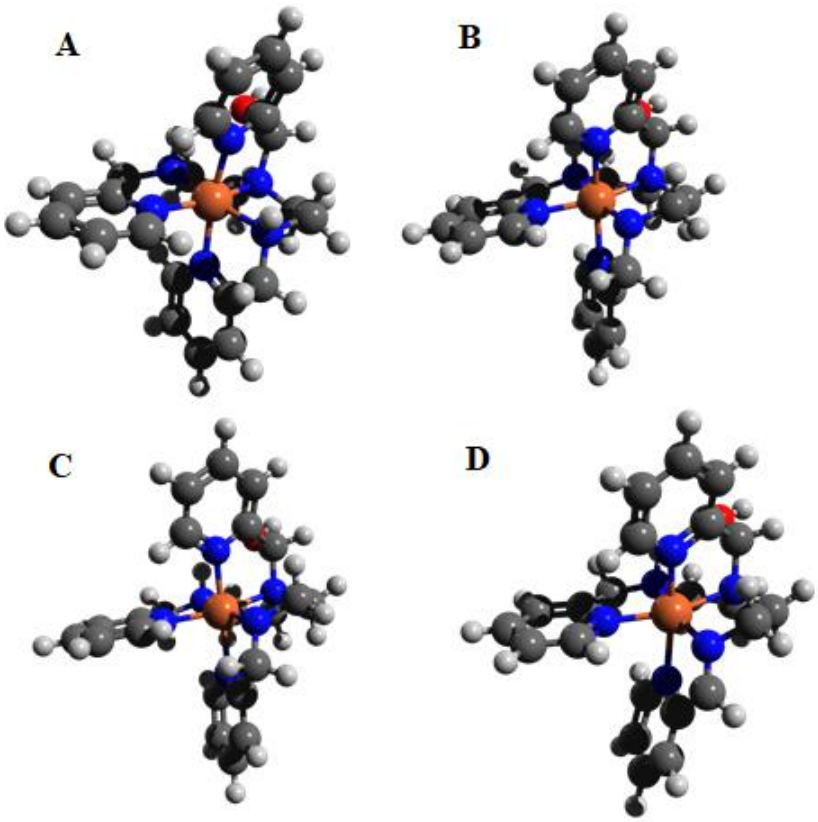

Figure 41. Reaction mechanism (def-TZVP) with water-synthesized ligand A) Stage 1 B) Stage 2 C) Stage 3 D) Stage 4

In Table 9 and 10, the computational results of each stage with def2-TZVP basis set are shown. The results obtained from the optimizations of each stage of the mechanism are shown in Table 9**.** Also, Table 10 shows the final energies of the system for each stage expressed in Hartree and transformed to kJ/mol to be compared. Finally, in Figure 42, an energy diagram to compare and resume the final energies for the mechanism is shown.

Table 9. Calculations of the mechanism with water-synthesized ligand (def2-TZVP)

def2-TZVP	Electrons	Charge	Spin	Energy (Hartree)
Stage A	233	3+	2	-2,521.591503
Stage B	233	2+	2	-2,521.399204
Stage C	232	3+	3	-2,520.930068
Stage D	232	2+	1	-2,520.807169

Table 10. Final energies of mechanism with water-synthesized ligand (def2-TZVP)

	Total Electrons	Final Energy (Hartree)	Energy Difference (Hartree)	Energy Difference (kJ/mol)
Stage A	269	-2,823.408597	0	0
Stage B	269	-2,823.868415	-0.459819	-1207.3
Stage C	269	-2,823.465046	-0.056449	-148.2
Stage D	269	-2,823.994265	-0.585668	-1537.7

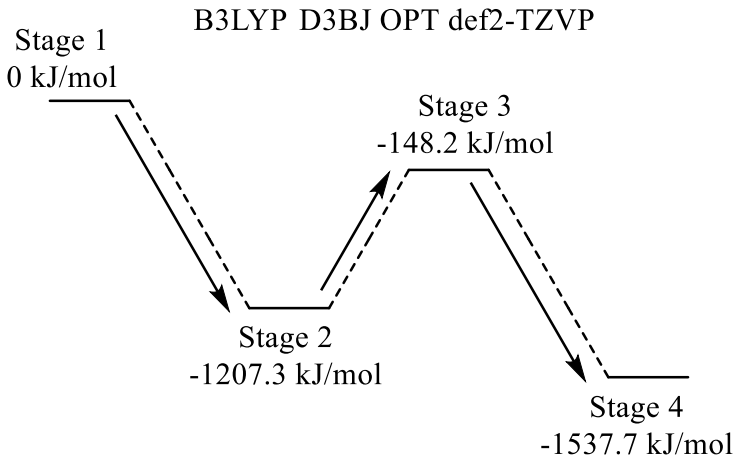

Figure 42. Energy diagram for the mechanism with water-synthesized ligand (def2-TZVP)

4.2. Reaction mechanism in methanol

In this case, the first stage proposed for the methanol-synthesized ligand mechanism was optimized considering that the mechanism of water presented before is precisely equal in the conditions of calculation. The difference is based on the diol formation with the solvent that is methanol, so the structure change, however the oxidation states and the multiplicities along all the mechanisms were the same. The optimization results for each mechanism stage are shown in Figure 43.

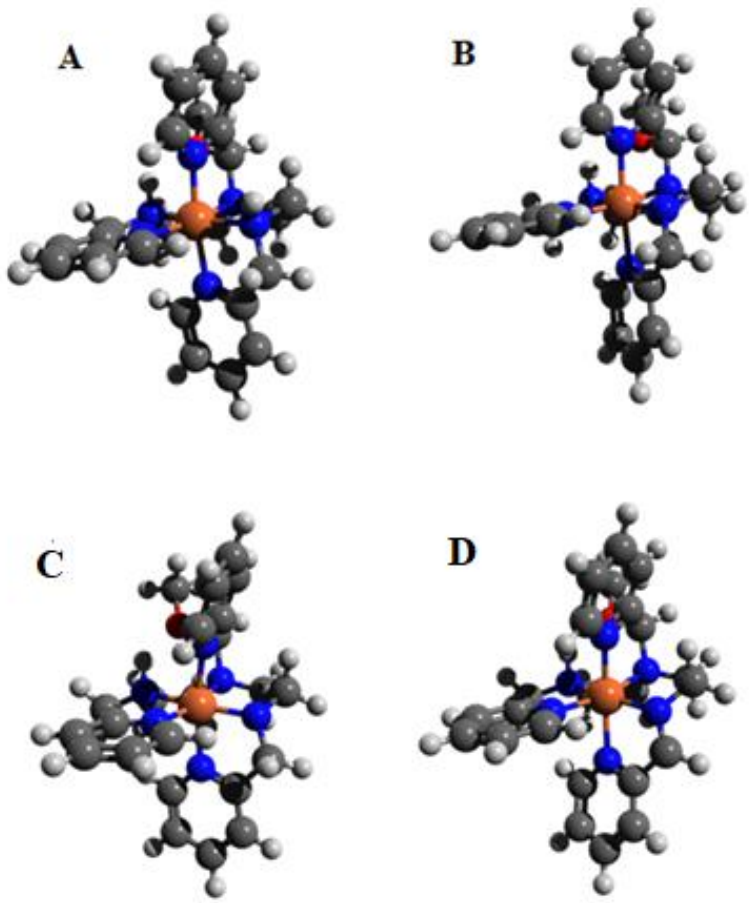

Figure 43. Reaction mechanism (def2-SVP) with methanol-synthesized ligand A) Stage 1 and B) Stage 2 C) Stage 3 D) Stage 4

In Table 11 and Table 12, the computational results of each stage with def2-SVP basis set are shown. The results obtained from the optimizations of each stage of the mechanism are shown in Table 11. Also, in Table 12, are shown the final energies of all the system for each stage expressed in Hartree and transformed to kJ/mol to be compared. Finally, in Figure 44, an energy diagram to compare and resume the final energies for the mechanism is shown.

Table 11. Calculations of the mechanism with methanol-synthesized ligand (def2-SVP)

def2-SVP	Electrons	Charge	Spin	Energy (Hartree)
Stage A	241	3	2	-2,559.322500
Stage B	241	2	2	-2,559.127615
Stage C	240	3	3	-2,558.661074
Stage D	240	2	1	-2,558.535729

Table 12. Final Energies of Mechanism with methanol-synthesized ligand (def2-SVP)

	Electrons	Final Energy (Hartree)	Energy Difference (Hartree)	Energy Difference (kJ/mol)
Stage A	293	-2,939.259477	0	0
Stage B	293	-2,939.705803	-0.446326	-1171.8
Stage C	293	-2,939.275848	-0.016372	-43.0
Stage D	293	-2,939.791713	-0.532236	-1,397.4

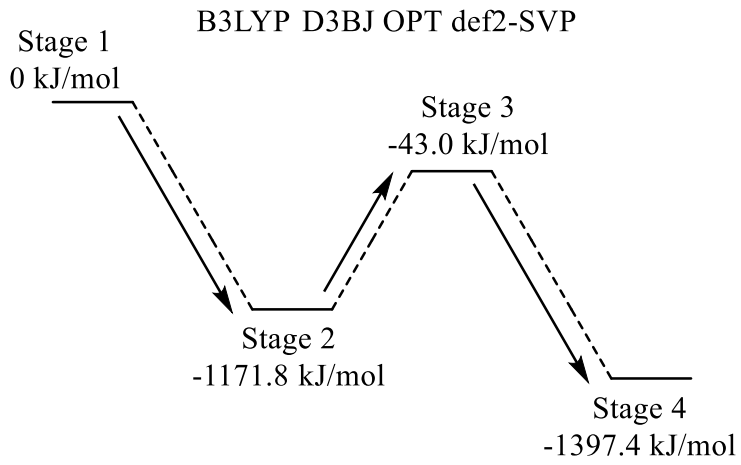

Figure 44. Energy diagram for the mechanism with methanol-synthesized ligand (def2-SVP)

Similarly, for obtaining accurate and supported results, the same mechanism calculations were performed using the def2-TZVP basis set (see Figure 45). The results have minor variations presented in Hartree, but they could have considerable importance in kJ/mol.

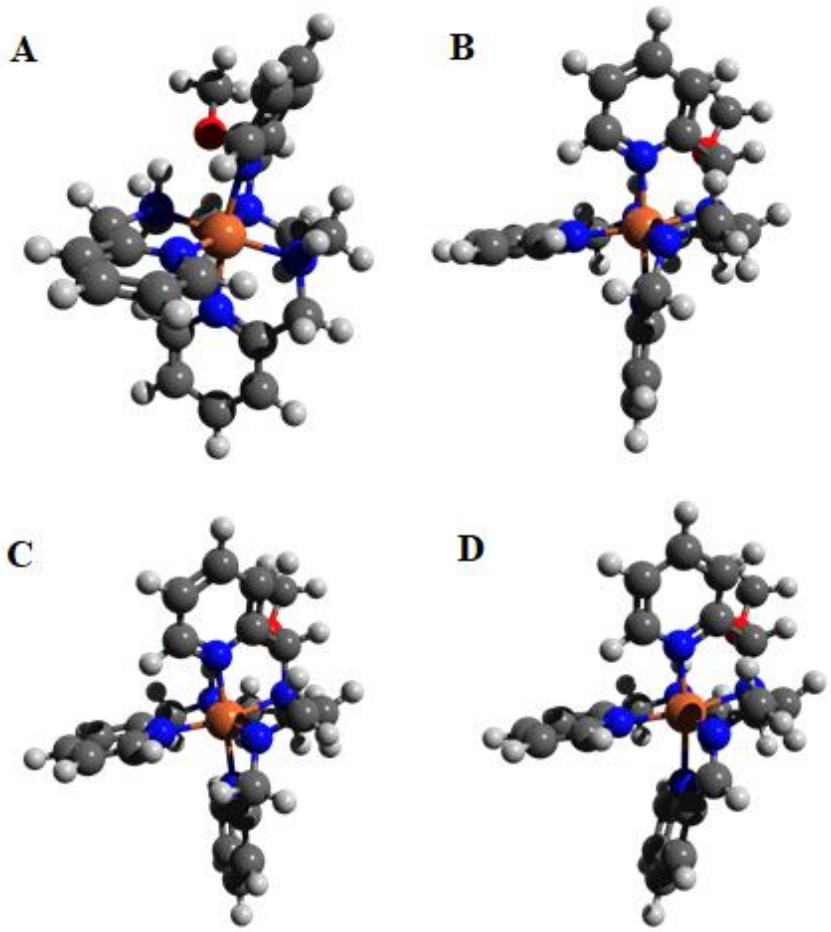

Figure 45. Reaction mechanism (def2-TZVP) with methanol-synthesized ligand A) Stage 1 B) Stage 2 C) Stage 3 D) Stage 4

In Table 13 and Table 14, the computational results of each stage with def2-TZVP basis set are shown. The results obtained from the optimizations of each stage of the mechanism are shown in Table 13. Also, in Table 14, are shown the final energies of all the system for each stage expressed in Hartree and transformed to kJ/mol to be compared. Finally, in Figure 46, an energy diagram to compare and resume the final energies for the mechanism is shown.

Table 13. Calculations of the mechanism with methanol-synthesized ligand (def2-TZVP)

def2-TZVP	Electrons	Charge	Spin	Energy (Hartree)
Stage A	241	3	2	-2,560.888533
Stage B	241	2	2	-2,560.693595
Stage C	240	3	3	-2,560.227347
Stage D	240	2	1	-2,560.101415

Table 14. Final energies of mechanism with methanol-synthesized ligand (def2-TZVP)

	Total Electrons	Final Energy (Hartree)	Energy Difference (Hartree)	Energy Difference (kJ/mol)
Stage A	293	-2,941.329667	0	0
Stage B	293	-2,941.760849	-0.431182	-1,132.1
Stage C	293	-2,941.360367	-0.030700	-80.6
Stage D	293	-2,941.860555	-0.530888	-1,393.8

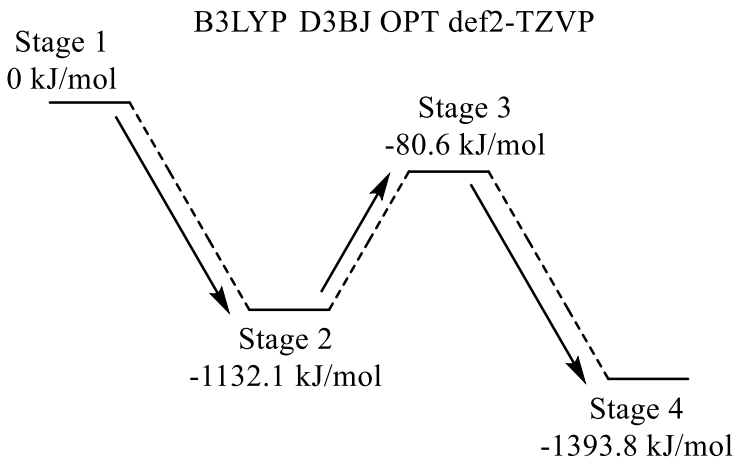

Figure 46. Energy diagram for the mechanism with methanol-synthesized ligand (def2-TZVP)

4.3. Reaction mechanism in ethanol

The same analysis is carried out for ethanol-synthesized ligand mechanism, as before, the difference is based on the diol formation with the solvent that is ethanol. The optimization results for each mechanism stage are shown in Figure 47.

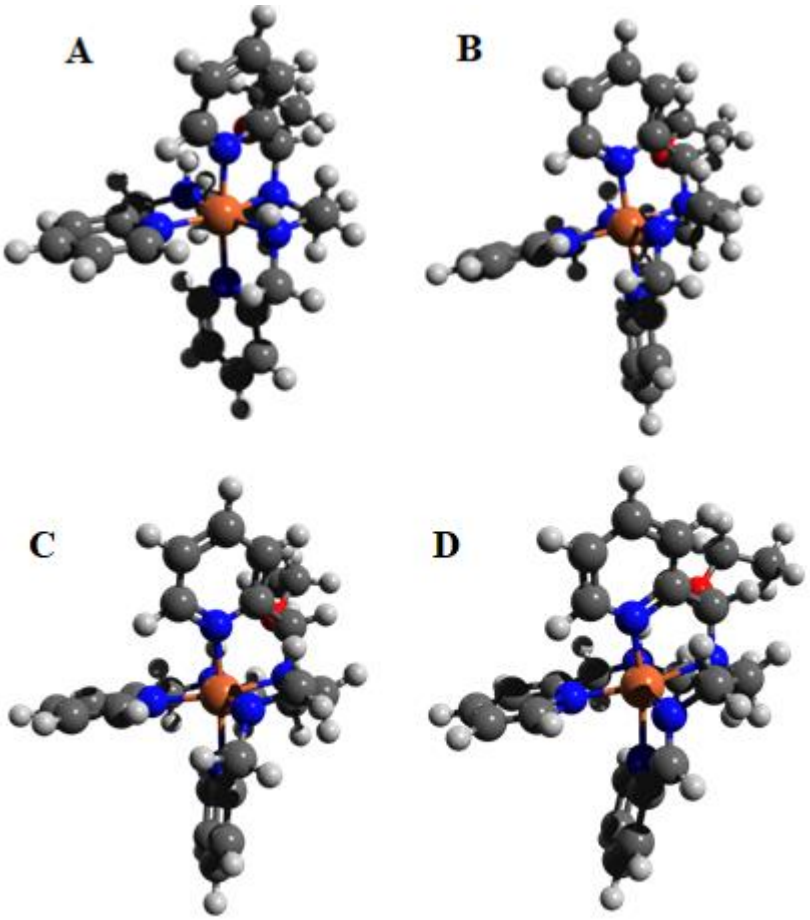

Figure 47. Reaction mechanism (def2-SVP) with ethanol-synthesized ligand A) Stage 1 B) Stage 2 C) Stage 3 D) Stage 4

In Table 15 and Table 16, the computational results of each stage with def2-SVP basis set are shown. The results obtained from the optimizations of each stage of the mechanism are shown in Table 15. Also, in Table 16, are shown the final energies of all the system for each stage expressed in Hartree and transformed to kJ/mol to be compared. Finally, in Figure 48, an energy diagram to compare and resume the final energies for the mechanism is shown.

Table 15. Calculations of the mechanism with ethanol-synthesized ligand (def2-SVP)

def2-SVP	Electrons	Charge	Spin	Energy (Hartree)
Stage A	249	3	2	-2,598.592406
Stage B	249	2	2	-2,598.395208
Stage C	248	3	3	-2,597.931644
Stage D	248	2	1	-2,597.803186

Table 16. Calculations of the mechanism with ethanol-synthesized ligand (def2-SVP)

	Total Electrons	Final Energy (Hartree)	Energy Difference (Hartree)	Energy Difference (kJ/mol)
Stage A	317	-3,057.074263	0	0
Stage B	317	-3,057.512078	-0.437815	-1,149.5
Stage C	317	-3,057.085100	-0.010837	-28.45
Stage D	317	-3,057.591656	-0.517393	-1,358.4

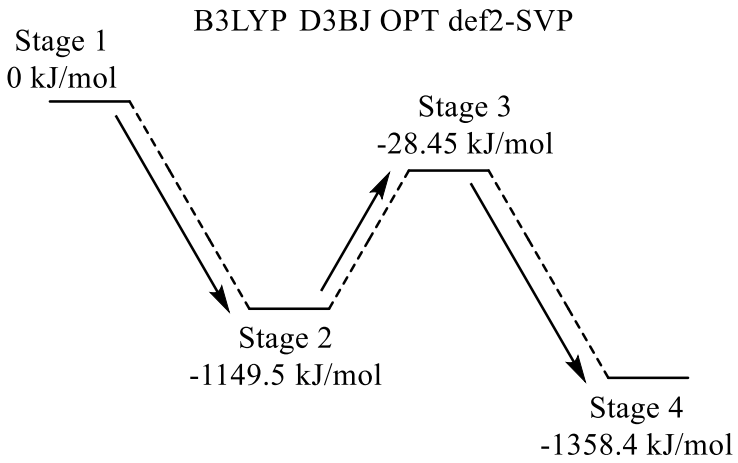

Figure 48. Energy diagram for the mechanism with ethanol-synthesized ligand (def2-SVP)

Following the same methodology, the same mechanism calculations were performed using the def2-TZVP basis set for obtaining accurate and supported results (see Figure 49). The results have minor variations presented in Hartree, but they could have considerable importance in kJ/mol.

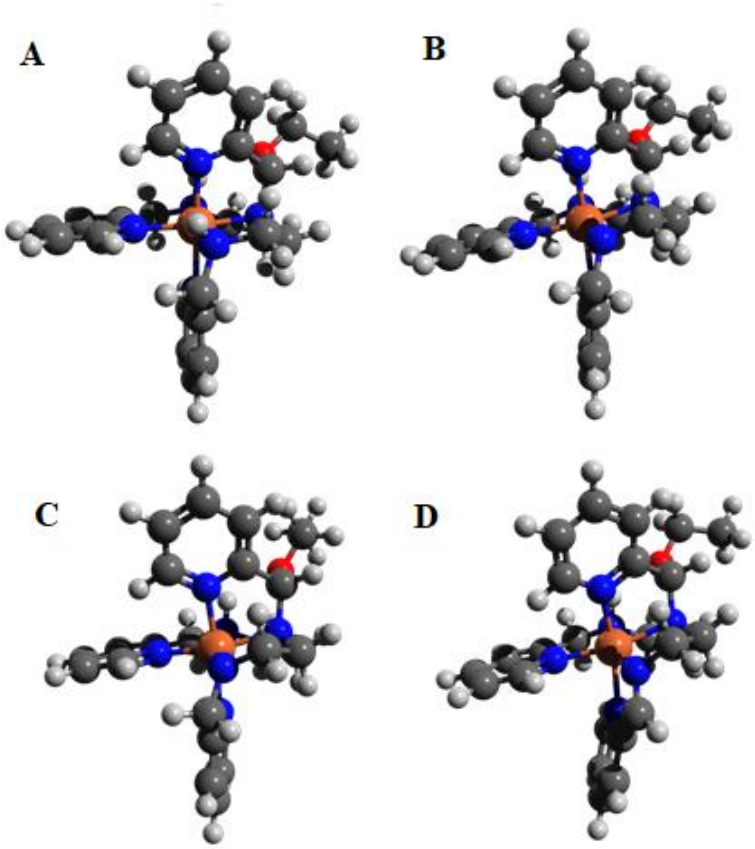

Figure 49. Reaction mechanism (def2-TZVP) with ethanol-synthesized ligand A) Stage 1 B) Stage 2 C) Stage 3 D) Stage 4

In Table 17 and Table 18, the computational results of each stage with def2-TZVP basis set are shown. The results obtained from the optimizations of each stage of the mechanism are shown in Table 17. Also, Table 18 are shown the final energies of all the systems for each stage in Hartree and transformed to kJ/mol to be compared. Finally, in Figure 50, an energy diagram to compare and resume the final energies for the mechanism is shown.

Table 17. Calculations of the mechanism with ethanol-synthesized ligand (def2-TZVP)

def2-TZVP	Electrons	Charge	Spin	Energy (Hartree)
Stage A	249	3	2	-2,600.200669
Stage B	249	2	2	-2,600.003333
Stage C	248	3	3	-2,599.540709
Stage D	248	2	1	-2,599.411043

Table 18. Calculations of the mechanism with ethanol-synthesized ligand (def2-TZVP)

	Total Electrons	Final Energy (Hartree)	Energy Difference (Hartree)	Energy Difference (kJ/mol)
Stage A	317	-3,059.271375	0	0
Stage B	317	-3,059.693953	-0.422578	-1,109.5
Stage C	317	-3,059.297095	-0.025720	-67.5
Stage D	317	-3,059.787343	-0.515968	-1,354.7

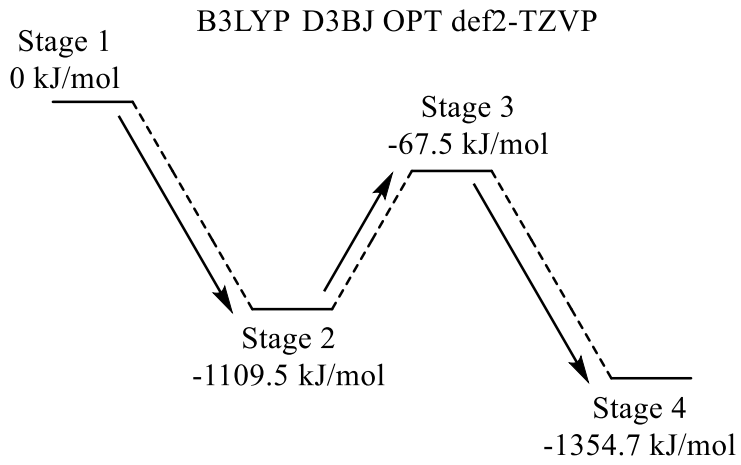

Figure 50. Energy diagram for the mechanism with ethanol-synthesized ligand (def2-TZVP)

4.4. Discussion

From the results exposed in the last section, in all cases, the energy diagram for the different solvent possibilities and the two different basis set shows a thermodynamically benefit mechanism. It can be observed that the difference of energy between the stages of the mechanism supports the hypothesis that OD is achieved through a 3-step mechanism, and that sustains the catalytic behavior of the system. Furthermore, if the final energy of the system in each stage is comparable, it can be observed that the thermodynamics of the mechanism favors the OD reaction. For both basis sets, it can be observed that the energy difference between the first and the last stage is negative. That means that, in terms of stability, the final stage of the system is most stable than the first, favoring the reaction.

To compare the energies of the mechanism in different solvents and optimized with two different basis set, the Figure 51 and Figure 52 show the energy differences between each stage in the mechanism. In Figure 51, the reaction mechanism with different modified ligands was calculated with a def2-SVP basis set; the water-modified reaction mechanism is more stable than the mechanism modified with methanol and ethanol. Furthermore, the methanol and ethanol modifications seem to be close in the final energy stage in the

proposed mechanism; however, the energy differences slightly favor methanol-modified reaction mechanism than ethanol-modified. The reaction with ethanol-modified mechanism seems to have very similar behavior, reducing the energy from the first stage compared to the last stage; this behavior is still thermodynamically favored. However, the energy of each stage is higher than in the cases of water and methanol modifications, which means this is not the preferred solvent in the possible options. This tendency can be extrapolated to other linear alcohols to show similar behavior as methanol and ethanol. Notably, in Figure 52, the mechanisms calculated with def2-TZVP show the same behavior as the calculated with def2-SVP, not only in the energy of each stage for the mechanisms, both also in the preference of the modification of the ligand. As in the case of the mechanisms calculated with def2-SVP for the ligand synthesized in methanol and ethanol, the calculations of def2-TZVP still have very similar behavior with a minor preference for methanol.

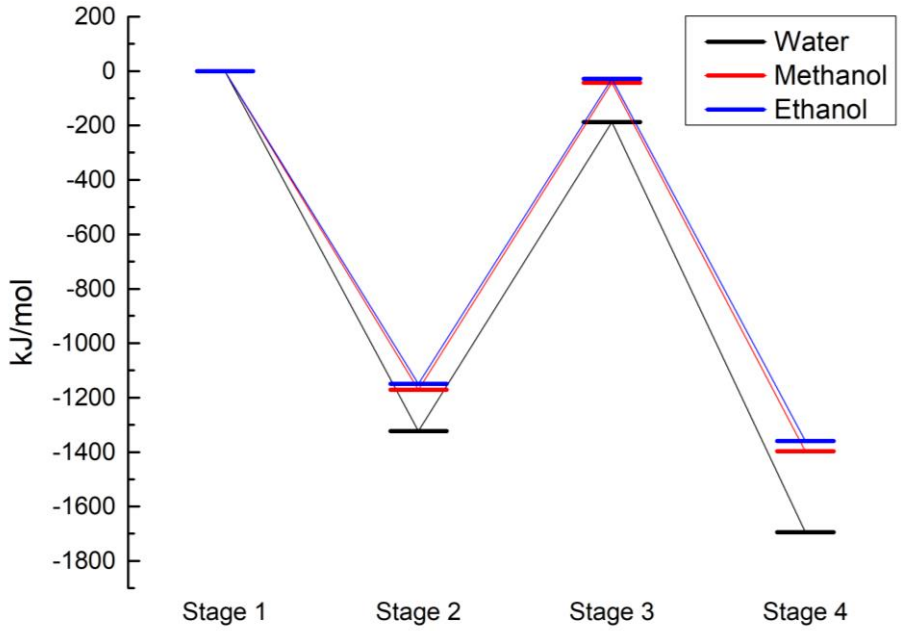

Figure 51. Comparison of the mechanism with ligand synthesized in water, methanol, and ethanol (def2-SVP)

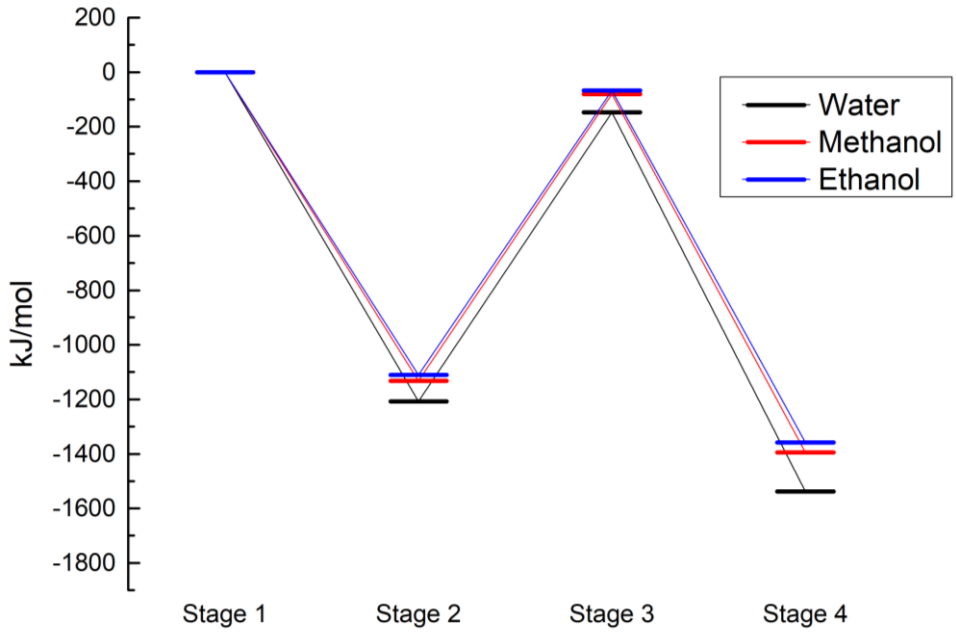

Figure 52. Comparison of the mechanism with ligand synthesized in water, methanol, and ethanol (def2-TZVP)

The MOs considered for the analysis were the HOMO (if the case), the SOMO (if the case), and LUMO. The Figures for each stage can be observed in Figures 33 – 35 – 37 – 39, respectively. The spatial analysis of the MOs support the events proposed by the reaction mechanism, supporting the electrons' location, the oxidation state changes, and the charges rearrangements.

5. Transition States

The proposed mechanism showed the existence of two transition states. Each transition state corresponds to the transference of the protons from the coordination complex to the solvent molecule to establish the OD unsaturation. The first transition state is located between stage 1 and stage 2 of the reaction mechanism, where the first proton is transferred. In Figure 53, it can be observed the transition state for the first proton remotion.

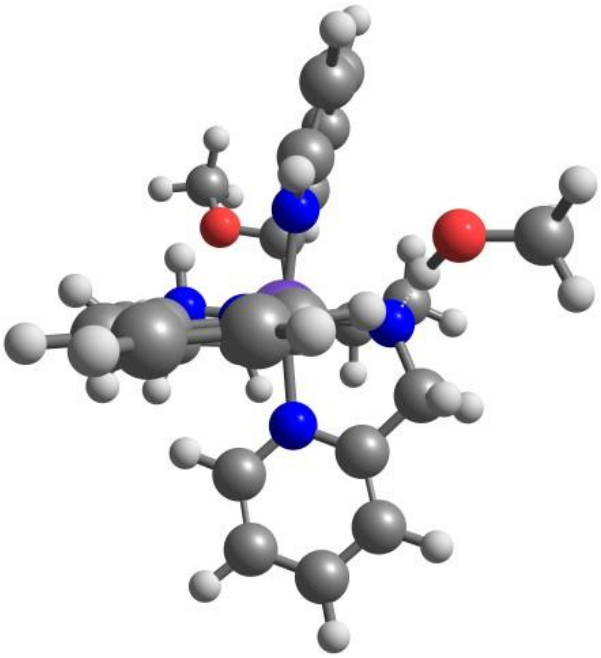

Figure 53. First transition state.

It can also be observed that the bond distance in the transition state from the hydrogen to the carbon in the pyridine ring is 1.32 Å and from the hydrogen to the oxygen of the solvent is 1.11 Å. Furthermore, the frequency that corresponds to the transition state is -1416.73 cm^{-1}. This value supports the existence of the transition state and rejects the possibility of obtaining a local minimum. Besides, the optimization energy obtained for the transition state was 22.45 kJ/mol compared to the first stage of the mechanism.

Similarly, the second transition state is located between stage 3 and stage 4 of the reaction mechanism, where the second proton is transferred, and the OD unsaturation is formed. In Figure 54, it can be observed the transition state for the second proton remotion.

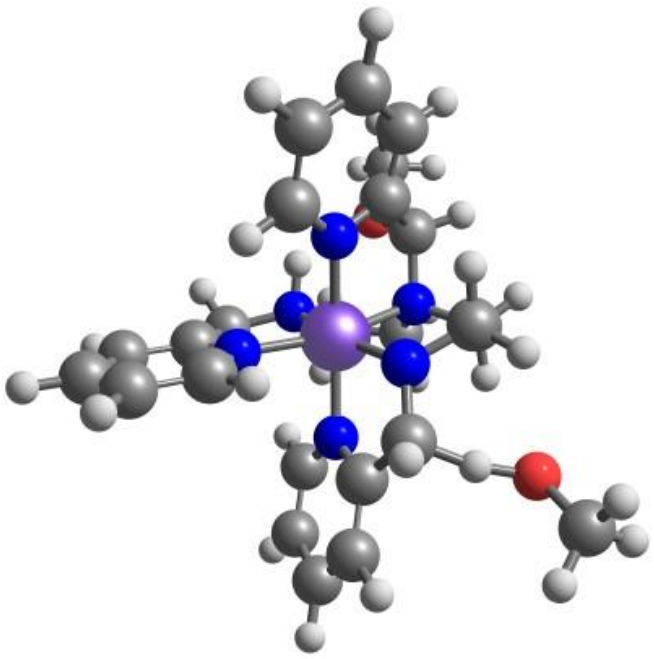

Figure 54. Second transition state.

As before, it can also be observed that the bond distance in the transition state from the hydrogen to the carbon in the pyridine ring is 1.33 Å and from the hydrogen to the oxygen of the solvent is 1.21 Å. Furthermore, the frequency that corresponds to the transition state is -1746.22 cm^{-1}. This value supports the existence of the transition state and rejects the possibility of obtaining a local minimum. Besides, the optimization energy obtained for the transition state was 39.36 kJ/mol compared to the third stage of the mechanism.

5.1. Discussion

The transition states corresponding to the proposed mechanism showed that the proton remotion and the electronic rearrangements are possible. The transition state corresponding to the first proton remotion showed a slight endothermic character compared to the first stage of the mechanism; then, the second transition state showed an endothermic character following the energy tendency of the proposed mechanism. With these conclusions, it can be inferred that both transition states are fast; this makes sense due to the small endothermic energy of both transition states.

The energy shown by the transition states allows a relatively easy way to achieve the reaction, and due to the value of the negative frequency for both transition states, the potential energy surface near the transition states is not plane. Furthermore, considering the hydrogen position in both transition states, it is not the case of an early or late transition state.

6. Mechanism Solvent Stability

The Continuum Solvation Model was applied for the three mechanisms calculated with the def2-SVP basis set in the final study. The model used for the calculations was the Conductor-like Polarizable Continuum model (CPCM) principally by its efficiency simulating solvents in quantum chemical calculations.

6.1. Reaction mechanism in water as solvent

At this point, for the implementation of the solvent in the calculation of the mechanism, the optimized structures for the mechanism presented in section 4.1 of the Results and Discussion section were considered. These calculations used a similar input for the calculation, B3LYP D3BJ CPCM(Water) OPT def2-SV. For the implementation of water into the mechanism, the dielectric constant (ε) implemented in ORCA was 80.4, and the refractive index 1.33 in this case. The results of the calculations with the def2-SVP basis set are shown in Table 19 and Table 20. As before, other molecules in the mechanism, such as dioxygen, oxide, water, and hydroxide, the corresponding results for the calculations for the def2-SVP basis set are shown in the Annexes section. In Figure 55, an energy diagram to compare and resume the final energies for the mechanism is shown.

Table 19. Calculations of the mechanism in water (def2-SVP)

def2-SVP	Electrons	Charge	Spin	Energy (Hartree)
Stage A	233	3	2	-2,520.558855
Stage B	233	2	2	-2,520.098914
Stage C	232	3	3	-2,519.894578
Stage D	232	2	1	-2,519.505714

Table 20. Calculations of the mechanism in water (def2-SVP)

Total Electrons	Final Energy (Hartree)	Energy Difference (Hartree)	Energy Difference (kJ/mol)
269	-2822.196296	0	0
269	-2822.291629	-0.095332	-250.3
269	-2822.251750	-0.055454	-145.6
269	-2822.418160	-0.221864	-582.5

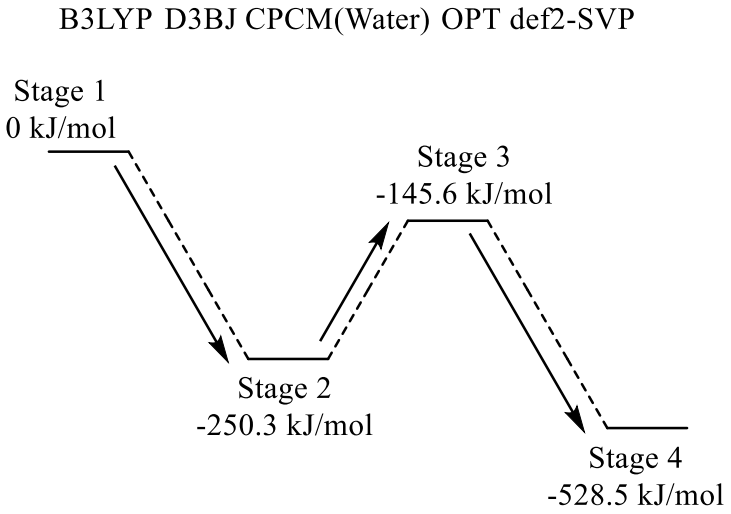

Figure 55. Energy diagram for the mechanism in water (def2-SVP)

6.2.Reaction mechanism in methanol as solvent

These calculations used a similar input for the calculation, B3LYP D3BJ CPCM(Methanol) OPT def2-SVP. For the implementation of methanol into the mechanism, the dielectric constant (ε) implemented in ORCA was 32.63, and the refractive index 1.329 in this case. The results of the calculations with the def2-SVP basis set are shown in Table 21 and Table 22. As before, other molecules in the mechanism, such as dioxygen, oxide, water, and hydroxide, the corresponding results for the calculations for the def2-SVP basis set are shown in the Annexes section. In Figure 56, an energy diagram to compare and resume the final energies for the mechanism is shown.

Table 21. Calculations of the mechanism in methanol (def2-SVP)

def2-SVP	Electrons	Charge	Spin	Energy (Hartree)
Stage A	241	3	2	-2,559.795150
Stage B	241	2	2	-2,559.340054
Stage C	240	3	3	-2,559.130618
Stage D	240	2	1	-2,558.746953

Table 22. Calculations of the mechanism in methanol (def2-SVP)

Total Electrons	Final Energy (Hartree)	Energy Difference (Hartree)	Energy Difference (kJ/mol)
293	-2,939.963120	0	0
293	-2,940.041740	-0.078620	-206.4
293	-2,939.994403	-0.031283	-82.1
277	-2,940.144454	-0.181333	-476.1

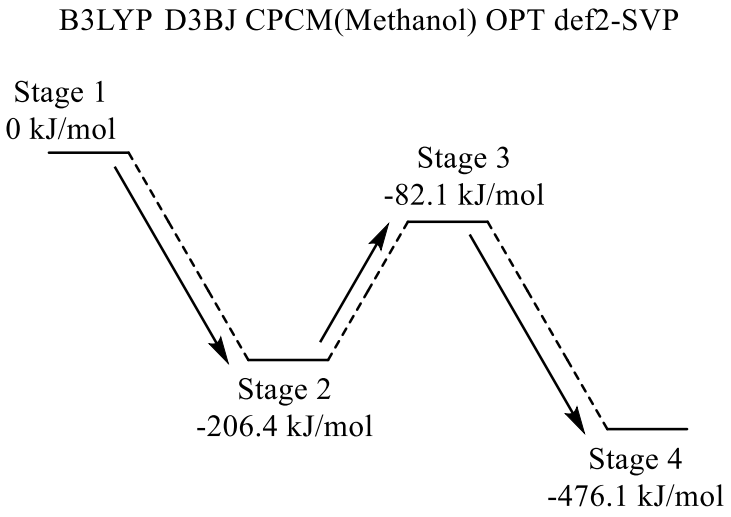

Figure 56. Energy diagram for the mechanism in methanol (def2-SVP)

6.3.Reaction mechanism in ethanol as solvent

For the implementation of the solvent in the calculation of the mechanism, the optimized structures for the mechanism presented in section 4.3 of the Results and Discussion were considered. These calculations used a similar input for the calculation, B3LYP D3BJ CPCM(Ethanol) OPT def2-SVP. For the implementation of ethanol into the mechanism, the dielectric constant (ε) implemented in ORCA was 24.3, and the refractive index 1.361 in this case. The results of the calculations are shown in Table 23 and Table 24. As before, other molecules in the mechanism, such as dioxygen, oxide, water, and hydroxide, the corresponding results for the calculations for the def2-SVP basis set are shown in the Annexes section. In Figure 57, an energy diagram to compare and resume the final energies for the mechanism is shown.

Table 23. Calculations of the mechanism in ethanol (def2-SVP)

def2-SVP	Electrons	Charge	Spin	Energy (Hartree)
Stage A	249	3	2	-2,599.051675
Stage B	249	2	2	-2,598.603192
Stage C	248	3	3	-2,598.392071
Stage D	248	2	1	-2,598.010148

Table 24. Calculations of the mechanism in ethanol (def2-SVP)

Total Electrons	Final Energy (Hartree)	Energy Difference (Hartree)	Energy Difference (kJ/mol)
317	-3,057.751910	0	0
317	-3,057.836970	-0.085060	-223.3
317	-3,057.786587	-0.034677	-91.0
317	-3,057.938207	-0.186297	-489.1

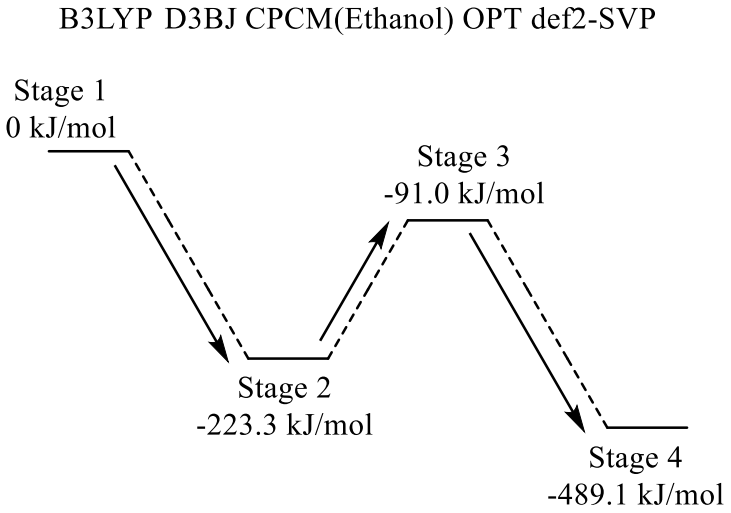

Figure 57. Energy diagram for the mechanism in ethanol (def2-SVP)

6.4. Discussion

This section shows the behavior of the mechanisms in the solvents that correspond to the variation of the ligand, which means the water-synthesized ligand was calculated in water, and so respectively. With the implementation of the solvents, the mechanism in different solvents is still showing the same catalytic behavior. However, the particular case of the energy diagram for the mechanism calculated with def2-SVP basis set shown in Figure 58 exposes preference for ethanol than methanol, in contrast with the calculations without solvent. Comparing the three possible solvents for the reaction, the water mechanism is still the higher favored mechanism. Furthermore, according to Christian et al. [14], the potential energy profile detailed shows highly similar behavior to the mechanism shown in this work. It should be considered that in both studies, the calculations were performed with the inclusion of the solvent in the system.

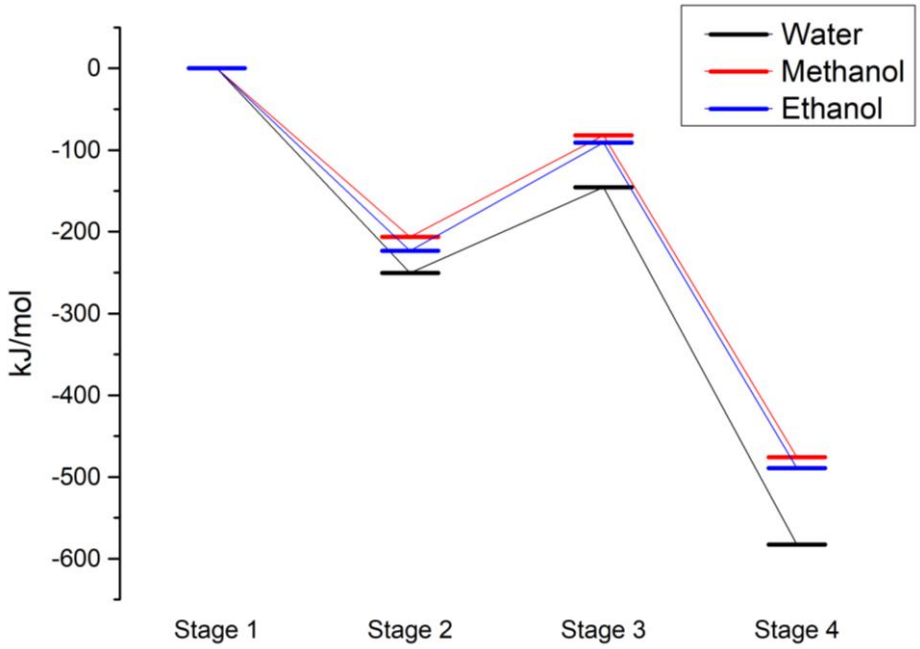

Figure 58. Comparison of the mechanism in water, methanol, and ethanol (def2-SVP).

CHAPTER V

Summary and Conclusions

- The optimization for L2 and L3 ligands showed an emphatic preference for L2 conformation over L3 before OD. In terms of energy, the stabilization of L2 is preferred by the system before. However, after OD, L3 conformation is preferred by the system.
- The difference in the stabilization of both ligands without an iron center is observed in the spatial conformation. For L3, the pyridine rings cannot adopt the octahedral center shape, while L2 shows a tendency to an octahedral center shape.
- The MOs for both ligands support the hindrance effect as the crucial factor for selecting the ligands. Significantly after OD, the HOMO of L3 changes its position to one of the pyridine rings instead of the linear section of the ligand, which could derive an impediment to achieving the coordination with the metallic center.
- According to the optimization energies, the hindrance effect, and the MOs analysis, it was demonstrated that L2 is thermodynamically favored before OD while, L3 is favored after OD.

- The modification of L2 with a solvent is a fundamental step to consider in the OD system, even inducing thermodynamic differences in the reaction.
- In terms of orientation and geometry, L4 in water, methanol, and ethanol show high similarity, both before and after OD. The difference was found in the energy optimization calculations that shows a preference (in stability) for L4 in ethanol over the other two possibilities.
- The analysis of MOs reveals no significant differences in HOMO and LUMO for the possible ligand modifications, nor before nor after OD. This result shows that all the possible ligand modifications show a similar reactivity to achieve coordination with the metal center with an octahedral center geometry. Any case presents an endothermic character, so it is demonstrated that all the possible modifications can accomplish the coordination.

- The spin of the ligands was probed to support the low spin character of the ligand. As expected, for $[Fe(L2)(DMSO)]^{3+}$, the low spin character was the

thermodynamically favored configuration. It is necessary to emphasize that with high spin and Jahn-Teller character, L2 still achieves the octahedral coordination, only differentiated by the stabilization energy.

- These last results are in concordance with the behavior of L3, which only achieves the coordination with the metal center in the calculation with low spin character. However, the geometry adopted by $[Fe(L3)(DMSO)]^{3+}$ was tetrahedral instead of octahedral. This result could be interesting as a selective reaction to obtain different geometries in this coordination compound.
- For high spin and Jahn-Teller effect, the geometry, the atoms coordinated, and the optimization energies are not possible or present endothermic character.

- As can be inferred from the previous results, the reaction mechanism with the different ligand modifications showed very similar behavior, even if the calculation is performed with different basis sets. These results also support the similar reactivity of the L4 possible changes.
- The proposed 3-step mechanism successfully explains all the events that should happen to reach the OD reaction. For all the ligand modifications, the OD reaction is achieved.
- The MOs orbital analysis of L4 in water mechanism showed a concordance with the oxidation states, and electron localization demonstrated that the study of the reaction is accomplished. The MOs analysis was performed only for L4 in water because the behavior in the rest of the cases was highly similar.
- Establishing a comparison among the possible modification of L4 in terms of optimization energy for each step, the L4 in methanol mechanism shows higher stability over the other possibilities. This result is supported by calculations with def2-SVP basis set and def2-TZVP. With this, methanol is initially proposed as the best environment for the catalytic reaction.

- With the proposed mechanism, the transition states for both hydrogen transferences can be obtained. The presence of the transition states supports the reaction kinetics and is in concordance with the energies obtained for the mechanism.

- The distances of the bonds in transition states enhance the solvent molecule's presence to achieve the proton transference; in both cases, the distances are similar. However, the spatial position of the solvent molecule is very different in each case.

- The calculation of the reaction mechanism in the presence of solvent was a fundamental supporting detail to probe the veracity of the obtained results. As expected, in the presence of a solvent, the mechanism in water was preferred over the methanol and ethanol possibility. Regarding the mechanism without the presence of the solvents, the results were the same.
- With this final result, it was demonstrated that water could improve the efficiency of the catalytic reaction considering that this reaction is not reported with water as an environment solvent.

Perspectives and Recommendations

- After finishing this work, it can be concluded that the OD reaction for this complex is efficient, especially in water. However, other solvents with less polarity (as methanol and methanol) showed to allow the reaction. An increasing number of carbons in the solvent and polarity changes can produce differences in the thermodynamics of the reaction.
- The 4-position substitution at the pyridine ring for the ligand could be proved. However, according to the results of this work, the kinetics of the reaction will not allow the OD reaction.
- Electrochemical studies may be performed to understand the chemical character of the electron transferences inside the complex. Furthermore, these studies will allow obtaining detailed information about the complex and the iron metal.

Bibliography

(1) Bruijnincx, P. C. A.; Buurmans, I. L. C.; Gosiewska, S.; Moelands, M. A. H.; Lutz, M.; Spek, A. L.; van Koten, G.; Klein Gebbink, R. J. M. Iron(II) Complexes with Bio-Inspired N,N,O Ligands as Oxidation Catalysts: Olefin Epoxidation Andcis-Dihydroxylation. *Chem. - A Eur. J.* **2008**, *14* (4), 1228–1237. https://doi.org/10.1002/chem.200700573.

(2) Tomyn, S.; Shylin, S. I.; Bykov, D.; Ksenofontov, V.; Gumienna-Kontecka, E.; Bon, V.; Fritsky, I. O. Indefinitely Stable Iron(IV) Cage Complexes Formed in Water by Air Oxidation. *Nat. Commun.* **2017**, *8* (1), 14099. https://doi.org/10.1038/ncomms14099.

(3) Drif, A.; Pineda, A.; Morvan, D.; Belliere-Baca, V.; De Oliveira Vigier, K.; Jérôme, F. Catalytic Oxidative Dehydrogenation of Malic Acid to Oxaloacetic Acid. *Green Chem.* **2019**. https://doi.org/10.1039/c9gc01768b.

(4) Shul'pin, G. B.; Kozlov, Y. N.; Shul'pina, L. S. Metal Complexes Containing Redox-Active Ligands in Oxidation of Hydrocarbons and Alcohols: A Review. *Catalysts*. 2019. https://doi.org/10.3390/catal9121046.

(5) Raleigh, C. J.; Martell, A. E. Oxidative Dehydrogenation of Coordinated 1,9-Bis(2-Pyridyl)-2,5,8-Triazanonane through Formation of a Cobalt Dioxygen Complex Intermediate. *Inorg. Chem.* **1985**, *24* (2), 142–148. https://doi.org/10.1021/ic00196a005.

(6) Ugalde-Saldívar, V. M.; Sosa-Torres, M. E.; Ortiz-Frade, L.; Bernès, S.; Höpfl, H. Novel Iron(Ii) Complexes with Hexadentate Nitrogen Ligands Obtained via Intramolecular Redox Reactions. *J. Chem. Soc. Dalt. Trans.* **2001**, No. 20, 3099. https://doi.org/10.1039/b100915j.

(7) Wang, X.; Miao, C.; Wang, S.; Xia, C.; Sun, W. Bioinspired Manganese and Iron Complexes with Tetradentate N Ligands for the Asymmetric Epoxidation of Olefins. *ChemCatChem* **2013**, *5* (8), 2489–2494. https://doi.org/10.1002/cctc.201300102.

(8) Bissette, A. J.; Fletcher, S. P. Mechanisms of Autocatalysis. *Angew. Chemie Int. Ed.* **2013**, *52* (49), 12800–12826. https://doi.org/10.1002/anie.201303822.

(9) van Leeuwen, P. W. N. M. *Homogeneous Catalysis*; Springer Netherlands: Dordrecht, 2004. https://doi.org/10.1007/1-4020-2000-7.

(10) Nielsen, M. T.; Padilla, R.; Nielsen, M. Homogeneous Catalysis by Organometallic Polynuclear Clusters. *Journal of Cluster Science*. Springer January 1, 2020, pp 11–61. https://doi.org/10.1007/s10876-019-01635-3.

(11) Witzke, R. J.; Chapovetsky, A.; Conley, M. P.; Kaphan, D. M.; Delferro, M. Nontraditional Catalyst Supports in Surface Organometallic Chemistry. *ACS Catalysis*. American Chemical Society October 16, 2020, pp 11822–11840. https://doi.org/10.1021/acscatal.0c03350.

(12) Li, B.; Zeng, H. C. Minimalization of Metallic Pd Formation in Suzuki Reaction with a Solid-State Organometallic Catalyst. *ACS Appl. Mater. Interfaces* **2020**, *12* (30), 33827–33837. https://doi.org/10.1021/acsami.0c09739.

(13) Herrmann, W. A.; Cornils, B. Organometallic Homogeneous Catalysis—Quo Vadis? *Angew. Chemie Int. Ed. English* **1997**, *36* (10), 1048–1067. https://doi.org/10.1002/anie.199710481.

(14) Christian, G. J.; Arbuse, A.; Fontrodona, X.; Martinez, M. A.; Llobet, A.; Maseras, F. Oxidative Dehydrogenation of an Amine Group of a Macrocyclic Ligand in the Coordination Sphere of a CuII Complex. *Dalt. Trans.* **2009**, No. 30, 6013. https://doi.org/10.1039/b902947h.

(15) Li, L.; Wang, H.; Han, J.; Zhu, X.; Ge, Q. Balancing the Activity and Selectivity of Propane Oxidative Dehydrogenation on NiOOH (001) and (010). *Trans. Tianjin Univ.* **2020**, *26* (5), 341–351. https://doi.org/10.1007/s12209-020-00267-3.

(16) Navlani-García, M.; Mori, K.; Salinas-Torres, D.; Kuwahara, Y.; Yamashita, H. New Approaches toward the Hydrogen Production from Formic Acid Dehydrogenation over Pd-Based Heterogeneous Catalysts. *Frontiers in Materials*. Frontiers Media S.A. March 8, 2019, p 44. https://doi.org/10.3389/fmats.2019.00044.

(17) Sun, X.; Han, P.; Li, B.; Mao, S.; Liu, T.; Ali, S.; Lian, Z.; Su, D. Oxidative Dehydrogenation Reaction of Short Alkanes on Nanostructured Carbon Catalysts: A Computational Account. *Chem. Commun.* **2018**, *54* (8), 864–875.

https://doi.org/10.1039/c7cc06941c.

(18) Zhang, L.; Chen, D.; Jang, L.; Vervaele, M.; Locquet, J. P.; Seo, J. W. Synthesis of Directly Spinnable Carbon Nanotube Carpets via the Oxidative Dehydrogenation Reaction of C2H2-CO2. In *Materials Today: Proceedings*; Elsevier Ltd, 2017; Vol. 4, pp 6966–6974. https://doi.org/10.1016/j.matpr.2017.07.026.

(19) Lopez-Taco, I. A.; Saucedo-Vázquez, J. P. Kinetics of the Oxidative Dehydrogenation of Polyamines in Iron Coordination Compounds, Yachay Tech University, 2020.

(20) *The IUPAC Compendium of Chemical Terminology*; Gold, V., Ed.; International Union of Pure and Applied Chemistry (IUPAC): Research Triangle Park, NC, 2019. https://doi.org/10.1351/goldbook.

(21) Shenvi, R. A.; O'Malley, D. P.; Baran, P. S. Chemoselectivity: The Mother of Invention in Total Synthesis. *Acc. Chem. Res.* **2009**, *42* (4), 530–541. https://doi.org/10.1021/ar800182r.

(22) Afagh, N. A.; Yudin, A. K. Chemoselectivity and the Curious Reactivity Preferences of Functional Groups. *Angew. Chemie Int. Ed.* **2010**, *49* (2), 262–310. https://doi.org/10.1002/anie.200901317.

(23) Gilbert, M. Relation of Structure to Chemical Properties. In *Brydson's Plastics Materials*; Elsevier, 2017; pp 75–102. https://doi.org/10.1016/B978-0-323-35824-8.00005-0.

(24) Roberts, John D. and Caserio, M. C. *Basic Principles of Organic Chemistry*; 1977.

(25) Wisniak, J. The History of Catalysis. From the Beginning to Nobel Prizes. *Educ. Química* **2010**, *21* (1), 60–69. https://doi.org/10.1016/S0187-893X(18)30074-0.

(26) Santen R. A Leeuwen P. W. N. M Mooulijn J. A. Averill B. A. Catalysis: An Integrated Approach. *Elsevier Sci. B.V., Amsterdam* **1999**, 602.

(27) Inglezakis, V. J.; Poulopoulos, S. G. *Adsorption, Ion Exchange and Catalysis*; Elsevier, 2006. https://doi.org/10.1016/B978-0-444-52783-7.X5000-9.

(28) Lloyd, L.; Ridler, D. E.; Twigg, M. V. Catalyst Handbook , 2nd Ed. *Wolfe Press. London* **1989**, 1989.

(29) J. -F. Le Page, J. Cosyns, P. Courty, E. Freund, J.-p. Franck, Y. Jacquin, B. Juguin., C. Marcilly, G. Martino, J. Miquel, R. Montarnal, A. Sugier, H. V. L. *Applied Heterogeneous Catalysis*; Technip, E., Ed.; Paris, 1987.

(30) Kakaei, K.; Esrafili, M. D.; Ehsani, A. Introduction to Catalysis. In *Interface Science and Technology*; 2019; pp 1–21. https://doi.org/10.1016/B978-0-12-814523-4.00001-0.

(31) Bhaduri, S.; Mukesh, D. *Homogeneous Catalysis*; John Wiley & Sons, Inc.: New York, USA, 2000. https://doi.org/10.1002/0471220388.

(32) Barceló, I.; Solís, H. *Cinética y Catálisis de Las Reacciones Químicas En Fase Homogénea*, 1st Editio.; 2010.

(33) Plasson, R.; Brandenburg, A.; Jullien, L.; Bersini, H. Autocatalyses. *J. Phys. Chem. A* **2011**, *115* (28), 8073–8085. https://doi.org/10.1021/jp110079p.

(34) Skorb, E. V.; Semenov, S. N. Mathematical Analysis of a Prototypical Autocatalytic Reaction Network. *Life* **2019**, *9* (2), 42. https://doi.org/10.3390/life9020042.

(35) Turek, T. Industrial Catalysis. Optimizing Catalysts and Processes, by R.J. Wijngaarden, A. Kronberg, K.R. Westerterp; Published by Wiley–VCH, Weinheim 1998, 268 Pages, Price DM 248,00. *Chem. Eng. Process. Process Intensif.* **1999**, *38* (3), 285. https://doi.org/10.1016/S0255-2701(99)00012-4.

(36) van Leeuwen, P. W. N. M. Homogeneous Metal Catalysis. In *Reference Module in Chemistry, Molecular Sciences and Chemical Engineering*; Elsevier, 2016. https://doi.org/10.1016/B978-0-12-409547-2.11101-1.

(37) Togni, A.; Venanzi, L. M. Nitrogen Donors in Organometallic Chemistry and Homogeneous Catalysis. *Angew. Chemie Int. Ed. English* **1994**, *33* (5), 497–526. https://doi.org/10.1002/anie.199404971.

(38) Denisov, E. T.; Sarkisov, O. M.; Likhtenshtein, G. I. Catalysis by Metal Complexes. In *Chemical Kinetics*; Elsevier, 2003; pp 472–501. https://doi.org/10.1016/B978-044450938-3/50039-9.

(39) Crichton, R. R. Basic Coordination Chemistry for Biologists. In *Biological Inorganic Chemistry*; Elsevier, 2012; pp 21–34. https://doi.org/10.1016/B978-0-444-53782-9.00002-4.

(40) Reedijk, J.; Bouwman, E. Introduction to Bioinorganic Chemistry. In *Bioinorganic Catalysis*; CRC Press, 1999; pp 1–12. https://doi.org/10.1201/9780203908457.ch1.

(41) Pal, S. Pyridine: A Useful Ligand in Transition Metal Complexes. In *Pyridine*; InTech, 2018. https://doi.org/10.5772/intechopen.76986.

(42) Ugalde-Saldivar, V.; Luna-Canut, M. A.; Sosa-Torres, M. E.; Rosales-Hoz, M. J.; Toscano, R. A.; Tobe, M. L. Preparation, Crystal Structure and Kinetics of Acid Hydrolysis of an Isomer of [Cr(Picdien)Cl][ZnCl 4][Picdien = 1,9-Bis(2′-Pyridyl)-2,5,8-Triazanonane]. *J. Chem. Soc., Dalt. Trans.* **1990**, No. 12, 3629–3634. https://doi.org/10.1039/DT9900003629.

(43) Bombieri, G.; Forsellini, E.; Del Pra, A.; Tobe, M. L.; Chatterjee, C.; Cooksey, C. J. The Crystal and Molecular Structure of an Isomer of Bromo [1,9-Bis(2-Pyridyl) 2,5,8-Triazononane] Cobalt(III), Perchlorate, [Co(Picdien)Br](ClO42and That of an Isomer of Nitro[1,9-Bis(2-Pyridyl)2,5,8-Triazanonane]Cobalt(III), Perchlorate, [Copicdien)(No2). *Inorganica Chim. Acta* **1983**, *75*, 93–101. https://doi.org/10.1016/S0020-1693(00)91195-2.

(44) Khan, M. M. T.; Halligudi, S. B.; Shukla, S.; Shaikh, Z. A. Reductive Carbonylation of Nitrobenzene to Phenylurethane Catalyzed by Ru(III)-Schiff Base Complexes. *J. Mol. Catal.* **1990**, *57* (3), 301–305. https://doi.org/10.1016/0304-5102(90)85004-2.

(45) Rosales, M. J.; Toscano, R. A.; Luna-Canut, M. A.; Sosa-Torres, M. E. Copper(II) and Nickel(II) Complexes with a Linear Pentadentate Ligand. The x-Ray Crystal Structure of [CuL][CuCl4] (L = 1,9-Bis-(2-Pyridyl)-2,5,8-Triazanonane). *Polyhedron* **1989**, *8* (7), 909–915. https://doi.org/10.1016/S0277-5387(00)86442-6.

(46) Sosa-Torres, M. E.; Ugalde-Saldívar, V. M.; Rosales-Hoz, M. J.; Toscano, R. A. Structure of [1,9-Bis(2-Pyridyl)-2,5,8-Triazanonane]Zinc(II) Tetrachlorozincate(II). *Acta Crystallogr. Sect. C Cryst. Struct. Commun.* **1993**,

49 (4), 796–799. https://doi.org/10.1107/S0108270192010564.

(47) Saucedo-Vázquez, J. P.; Kroneck, P. M. H.; Sosa-Torres, M. E. The Role of Molecular Oxygen in the Iron(<scp>iii</Scp>)-Promoted Oxidative Dehydrogenation of Amines. *Dalt. Trans.* **2015**, *44* (12), 5510–5519. https://doi.org/10.1039/C4DT03606A.

(48) Richard Keene, F. Metal-Ion Promotion of the Oxidative Dehydrogenation of Coordinated Amines and Alcohols. *Coord. Chem. Rev.* **1999**, *187* (1), 121–149. https://doi.org/10.1016/S0010-8545(99)00034-X.

(49) Ochiai, E.-I. Iron versus Copper, II: Principles and Applications in Bioinorganic Chemistry. *J. Chem. Educ.* **1986**, *63* (11), 942. https://doi.org/10.1021/ed063p942.

(50) Christian, G. J.; Llobet, A.; Maseras, F. Mechanistic Study of Amine to Imine Oxidation in a Dinuclear Cu(II) Complex Containing an Octaaza Dinucleating Ligand. *Inorg. Chem.* **2010**, *49* (13), 5977–5985. https://doi.org/10.1021/ic100502x.

(51) Zassinovich, G.; Mestroni, G.; Gladiali, S. Asymmetric Hydrogen Transfer Reactions Promoted by Homogeneous Transition Metal Catalysts. *Chem. Rev.* **1992**, *92* (5), 1051–1069. https://doi.org/10.1021/cr00013a015.

(52) Mayer, J. M. PROTON-COUPLED ELECTRON TRANSFER: A Reaction Chemist's View. *Annu. Rev. Phys. Chem.* **2004**, *55* (1), 363–390. https://doi.org/10.1146/annurev.physchem.55.091602.094446.

(53) Blomberg, M. R. A.; Siegbahn, P. E. M. Different Types of Biological Proton Transfer Reactions Studied by Quantum Chemical Methods. *Biochim. Biophys. Acta - Bioenerg.* **2006**, *1757* (8), 969–980. https://doi.org/10.1016/j.bbabio.2006.01.002.

(54) Szabo, A.; Ostlund, N. *Modern Quantum Chesmitry Introduction to Advanced Electronic Structure Theory*; General Publishing Company, Ltd.: New York, 1996.

(55) Mendez, A. M. P.; Mitnik, D. M.; Miraglia, J. E. Local Effective Hartree–Fock Potentials Obtained by the Depurated Inversion Method. In *Advances in*

Quantum Chemistry; 2018; pp 117–132. https://doi.org/10.1016/bs.aiq.2017.07.004.

(56) Amusia, M. Y.; Msezane, A. Z.; Shaginyan, V. R. Density Functional Theory versus the Hartree–Fock Method: Comparative Assessment. *Phys. Scr.* **2003**, *68* (6), C133–C140. https://doi.org/10.1238/physica.regular.068ac0133.

(57) Pederson, M. R.; Baruah, T. Self-Interaction Corrections Within the Fermi-Orbital-Based Formalism. In *Advances in Atomic, Molecular and Optical Physics*; 2015; pp 153–180. https://doi.org/10.1016/bs.aamop.2015.06.005.

(58) Toulhoat, H. Heterogeneous Catalysis: Use of Density Functional Theory. In *Encyclopedia of Materials: Science and Technology*; Elsevier, 2010; pp 1–7. https://doi.org/10.1016/B978-008043152-9.02243-0.

(59) Kurth, S.; Marques, M. A. L.; Gross, E. K. U. Density-Functional Theory. In *Encyclopedia of Condensed Matter Physics*; Elsevier, 2005; pp 395–402. https://doi.org/10.1016/B0-12-369401-9/00445-9.

(60) Frisch, M. J.; Trucks, G. W.; Cheeseman, J. R. Systematic Model Chemistries Based on Density Functional Theory: Comparison with Traditional Models and with Experiment. In *Theoretical and Computational Chemistry*; Elsevier, 1996; Vol. 4, pp 679–707. https://doi.org/10.1016/S1380-7323(96)80100-2.

(61) Bal, H. E.; Kaashoek, M. F.; Tanenbaum, A. S. Orca: A Language for Parallel Programming of Distributed Systems. *IEEE Trans. Softw. Eng.* **1992**, *18* (3), 190–205. https://doi.org/10.1109/32.126768.

(62) Neese, F. Software Update: The ORCA Program System, Version 4.0. *WIREs Comput. Mol. Sci.* **2018**, *8* (1). https://doi.org/10.1002/wcms.1327.

(63) Neese, F. The ORCA Program System. *WIREs Comput. Mol. Sci.* **2012**, *2* (1), 73–78. https://doi.org/10.1002/wcms.81.

(64) Kim, K.; Jordan, K. D. Comparison of Density Functional and MP2 Calculations on the Water Monomer and Dimer. *Journal of Physical Chemistry*. American Chemical Society 1994, pp 10089–10094. https://doi.org/10.1021/j100091a024.

(65) Stephens, P. J.; Devlin, F. J.; Chabalowski, C. F.; Frisch, M. J. Ab Initio Calculation of Vibrational Absorption and Circular Dichroism Spectra Using

Density Functional Force Fields. *J. Phys. Chem.* **1994**, *98* (45), 11623–11627. https://doi.org/10.1021/j100096a001.

(66) Tirado-Rives, J.; Jorgensen, W. L. Performance of B3LYP Density Functional Methods for a Large Set of Organic Molecules. *J. Chem. Theory Comput.* **2008**, *4* (2), 297–306. https://doi.org/10.1021/ct700248k.

(67) Grimme, S.; Ehrlich, S.; Goerigk, L. Effect of the Damping Function in Dispersion Corrected Density Functional Theory. *J. Comput. Chem.* **2011**, *32* (7), 1456–1465. https://doi.org/10.1002/jcc.21759.

(68) Tsuzuki, S.; Uchimaru, T. Accuracy of Intermolecular Interaction Energies, Particularly Those of Hetero-Atom Containing Molecules Obtained by DFT Calculations with Grimme's D2, D3 and D3BJ Dispersion Corrections. *Phys. Chem. Chem. Phys.* **2020**, *22* (39), 22508–22519. https://doi.org/10.1039/D0CP03679J.

(69) Neese Frank, W. F. Orca Manual -An Ab Initio, DFT and Semiempirical SCF-MO Package-. *Input Descr.* **2011**.

(70) Neese, F.; Wennmohns, F. Orca 4.0.1 Manual. *Wiley Interdiscip. Rev. Comput. Mol. Sci.* **2017**.

(71) Zheng, J.; Xu, X.; Truhlar, D. G. Minimally Augmented Karlsruhe Basis Sets. *Theor. Chem. Acc.* **2011**, *128* (3), 295–305. https://doi.org/10.1007/s00214-010-0846-z.

(72) Weigend, F.; Ahlrichs, R. Balanced Basis Sets of Split Valence, Triple Zeta Valence and Quadruple Zeta Valence Quality for H to Rn: Design and Assessment of Accuracy. *Phys. Chem. Chem. Phys.* **2005**, *7* (18), 3297. https://doi.org/10.1039/b508541a.

(73) Hill, J. G. Gaussian Basis Sets for Molecular Applications. *International Journal of Quantum Chemistry*. January 5, 2013, pp 21–34. https://doi.org/10.1002/qua.24355.

(74) Takano, Y.; Houk, K. N. Benchmarking the Conductor-like Polarizable Continuum Model (CPCM) for Aqueous Solvation Free Energies of Neutral and Ionic Organic Molecules. *J. Chem. Theory Comput.* **2005**, *1* (1), 70–77.

https://doi.org/10.1021/ct049977a.

(75) Jesus, A. J. L.; Tomé, L. I. N.; Eusébio, M. E. S.; Redinha, J. S. Determination of the Enthalpy of Solute-Solvent Interaction from the Enthalpy of Solution: Aqueous Solutions of Erythritol and L-Threitol. *J. Phys. Chem. B* **2006**, *110* (18), 9280–9285. https://doi.org/10.1021/jp0561221.

(76) Saucedo-Vázquez, J. P.; Ugalde-Saldívar, V. M.; Toscano, A. R.; Kroneck, P. M. H.; Sosa-Torres, M. E. On the Mechanism of Iron(III)-Dependent Oxidative Dehydrogenation of Amines. *Inorg. Chem.* **2009**, *48* (3), 1214–1222. https://doi.org/10.1021/ic8016968.

APPENDIX

APPENDIX A:

Results of the calculations for the extra molecules intervening in the mechanisms of Section 4

Stage A	OH-				OH-				O2			
	Electrons	Charge	Spin	Energy (Hartree)	Electrons	Charge	Spin	Energy (Hartree)	Electrons	Charge	Spin	Energy (Hartree)
	10	-1	1	-75.92537055	10	-1	1	-75.92537055	16	0	1	-150.2698208
Stage B	OH-				O2				H2O			
	Electrons	Charge	Spin	Energy (Hartree)	Electrons	Charge	Spin	Energy (Hartree)	Electrons	Charge	Spin	Energy (Hartree)
	10	-1	1	-75.92537055	16	0	1	-150.2698208	10	0	1	-76.43834815
Stage C	OH-				O2-				H2O			
	Electrons	Charge	Spin	Energy (Hartree)	Electrons	Charge	Spin	Energy (Hartree)	Electrons	Charge	Spin	Energy (Hartree)
	10	-1	1	-75.92537055	17	-1	2	-150.459955	10	0	1	-76.43834815
Stage D	O2-				H2O				H2O			
	Electrons	Charge	Spin	Energy (Hartree)	Electrons	Charge	Spin	Energy (Hartree)	Electrons	Charge	Spin	Energy (Hartree)
	17	-1	2	-150.459955	10	0	1	-76.43834815	10	0	1	-76.43834815

Table 25. Additional molecules for the mechanism with ligand synthesized in water, methanol (def2-SVP)

Stage A	OH-				OH-				O2			
	Electrons	Charge	Spin	Energy (Hartree)	Electrons	Charge	Spin	Energy (Hartree)	Electrons	Charge	Spin	Energy (Hartree)
	10	-1	1	-75.774370	10	-1	1	-75.774370	16	0	1	-150.268354
Stage B	OH-				O2				H2O			
	Electrons	Charge	Spin	Energy (Hartree)	Electrons	Charge	Spin	Energy (Hartree)	Electrons	Charge	Spin	Energy (Hartree)
	10	-1	1	-75.774370	16	0	1	-150.268354	10	0	1	-76.426488
Stage C	OH-				O2-				H2O			
	Electrons	Charge	Spin	Energy (Hartree)	Electrons	Charge	Spin	Energy (Hartree)	Electrons	Charge	Spin	Energy (Hartree)
	10	-1	1	-75.774370	17	-1	2	-150.334120	10	0	1	-76.426488
Stage D	O2-				H2O				H2O			
	Electrons	Charge	Spin	Energy (Hartree)	Electrons	Charge	Spin	Energy (Hartree)	Electrons	Charge	Spin	Energy (Hartree)
	17	-1	2	-150.334120	10	0	1	-76.426488	10	0	1	-76.426488

Table 26. Additional molecules for the mechanism with ligand synthesized in water (def2-TZVP)

Stage A	CH3O-				CH3O-				O2			
	Electrons	Charge	Spin	Energy (Hartree)	Electrons	Charge	Spin	Energy (Hartree)	Electrons	Charge	Spin	Energy (Hartree)
	18	-1	1	-114.927474	18	-1	1	-114.927474	16	0	1	-150.082029
Stage B	CH3O-				O2				CH3OH			
	Electrons	Charge	Spin	Energy (Hartree)	Electrons	Charge	Spin	Energy (Hartree)	Electrons	Charge	Spin	Energy (Hartree)
	18	-1	1	-114.927474	16	0	1	-150.082029	18	0	1	-115.5686846
Stage C	CH3O-				O2-				CH3OH			
	Electrons	Charge	Spin	Energy (Hartree)	Electrons	Charge	Spin	Energy (Hartree)	Electrons	Charge	Spin	Energy (Hartree)
	18	-1	1	-114.927474	17	-1	2	-150.118615	18	0	1	-115.5686846
Stage D	O2-				CH3OH				CH3OH			
	Electrons	Charge	Spin	Energy (Hartree)	Electrons	Charge	Spin	Energy (Hartree)	Electrons	Charge	Spin	Energy (Hartree)
	17	-1	2	-150.118615	18	0	1	-115.5686846	18	0	1	-115.5686846

Table 27. Additional molecules for the mechanism with ligand synthesized in methanol (def2-SVP)

Stage A	CH3O-				CH3O-				O2			
	Electrons	Charge	Spin	Energy (Hartree)	Electrons	Charge	Spin	Energy (Hartree)	Electrons	Charge	Spin	Energy (Hartree)
	18	-1	1	-115.0863899	18	-1	1	-115.0863899	16	0	1	-150.268354
Stage B	CH3O-				O2				CH3OH			
	Electrons	Charge	Spin	Energy (Hartree)	Electrons	Charge	Spin	Energy (Hartree)	Electrons	Charge	Spin	Energy (Hartree)
	18	-1	1	-115.0863899	16	0	1	-150.268354	18	0	1	-115.7125098
Stage C	CH3O-				O2-				CH3OH			
	Electrons	Charge	Spin	Energy (Hartree)	Electrons	Charge	Spin	Energy (Hartree)	Electrons	Charge	Spin	Energy (Hartree)
	18	-1	1	-115.0863899	17	-1	2	-150.334120	18	0	1	-115.7125098
Stage D	O2-				CH3OH				CH3OH			
	Electrons	Charge	Spin	Energy (Hartree)	Electrons	Charge	Spin	Energy (Hartree)	Electrons	Charge	Spin	Energy (Hartree)
	17	-1	2	-150.334120	18	0	1	-115.7125098	18	0	1	-115.7125098

Table 28. Additional molecules for the mechanism with ligand synthesized in methanol (def2-TZVP)

Stage A	CH3CH2O-				CH3CH2O-				O2			
	Electrons	Charge	Spin	Energy (Hartree)	Electrons	Charge	Spin	Energy (Hartree)	Electrons	Charge	Spin	Energy (Hartree)
	26	-1	1	-154.1999138	26	-1	1	-154.1999138	16	0	1	-150.0820292
Stage B	CH3CH2O-				O2				CH3CH2OH			
	Electrons	Charge	Spin	Energy (Hartree)	Electrons	Charge	Spin	Energy (Hartree)	Electrons	Charge	Spin	Energy (Hartree)
	26	-1	1	-154.1999138	16	0	1	-150.0820292	26	0	1	-154.834927
Stage C	CH3CH2O-				O2-				CH3CH2OH			
	Electrons	Charge	Spin	Energy (Hartree)	Electrons	Charge	Spin	Energy (Hartree)	Electrons	Charge	Spin	Energy (Hartree)
	26	-1	1	-154.1999138	17	-1	2	-150.1186153	26	0	1	-154.834927
Stage D	O2-				CH3CH2OH				CH3CH2OH			
	Electrons	Charge	Spin	Energy (Hartree)	Electrons	Charge	Spin	Energy (Hartree)	Electrons	Charge	Spin	Energy (Hartree)
	17	-1	2	-150.1186153	26	0	1	-154.834927	26	0	1	-154.834927

Table 29. Additional molecules for the mechanism with ligand synthesized in ethanol (def2-SVP)

Stage A	CH3CH2O-				CH3CH2O-				O2			
	Electrons	Charge	Spin	Energy (Hartree)	Electrons	Charge	Spin	Energy (Hartree)	Electrons	Charge	Spin	Energy (Hartree)
	26	-1	1	-154.4011756	26	-1	1	-154.4011756	16	0	1	-150.268354
Stage B	CH3CH2O-				O2				CH3CH2OH			
	Electrons	Charge	Spin	Energy (Hartree)	Electrons	Charge	Spin	Energy (Hartree)	Electrons	Charge	Spin	Energy (Hartree)
	26	-1	1	-154.4011756	16	0	1	-150.268354	26	0	1	-155.0210899
Stage C	CH3CH2O-				O2-				CH3CH2OH			
	Electrons	Charge	Spin	Energy (Hartree)	Electrons	Charge	Spin	Energy (Hartree)	Electrons	Charge	Spin	Energy (Hartree)
	26	-1	1	-154.4011756	17	-1	2	-150.334120	26	0	1	-155.0210899
Stage D	O2-				CH3CH2OH				CH3CH2OH			
	Electrons	Charge	Spin	Energy (Hartree)	Electrons	Charge	Spin	Energy (Hartree)	Electrons	Charge	Spin	Energy (Hartree)
	17	-1	2	-150.334120	26	0	1	-155.0210899	26	0	1	-155.0210899

Table 30. Additional molecules for the mechanism with ligand synthesized in ethanol (def2-TZVP)

APPENDIX B:

Results of the calculations for the extra molecules intervening in the mechanisms of Section 6

Stage A	OH-				OH-				O2			
	Electrons	Charge	Spin	Energy (Hartree)	Electrons	Charge	spin	Energy (Hartree)	Electrons	Charge	Spin	Energy (Hartree)
	10	-1	1	-75.776957	10	-1	1	-75.776957	16	0	1	-150.083527
Stage B	OH-				O2				H2O			
	Electrons	Charge	Spin	Energy (Hartree)	Electrons	Charge	spin	Energy (Hartree)	Electrons	Charge	Spin	Energy (Hartree)
	10	-1	1	-75.776957	16	0	1	-150.083527	10	0	1	-76.3322311
Stage C	OH-				O2-				H2O			
	Electrons	Charge	Spin	Energy (Hartree)	Electrons	Charge	spin	Energy (Hartree)	Electrons	Charge	Spin	Energy (Hartree)
	10	-1	1	-75.776957	17	-1	2	-150.2479838	10	0	1	-76.332231
Stage D	O2-				H2O				Electrons			
	Electrons	Charge	Spin	Energy (Hartree)	Electrons	Charge	spin	Energy (Hartree)	n of electrons	Charge	Spin	Energy (Hartree)
	17	-1	2	-150.247984	10	0	1	-76.332231	10	0	1	-76.332231

Table 31. Additional molecules for the mechanism in water as solvent (def2-SVP)

Stage A	CH3O-				CH3O-				O2			
	Electrons	Charge	Spin	Energy (Hartree)	Electrons	Charge	Spin	Energy (Hartree)	Electrons	Charge	Spin	Energy (Hartree)
	18	-1	1	-115.042235	18	-1	1	-115.042235	16	0	1	-150.083499
Stage B	CH3O-				O2				CH3OH			
	Electrons	Charge	Spin	Energy (Hartree)	Electrons	Charge	Spin	Energy (Hartree)	Electrons	Charge	Spin	Energy (Hartree)
	18	-1	1	-115.042235	16	0	1	-150.083499	18	0	1	-115.575952
Stage C	CH3O-				O2-				CH3OH			
	Electrons	Charge	Spin	Energy (Hartree)	Electrons	Charge	Spin	Energy (Hartree)	Electrons	Charge	Spin	Energy (Hartree)
	18	-1	1	-115.042235	17	-1	2	-150.245597	18	0	1	-115.575952
Stage D	O2-				CH3OH				CH3OH			
	Electrons	Charge	Spin	Energy (Hartree)	Electrons	Charge	Spin	Energy (Hartree)	Electrons	Charge	Spin	Energy (Hartree)
	17	-1	2	-150.245597	18	0	1	-115.575952	18	0	1	-115.575952

Table 32. Additional molecules for the mechanism in methanol as solvent (def2-SVP)

Stage A	CH3CH2O-				CH3CH2O-				O2			
	Electrons	Charge	Spin	Energy (Hartree)	Electrons	Charge	Spin	Energy (Hartree)	Electrons	Charge	Spin	Energy (Hartree)
	26	-1	1	-154.3083758	26	-1	1	-154.3083758	16	0	1	-150.083483
Stage B	CH3CH2O-				O2				CH3CH2OH			
	Electrons	Charge	Spin	Energy (Hartree)	Electrons	Charge	Spin	Energy (Hartree)	Electrons	Charge	Spin	Energy (Hartree)
	26	-1	1	-154.3083758	16	0	1	-150.083483	26	0	1	-154.8419190
Stage C	CH3CH2O-				O2-				CH3CH2OH			
	Electrons	Charge	Spin	Energy (Hartree)	Electrons	Charge	Spin	Energy (Hartree)	Electrons	Charge	Spin	Energy (Hartree)
	26	-1	1	-154.3083758	17	-1	2	-150.244221	26	0	1	-154.8419190
Stage D	O2-				CH3CH2OH				CH3CH2OH			
	Electrons	Charge	Spin	Energy (Hartree)	Electrons	Charge	Spin	Energy (Hartree)	Electrons	Charge	Spin	Energy (Hartree)
	17	-1	2	-150.244221	26	0	1	-154.8419190	26	0	1	-154.8419190

Table 33. Additional molecules for the mechanism in ethanol as solvent (def2-SVP)